3-26-2002

Effects of Shot-Peening on High Cycle Fretting Fatigue Behavior of Ti-6Al-4V

Halil I. Yuksel

EFFECTS OF SHOT-PEENING ON HIGH CYCLE FRETTING FATIGUE BEHAVIOR OF Ti-6Al-4V

THESIS

Halil I Yuksel, 1LT, TUAF

AFIT/GAE/ENY/02-12

DEPARTMENT OF THE AIR FORCE
AIR UNIVERSITY

AIR FORCE INSTITUTE OF TECHNOLOGY

Wright-Patterson Air Force Base, Ohio

Report Documentation Page

Report Date	Report Type	Dates Covered (from... to)
26 Mar 02	Final	Sep 2000 - Mar 2002

Title and Subtitle Effects of Shot-Peening on High Cycle Fretting Fatigue Behavior of Ti-6Al-4V	**Contract Number**
	Grant Number
	Program Element Number
Author(s) 1Lt Halil I. Yuksel, TUAF	**Project Number**
	Task Number
	Work Unit Number
Performing Organization Name(s) and Address(es) Air Force Institute of Technology Graduate School of Engineering and Management (AFIT/EN) 2950 P Street, Bldg 640 WPAFB, OH 45433-7765	**Performing Organization Report Number** AFIT/GAE/ENY/02-12
Sponsoring/Monitoring Agency Name(s) and Address(es) Dr. Jeffrey Calcaterra AFRL/MLLMN 2230 Tenth Street, Suite 1 WPAFB, OH 45433-7817	**Sponsor/Monitor's Acronym(s)**
	Sponsor/Monitor's Report Number(s)

Distribution/Availability Statement
Approved for public release, distribution unlimited

Supplementary Notes
The original document contains color images.

Abstract
Effects of Shot-peening on High Cycle Fretting Fatigue behavior of Ti-6Al-4V were investigated. Experiments were performed with 6.35 mm thick specimens which provided S/N curves. After the tests, it was observed that the specimens failed near the trailing edge of contact. Scanning Electron Microscopy showed that cracks initiated on the contact surface for 6.35 mm, and at the depth of specimen ranging from 200 to 300 microns for 3.81 mm thick specimens. Initial crack orientation was around 37 and 42 degrees respectively for 6.35 and 3.81 mm thicknesses. Finite Element Analysis (FEA) was conducted, and using FEA results, Smith-Watson-Topper, Findley, Shear Stress Range and Modified Shear Stress Range parameters were evaluated. Stress relazation was observed after the failure of the specimens, and evaluations were repeated for differment percentages of stress relaxation. Based on specific assumptions aout stress relaxation. Modified Shear Stress range parameter was determined to be the only appropriate fatigue parameter that could meet all the required conditions for shot-peened fretting fatigue specimens. Also thickness effects on shot-peened specimens were investigated and discussed in this study.

Subject Terms Fretting Fatigue, High Cycle Fatigue, Shot-Peening, Shot-Peening Effets in Fretting Fatigue	
Report Classification unclassified	**Classification of this page** unclassified
Classification of Abstract unclassified	**Limitation of Abstract** UU
Number of Pages 142	

The views expressed in this thesis are those of the author and do not reflect the official policy or position of the Department of Defense, the U. S. Government, or the Government of Turkish Republic.

AFIT/GAE/ENY/02-12

EFFECTS OF SHOT-PEENING ON HIGH CYCLE FRETTING FATIGUE BEHAVIOR OF Ti-6Al-4V

THESIS

Presented to the Faculty

Department of Aeronautical and Astronautical Engineering

Graduate School of Engineering and Management

Air Force Institute of Technology

Air University

Air Education And Training Command

In Partial Fulfillment of the Requirements for the

Degree of Master of Science in Aeronautical Engineering

Halil I Yuksel, BS

1 LT, TUAF

March 2002

AFIT/GAE/ENY/02-12

EFFECTS OF SHOT-PEENING ON HIGH CYCLE FRETTING FATIGUE BEHAVIOR OF Ti-6Al-4V

Halil I Yuksel, BS
1 LT, TUAF

Approved:

_____//signed//_____	_____
Shankar Mall (Chairman)	date
_____//signed//_____	_____
Vinod K. Jain (Member)	date
_____//signed//_____	_____
Robert A. Canfield (Member)	date

Acknowledgements

I would like to express my sincere appreciation to my faculty advisor and my thesis advisor Dr. Mall for his guidance and support throughout this thesis project. I would also like to thank my sponsor Dr. Jeffrey Calcaterra, from Air Force Research Laboratory, Materials and Manufacturing Directorate (AFRL/MLLMN).

I would like to thank Oh-Chang Jin and Shantanu Namjoshi who gave me technical support while performing the tests, and S. Naboulsi who helped me with the Finite Element Analysis of the fretting fatigue experimental configuration.

I would also like to thank my academic advisor Dr. King for his helps throughout the whole academic year, and special thanks to Lt. Col. Canfield for his patience and valuable helps while teaching Finite Element Analysis.

Finally, I would like to express my gratitude to Turkish Air Forces who believed in me and gave me the chance and honor of completing my Master of Science degree in Aeronautical Engineering in AFIT in USA.

Halil I Yuksel

Table of Contents

Page

List of Figures

Figure Page

Figure Page

List of Tables

Nomenclature

a	contact half width
a_{EXP}	experimentally observed contact half width
a_{FEA}	FEA predicted contact half width
A	cross sectional area
A^*	composite compliance
b	half length of the specimen thickness
b'	fatigue strength exponent
c	stick zone boundary
c'	fatigue ductility exponent
C_1, C_2, C_3, C_4	material fitting parameters
e	x coordinate shift of the stick zone
E	modulus of elasticity
f	coefficient of friction
G	shear modulus
k	radius of curvature
k'	material fitting parameter
m	material fitting parameter
N_f	number of cycles to failure
N_i	number of cycles to crack initiation
p_0	maximum normal pressure in contact zone
P	normal load

q	surface shear stress
Q	tangential load
Q_{max}	maximum tangential load
Q_{min}	minimum tangential load
r	fretting pad radius
R	axial stress ratio
R_1	principal strain ratio
R_ε	strain ratio in x direction
R_τ	shear stress ratio
S_y	yield stress
u	displacement
w	specimen width
β	Dundar's parameter
$\varepsilon_{1,max}$	maximum principal strain
$\varepsilon_{1,R1}$	maximum principal strain corrected for strain ratio
ε_a	strain amplitude
ε_f'	fatigue ductility coefficient
ε_{max}	maximum strain in x-direction
$\varepsilon_{max,R\varepsilon}$	maximum strain in x-direction corrected for strain ratio
γ_{crit}	critical plane shear stress amplitude fatigue parameter
γ^*_{crit}	γ_{crit} fatigue parameter adjusted for multi axial loading
Γ	maximum ($\sigma_{max}\,\varepsilon_a$) fatigue parameter at the critical plane

ν	Poisson's ratio
θ	observed angle of orientation
σ_{axial}	axial stress
$\sigma_{axial,max}$	maximum axial stress
$\sigma_{axial,min}$	minimum axial stress
$\sigma_{n,max}$	maximum normal stress on critical plane
σ_f'	fatigue strength coefficient
σ_R	fatigue strength reduction
σ_T	tangential stress, stress in x- direction in this study
σ_{xx}	normal stress in longitudinal direction (X-axis)
$\sigma_{xx,FEA}$	FEA predicted stress in the X-direction
σ_{yy}	normal stress in the Y-direction
τ	shear stress
τ_{max}	maximum shear stress on critical plane
τ_f'	shear fatigue ductility coefficient
τ_{xy}	shear stress on X-Y plane

Abstract

Effects of shot-peening on high cycle fretting fatigue behavior of Ti-6Al-4V were investigated. S-N curves were obtained with 6.35 mm thick specimens. Scanning Electron Microscopy showed that for 6.35 mm thickness, cracks initiated on the contact surface whereas the crack initiation location was found to be at the depth ranging from 200 to 300 microns from the contact surface for 3.81 mm thick specimens tested in a previous study at AFIT. The orientation of the primary crack for 6.35 mm thickness was around -37 degrees, and the orientation of the secondary crack was around -28 degrees. Failure location was near the trailing edge of contact for both thicknesses. Commercially available finite element code ABAQUS was used to analyze the specimens. Axial stress (σ_{xx}) distribution along the longitudinal direction and within depth of the specimen was found to determine where the stress concentration was maximum that may have caused crack initiation. Maximum stress concentration was found in the trailing edge of contact where the specimens failed. Also transverse (σ_{yy}), and shear (τ_{xy}) stresses were found. Using σ_{xx}, σ_{yy}, and τ_{xy} values of FEA output data, Smith-Watson-Topper, Findley, Shear Stress Range and Modified Shear Stress Range (MSSR) parameters were evaluated. Stress relaxation was observed after the failure of specimens, and based on specific assumptions about stress relaxation, evaluations were repeated for different percentages of stress relaxation. MSSR Parameter was determined to be the only appropriate fatigue parameter that could meet all the required conditions for shot-peened specimens. Also, thickness effects on shot-peened specimens were investigated and discussed in this study.

EFFECTS OF SHOT-PEENING ON HIGH CYCLE FRETTING FATIGUE BEHAVIOR OF Ti-6Al-4V

1. Introduction

1.1. Fretting Fatigue Problem

Fretting fatigue is one of the most important areas of interest to the United States Air Force as a cause of high cycle fatigue failure. Fretting fatigue is the damage caused by localized relative motion between the components under vibratory load, and results in premature crack initiation and failure. It is the form of contact fatigue occurring especially in certain, important structural components such as aircraft turbine engines and fuselage lap joints with critical cracks being initiated at contact interfaces. Fretting increases tensile and shear stresses at the contact surface and generates flaws which lead to premature crack nucleation, and finally it results in failure due to the reduction of fatigue resistance of materials. The blade/disk dovetail joint in aircraft turbine engines mostly fails due to fretting fatigue (Figure 1.1). Fretting fatigue leads to both failures and increases in the maintenance costs due to the reduced part lives. In order to minimize these maintenance costs and increase the parts' lives, the United States Air Force and several researchers have worked on the fretting fatigue problem. They have performed numerous studies on different areas of fretting fatigue. They tried to formulate different fatigue parameters that would help determining the causes of the reduction in the lives of

different materials due to fretting fatigue when compared to plain fatigue, and they tried to find new methods that would help increasing the lives and decreasing the maintenance costs of the materials. They also tried various methods involving surface modifications such as shot-peening [1,2], coatings [3,4], and soft shims [5]. Earlier studies performed by different authors will be explained in Chapter 2 in detail.

1.2. Shot-Peening in Fretting Fatigue

The purpose of this study is to investigate the effects of shot-peening on high cycle fretting fatigue behavior of Ti-6Al-4V in detail. Shot-peeing is the most commonly used cold working procedure that involves bombarding the surface of the material with small, hard, often steel balls. These cause biaxial yielding in compression under each point of impact, hence a biaxial compressive residual stress occurs on the surface due to the elastic recovery of the unyielded material beneath. Shot-peening changes physical and mechanical properties of a material. It introduces a residual compressive stress on the surface with a changing profile within depth of the material, and a compensatory residual tensile stress within the material. It changes the surface roughness of the material, thereby potentially changing the coefficient of friction, and work hardening of the material, again thereby changing the coefficient of friction. Also distortion of the grains near the surface reduces the propensity for crack propagation in this region. All these properties may vary when the severity of shot-peening changes. In shot-peened specimens, when there is no stress relaxation, cracks occur within depth of the material due to the compressive zone created by shot-peening, whereas the cracks occur on the surface of the unshot-peened

specimens. This compressive zone tends to cancel out the effects of the tensile stresses up to a specific level which act as the opening mode for the cracks. Cracks also do not propagate in this compressive zone. This phenomenon leads us to a point that shot-peening improves fatigue life, strength operation, and corrosion resistance due to the introduction of compressive residual stress. In addition, shot-peening can close the preexisting cracks if the depth of the residual compressive stress generated due to shot-peening is greater than the depth of the cracks. But if it is too severe then there may not be any beneficial effects. Instead it may result in a brittle material with higher notch sensitivity, which is not desired from the shot-peening. Surface residual stresses are beneficial only where subsequent yielding does not occur due to loads that occur in service, as this may remove the compressive residual stress or even change it to a harmful tensile one.

1.3. Methodology

The objective in this study was to show the effects of shot-peening on high cycle fretting fatigue behavior of titanium alloy, Ti-6Al-4V. For this reason, the first part was to get the S-N curves of the 6.35 mm thick shot-peened specimens by performing tests (7 tests) in the laboratory under different loading conditions. Also, crack initiation location and the initial crack orientations of the primary and the secondary cracks were found by doing Scanning Electron Microscopy (SEM). A previous study performed by Namjoshi, Jain, and Mall [6] with 3.81 mm thick shot-peened fretting specimens showed that the crack initiation location was different from the as received specimens. It was

inside the specimen at a depth ranging from 200 to 300 microns rather than on the surface due to the residual compressive stress created by shot-peening. In this study, the author found the crack initiation location and initial crack orientations of 6.35 mm thick shot-peened fretting specimens, and compared with the results from 3.81 mm thick specimens, found by Namjoshi, Jain, and Mall [6]. The author conducted Finite Element Analysis (FEA) using ABAQUS [7]. Axial stress distribution along the longitudinal and transverse directions was found to determine where the stress concentration was maximum that might be the main reason of the crack initiation along the contact interface. Besides the axial stresses, transverse and shear stresses were found too. By using axial, transverse and shear stresses, several fatigue parameters were evaluated along the contact surface, and within depth of the material. Theoretical details about these fatigue parameters are given in Chapter 2. The author made some comparisons between the observed crack initiation location and initial orientation of the primary crack (SEM Results) and predicted location and orientation of the primary crack that causes failure (Fatigue Parameters Results). The author also compared the results of 6.35 mm thick specimens found in this study with the results of 3.81 mm thick specimens obtained by Namjoshi, Jain, and Mall [6]. In addition, the author investigated the thickness effects on the crack initiation behavior of shot-peened specimens. Finally, the author tried to predict the crack initiation cycles of shot-peened fretting fatigue specimens using the plain fatigue and as received fretting fatigue data.

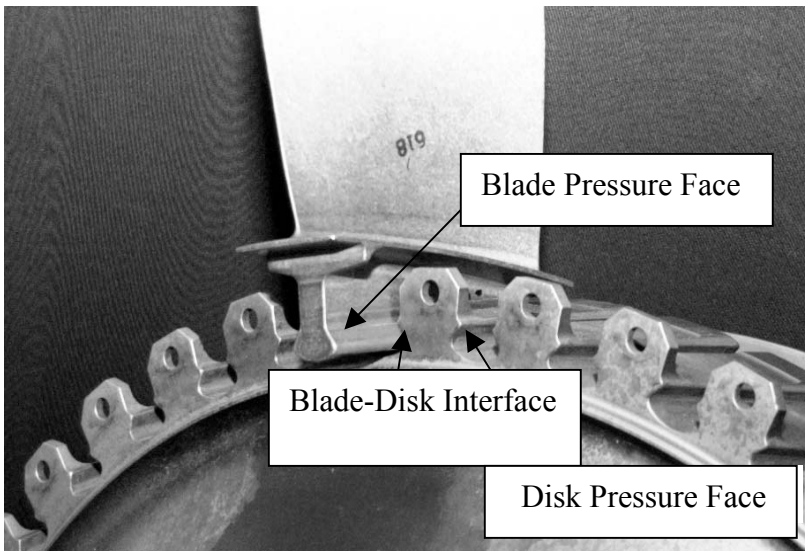

Figure 1.1. Turbine Engine Blade-Disk Interface

2. Literature Review

2.1. General Issue

In this chapter, different approaches and different formulations developed by several researchers to investigate the fretting fatigue problem are reviewed in three main sections. The first section will review the studies done in fatigue parameters area. These parameters were used to describe the fretting fatigue crack initiation behavior. The second section will review the analytical techniques (mainly contact mechanics) that would help to validate the Finite Element Model of the fretting fatigue experimental configuration used in this study. The third section will review details of the previous study about shot-peening performed by Namjoshi, Jain, and Mall [6], which will also be a basis for this thesis. In the previous study, some specific techniques were used while analyzing the test results of 3.81 mm thick shot-peened specimens. Some of the steps described in the third section will be used in the next chapters while analyzing the test data of 6.35 mm thick shot-peened specimens in this study.

2.2. Fatigue Parameters

The studies done in Fatigue Parameters area were categorized by Lykins [8] under four main, important areas. These areas are *"Empirical Techniques, Fracture Mechanics Techniques, Fretting Fatigue Specific Techniques, and Plain Fatigue Techniques"*. These techniques will be reviewed in detail in the following sections.

2.2.1. Empirical Techniques. In the history of the fretting fatigue, several researchers attempted to predict the failure cycles of the fretting fatigue specimens using many different empirical techniques. In the studies done up to this time, the life debit due to fretting has been correlated using one or more test variables, generally on the basis of the applied stress. Most of the authors tried to explain the reduction in the life due to fretting as a function of the alternating applied stress, but they ignored that under fretting fatigue conditions, there is a stress concentration that develops at the edge of the contact as a result of the applied normal, tangential and the axial load which causes the life debit. In his studies, Harris [9] developed a sensitivity index for fretting fatigue of Ti-6Al-4V. He made some normal pressure modifications and changed the magnitude of the stress concentration at the edge of the contact, and showed that the important thing for developing a fatigue parameter was making modifications on the stress concentration, not the applied normal pressure.

Hoeppner and Goss [10] showed that fretting damage is produced after a certain percentage of fatigue life with the fretting pads in contact with the fretting specimen. Endo and Goto [11] also noticed this phenomenon when they worked on a different material.

In the empirical techniques described above, the authors did not try to establish the relationship between the change in applied loading condition and the change in the stress or strain along the contact surface. Instead they just tried to show that fretting fatigue reduced the strength of plain fatigue due to parametric variations of certain loading conditions, specifically the applied normal pressure.

2.2.2. Fracture Mechanics Techniques. As mentioned in the previous section, there is a high stress concentration at the edge of contact as a result of the applied axial, normal and tangential loads in fretting fatigue. Lindley and Nix [12,13] developed a stress intensity factor for this highly stressed contact edge region. Using this stress intensity factor, loading conditions leading to crack growth and arrest behavior would be determined.

In fracture mechanics technique, there is a limitation. Either an initial crack length is assumed or an estimate of threshold of the flaw size that can be tolerated for infinite fretting fatigue life is provided. It is known from the previous studies that crack initiation begins at around % 50 to % 90 of the total fatigue life for high cycle fretting fatigue conditions, but it is impossible to find the exact life spent to reach an initial crack length. As it is not easy to understand the crack initiation phase of the fretting fatigue, it is getting more difficult to develop a fatigue parameter using fracture mechanics techniques under high cycle fretting fatigue conditions. Also, fracture mechanics techniques do not provide or predict the remaining life until failure after the point where there is an initial crack length. In addition, the crack orientation must be assumed or known to conduct the analyses using fracture mechanics techniques.

As a result, it can be said that fracture mechanics approach is not applicable under high cycle fretting fatigue conditions, because fracture mechanics approach can be used to analyze fatigue failure where a large part of life is spent in crack propagation, but it is known that under high cycle fretting fatigue (HCF) conditions, a large part of the life is spent during the crack nucleation and growth to a detectable size. So, there is no

distinction made between the crack formation and crack propagation in HCF conditions.

2.2.3. Fretting Fatigue Specific Techniques. Ruiz and some other authors [14] proposed two parameters that may be applicable specifically to fretting fatigue. These parameters are as follows

$$\kappa_1 = (\sigma_T)_{max}\,(\tau\delta)_{max} \tag{1}$$

$$\kappa_2 = (\sigma_T \tau\delta)_{max} \tag{2}$$

where $(\sigma_T)_{max}$ is the maximum tangential stress, and $(\tau\delta)_{max}$ is the maximum frictional work. Ruiz proposed that damage from fretting fatigue depends on the work done by the frictional force between contacting bodies. His first parameter is a measure of the frictional energy expenditure density. In equations (1) and (2), frictional work term ($\tau\delta$) represents the mechanism that nucleates cracks, and the maximum tangential stress term $(\sigma_T)_{max}$ opens and then propagates the nucleated cracks. The tangential stress defined here is analogous to the stress in the longitudinal direction in this study (Figure 2.1). The second parameter is the modified form of the first parameter. It asserts that crack nucleation in the fretting fatigue can also depend on the maximum tangential stress. Several authors found that maximum value of the second parameter (κ_2) had good agreement with the location of fretting fatigue crack initiation along the interface, but Mall, Jain and Lykins [15] showed that these parameters were inadequate to predict the fretting fatigue crack initiation behavior. Lykins [8] found that there was not a distinct trend between the Ruiz parameter and the fretting fatigue cycles to crack initiation, and there was inconsistency about the crack initiation location when compared with the

experimental observations.

Elkholy [16] developed a parameter as follows

$$(\sigma_R / p_0) = 2f\,[1-\exp(-E\,u / a\,p_0)] \quad (3)$$

where σ_R is the fretting fatigue strength reduction, p_0 is the maximum pressure due to the normal load (Hertzian Peak Pressure), f is the coefficient of friction, E is the elasticity modulus, u is the slip distance, and a is the contact half length. He suggested subtracting the fretting fatigue reduction factor from the plain fatigue strength of the material. He also included the effects of the slip distance to his parameter. This method is applicable only when the same stress ratio is used in fretting fatigue tests.

Lindley and Nix [12,13] included the effects of the slip distance in their studies too, like Elkholy [16] did. Fouvry [17] recognized that the transition from the gross sliding contact condition to the partial slip condition was an important threshold condition for fretting fatigue. They all realized that the effects of the slip distance at the transition point were the most important points while working on the fretting fatigue problem.

2.2.4. Plain Fatigue Techniques. Several authors formulated different plain fatigue parameters, based on stress or strain history of the plain fatigue specimens. They then used these parameters to estimate the lives of the fretting fatigue specimens. These plain fatigue techniques can be applied in fretting fatigue problem at the trailing edge of the contact where the stress concentration is maximum.

As a plain fatigue technique, Coffin [18] and Manson [19] showed the relation of the strain and number of cycles to failure as follows

$$(\Delta\varepsilon / 2)_p = \varepsilon_f' (2N_f)^{c'} \quad (4)$$

where $(\Delta\varepsilon / 2)_p$ is the plastic strain amplitude, ε_f' is the fatigue ductility coefficient, N_f is the number of strain reversals to failure (1 reversal = 0.5 cycle), and c' is the fatigue ductility exponent.

Basquin [20] showed a similar relation as follows

$$(\Delta\varepsilon / 2)_e = \sigma_f' / E * (2N_f)^{b'} \quad (5)$$

where $(\Delta\varepsilon / 2)_e$ is the elastic strain amplitude, σ_f' is the fatigue strength coefficient and b' is the fatigue strength exponent.

Using the previous equations, the total strain amplitude can be written as follows

$$\varepsilon_a = \sigma_f' / E * (2N_i)^{b'} + \varepsilon_f' (2N_i)^{c'} \quad (6)$$

Equation (6) is known as strain life equation. It is a good fatigue parameter under constant strain ratio conditions. It does not give accurate results when different strain ratios are used while collecting data.

Walker [21] developed a method that also works with different strain ratios. His method can be expressed as follows

$$\varepsilon_{max,R\varepsilon} = \varepsilon_{max} (1 - R_\varepsilon)^m \quad (7)$$

where $\varepsilon_{max,R\varepsilon}$ represents the maximum strain corrected for the given strain ratio, ε_{max} is the maximum strain, R_ε is the strain ratio ($R_\varepsilon = \varepsilon_{min} / \varepsilon_{max}$), and m is a material fitting parameter. Lykins [8] showed that this parameter was in good agreement with the

experimental results in predicting the number of cycles to crack initiation, and crack initiation location along the contact surface, but not the initial crack orientation.

Socie [22] showed that the maximum principal strain could be used as a fatigue parameter for multiaxial plain fatigue loading. The maximum principal strain corrected for strain ratio can be formulated using the Walker [21] method in the same manner as follows

$$\varepsilon_{1,R1} = \varepsilon_{1,max} (1- R_1)^{m} \tag{8}$$

where $\varepsilon_{1,R1}$ is maximum principal strain corrected for strain ratio, $\varepsilon_{1,max}$ is maximum principal strain, and R_1 is principal strain ratio. Lykins [8] found that this parameter was not in good agreement with the experimental results while predicting the number of cycles to crack initiation and initial crack orientation. It could just predict the crack initiation location along the contact surface (the location where the parameter has its maximum value is accepted as the predicted crack initiation location).

Nishioka and Hirokawa [23,24] showed that the maximum principal stress could be used as a fatigue parameter to predict the crack initiation location. Also they found that the initial crack orientation was around 45^{o} from the maximum principal stress plane.

Smith-Watson-Topper [25] formulated another considerable fatigue parameter finding the number of cycles to crack initiation as follows

$$\Gamma = \sigma_{max}\varepsilon_a = (\sigma_f')^2 / E * (2N_i)^{2b'} + \sigma_f'\varepsilon_f'(2N_i)^{b'+c'} \tag{9}$$

where σ_f' is fatigue strength coefficient, b' is fatigue strength exponent, ε_f' is fatigue ductility coefficient, c' is fatigue ductility exponent, E is the elasticity modulus, and N_i is

cycles to crack initiation. This equation is widely known as Smith-Watson-Topper (SWT) [25] parameter. Mall, Jain, Namjoshi, and Lykins [26] evaluated this parameter in their studies. They found that this parameter was effective in predicting the number of cycles to crack initiation, and the crack initiation location, but not the initial crack orientation along the contact surface.

In fretting fatigue, crack nucleation occurs in the contact region between the two bodies where the state of stress is of a multiaxial nature. Based on this approach, Socie [22] modified SWT parameter that it could also be used as a critical plane multiaxial parameter. He changed the left hand side of equation (9) to represent the maximum principal strain amplitude and the maximum principal stress.

In critical plane methods, it is possible to predict the orientation of crack and it can provide an estimate of the crack size. Szolwinski and Farris [27] also made further modifications to SWT parameter and proposed a critical plane approach for fretting fatigue. Their modified parameter assumed that crack initiation occurs on the plane where the product of the normal strain amplitude, ε_a, and the stress normal to this plane, σ_{max} was maximum. Their parameter, $\Gamma = \sigma_{max}\,\varepsilon_a$, worked in predicting the crack initiation location and orientation. The initial crack orientation was found to be perpendicular to the applied axial stress.

Fatemi and Socie [28] showed that using the same strain amplitude in torsion tests when compared to tension tests, it was possible to get longer lives. They created a model as follows

$$\gamma[\,1 + k'(\,\sigma_{n,max} / S_y)] = \tau_f' / G * (\,2N_i)^{b'} + \gamma_f'(\,2N_i)^{c'} \qquad (10)$$

where γ is the critical shear strain amplitude, k' is a fitting constant, $\sigma_{n,max}$ is the normal stress perpendicular to the critical plane, S_y is the yield stress of the material, τ_f' is the shear fatigue ductility coefficient, G is shear modulus, and γ_f' is the shear fatigue strength coefficient. Equation (10) is known as Fatemi and Socie (F-S) parameter.

Neu, Pape, Swalla-Michaud [29] found that Smith-Watson-Topper (SWT) critical plane parameter predicted the crack initiation location well, but not the initial crack orientation. However, they also found that Fatemi-Socie parameter predicted the crack initiation location and initial crack orientation well. In addition, they realized that the maximum shear strain amplitude did not coincide with the location of crack initiation under fretting fatigue conditions, whereas it was effective for plain fatigue.

Lundberg and Palmgren [30] found out that under rolling contact conditions, shear stress amplitude on the critical plane could be used to predict the bearing ring failures. It was also applicable to fretting fatigue configuration as the roller bearing fatigue configuration was similar to fretting fatigue configuration.

Fellows [31] and some other authors showed that for certain fretting fatigue configurations, the location of the maximum shear stress amplitude on the critical plane coincided with the observed crack initiation location. However they did not formulate any fatigue parameters to predict the number of cycles to crack initiation and they did not try to find any relations between the observed and the predicted angles of crack orientation along the contact surface.

Lykins [8] proposed a shear stress based critical plane parameter as follows

$$\gamma_{crit} = (\tau_{max} / G)(1-R_{\tau})]^{m} \qquad (11)$$

where τ_{max} is maximum shear stress, G is shear modulus, and R_τ is the shear stress ratio. In order to compare the plain fatigue and fretting fatigue conditions, he then modified and proposed this parameter as

$$\gamma^*_{crit} = (1 + \sigma_{yy} / \sigma_{xx}) \ \tau_{max} / [G (1-R_\tau)]^{m} \quad (12)$$

where σ_{yy} is the transverse stress, and σ_{xx} is the axial stress. This parameter involves the maximum shear stress range along with the local shear stress ratio and transverse stress ratio effects on the critical plane. This parameter was effective in predicting the number of cycles to crack initiation, crack initiation location and initial crack orientation along the contact surface.

Findley [32] proposed another multiaxial fatigue parameter, involving the normal stress effect besides the shear stress as

$$FP = \tau_a + k \ \sigma_{max} \quad (13)$$

where k is an influence factor (k = 0.35) (0.35 is found from plain fatigue data), and

$$\tau_a = (\tau_{max} - \tau_{min}) / 2 \quad (14)$$

In their studies, Mall, Jain, Namjoshi and Lykins [26] showed that Findley parameter was not effective in predicting the fretting fatigue lives from plain fatigue data, and also, the predicted crack orientations were different from those observed experimentally. So, in order to overcome this shortcoming of Findley parameter, they modified the Shear Stress Range parameter in the form of Findley parameter, and proposed the Modified Shear Stress Range (MSSR) parameter as follows

$$MSSR = A.\Delta\tau_{crit,eff}^{B} + C.\sigma_{max}^{D} \quad (15)$$

where Shear Stress Range parameter (SSR) was defined as

$$\Delta\tau_{crit,eff} = \tau_{max}(1\text{-}R_{\tau})^{m} \quad \text{and} \quad m = 0.45 \quad (16)$$

MSSR parameter explicitly included the effects of the shear stress as well as the normal stress as it should be the case in multiaxial fatigue loading. Mall, Jain, Namjoshi and Lykins [26] showed that MSSR parameter was effective in predicting the number of cycles to crack initiation, crack initiation location, and initial crack orientation along the contact surface, which were completely in agreement with their experimental counterparts.

In Chapter 5 of this thesis, some of these fatigue parameters mentioned above will be evaluated. These evaluations will be performed for different percentages of stress relaxation. For shot-peened specimens, there will be some stress relaxation, and in order to understand the crack initiation behavior of shot-peened specimens better, parameter results will be analyzed thoroughly. As also it will be explained in Chapter 5, the evaluations will be performed for Smith-Watson-Topper (SWT), Findley, Shear Stress Range (SSR), and Modified Shear Stress Range (MSSR) parameters. For each of the parameters, there will be comparisons between the experimentally observed crack initiation locations, and initial crack orientations. Also, maximum values of these parameters will be analyzed to find whether the crack initiation location is on the contact surface or inside the material. In addition, the author will try to predict the crack initiation cycles of shot-peened fretting fatigue specimens comparing the plain fatigue data and

shot-peened fretting fatigue data. Finally, the results of Scanning Electron Microscopy (SEM) and fatigue parameters will be discussed in Chapter 6.

2.3. Contact Mechanics

In this study, there is a cylindrical body (fretting pad) in contact with a flat body (fretting specimen), which is the form of fretting fatigue configuration. So, there is a contact problem between a cylindrical and a flat body to be solved. The analytical solution for this case will be reviewed in details in the following section solved by Hills and Nowell [33].

2.3.1. Contact Problem Between a Cylindrical and a Flat Body. The two bodies in contact are assumed to have infinite boundaries. In Figure 2.2, the diagram of the two bodies in contact are shown. In the figure, σ_{axial} represents the applied cyclic axial stress, P is the applied normal load, Q is the reacted tangential load, a is the contact half length, b is the specimen half thickness, and A is the cross sectional area of the specimen. The fretting pad has a constant radius, whereas the fretting specimen is infinite in the cross sectional plane.

Hills and Nowell [33] developed a relation for the contact region in Y-direction like

$$(1 / A^*)(\delta h / \delta x) = (1 / \pi) \int [p(\xi) / (x-\xi)] - \beta q(x) \qquad (17)$$

where $h(x) = v_1(x)-v_2(x)$, is the amount of the overlap in case the contacting bodies penetrate each other, p is the pressure in contact region and q is the surface shear stress. A* is the composite compliance defined as

$$A^* = 2\,[(1-\nu_1^2)/E_1 + (1-\nu_2^2)/E_2] \tag{18}$$

and Dundar's parameter, β, is defined as

$$\beta = (1/2A^*)\,[(1-2\nu_1)/E_1 - (1-2\nu_2)/E_2] \tag{19}$$

where E is the elasticity modulus and ν is the Poisson's ratio. A similar equation can be obtained as follows when tangential displacement is assumed as $g(x) = u_1(x) - u_2(x)$

$$(1/A^*)(\delta g/\delta x) = (1/\pi)\int [q(\xi)/(x-\xi)] + \beta p(x) \tag{20}$$

Equations (17) and (20) can be simplified, because the materials of the fretting pad and the fretting specimen are the same in this study which leads to $\beta = 0$.

According to Hertz solution, when a normal load P is applied, there will be a peak stress at the middle of the contact surface. Also, according to the Half Space assumption, if one half of the fretting specimen thickness, b, is at least ten times the contact half width, a, or b/a >10, it is accepted that a half space exists that can be interpreted as an infinite boundary. Finite Element Analysis needs to be conducted if b/a < 10. Fellows et al. [34] used b/a = 3 in their studies and showed that if the infinite boundary assumption is violated, there will be a deviation from the analytical solutions.

Hills and Nowell [33] found an expression using the equilibrium between the applied load and pressure distribution for the contact zone as

$$P = -\int_{-a}^{a} p(\xi)d\xi = (\pi k a^2)/2A^* \tag{21}$$

where $k = 1/R_1 + 1/R_2$. Here, R_1 is the radius of the fretting pad, and R_2 is the radius of the fretting specimen. Using the previous equation, the pressure distribution can be expressed as

$$p(x) = - p_0 [1 - (x / a)^2]^{0.5} \quad (22)$$

where p_0 is the maximum pressure (Hertzian Peak Pressure) defined as

$$p_0 = \frac{2P}{\pi a} \quad (23)$$

P is the applied normal load, and a is the contact half length. Contact half length, a, can be found using equation (21) as follows

$$a^2 = \frac{2PA^*}{\pi k} \quad (24)$$

In this study, for a fretting pad having a curvature of 50.8 mm, and a fretting specimen having a flat surface ($R = \infty$), contact half length can be found as follows after applying the variables

$$a = [((8PR_1) / \pi) ((1-\nu^2) / E)]^{0.5} \quad (25)$$

The axial stress (stress along longitudinal direction) resulting from the applied normal load P can be expressed in Cartesian coordinates as

$$(\sigma_{xx})_{normal} = -p_0 \{ [a^2 - x^2]^{0.5} / a \} \quad (26)$$

On the contact surface, after applying normal load P and tangential load Q, there will be a stick zone in the middle and slip zones at both sides. As shown in Figure 2.3, the distance between –c and c gives the sticking region whereas the distances between –a and –c, and c and a show the slipping regions. In the stick region, contacting points of the fretting specimen and the fretting pad move together, but in the slip zone the contacting points of the specimen and pad move freely.

Shear stress distribution along the contact surface is described as

$$q(x) = C / (a^2 - x^2)^{0.5} \tag{27}$$

where C is found as

$$C = Q / \pi \tag{28}$$

Q is the total shear stress along the contact length, which is obtained by integrating the shear stress distribution. It is also found by Hills and Nowell [33] as follows

$$Q = [(f p_0 \pi) / (2a)] (a^2 - c^2) \tag{29}$$

where f is the coefficient of friction, and stick zone size is described as follows

$$c / a = [1 - |Q / f P|]^{0.5} \tag{30}$$

Eventually, the stress distribution caused by the tangential load in the X-direction (longitudinal direction) is found as

$$(\sigma_{xx})_{tangential} = 2 f p_0 - \frac{2}{\pi} \int_{-a}^{a} \frac{q'(x)}{x+a} dx \quad (31)$$

where

$$q'(x) = -[(f p_0 c) / a] \{ 1-[(x - e) / c]^2 \}^{0.5} \quad (32)$$

and

$$e = (\sigma a) / (4 f p_0) \quad (33)$$

Total stress along the contact surface of the fretting specimen and the fretting pad in X-direction (longitudinal direction) can be expressed as the sum of the axial stresses caused by the normal and tangential loads, and the applied axial stress as follows

$$\sigma_{xx} = (\sigma_{xx})_{normal} + (\sigma_{xx})_{tangential} + (\sigma_{xx})_{axial} \quad (34)$$

Chan and Lee [35] wrote a program named "Ruiz program" which carries out the numerical solution of the equation (34). In this study, the results of the Finite Element Analysis (FEA) and Ruiz program will be compared, and by means of comparing FEA results with this alternative analytical solution technique, FEA results will be validated in Chapter 4. After validating the FEA results, σ_{xx}, σ_{yy}, and τ_{xy} values of the FEA output data will be used to evaluate the fatigue parameters mentioned in the previous section, along the contact surface and within depth of the specimen (along longitudinal and transverse directions). Also, it should be noted again that Finite Element Analysis is necessary for the configuration of cylindrical pad on a flat specimen in this study, because the thickness of the shot-peened specimens is 6.35 mm, and half of the thickness

is less than ten times b/a. It will be 7.2159 < 10, as it will be shown in Chapter 4.

2.4. Specific Techniques Used for 3.81 mm Thick Shot-Peened Specimens

As also mentioned in the previous chapter, various methods involving surface modifications such as shot-peening [1-2], coatings [3-4] and soft shims [5] have been used by several researchers to improve the fretting fatigue behavior of Ti-6Al-4V. This study will mostly focus on shot-peening, because the objective here is finding the effects of shot-peening on high cycle fretting fatigue behavior of Ti-6Al-4V rather than the other methods.

In their studies, De Los Rios, Brown, Trooll and Levers [36-37] have shown that shot-peening improves the fretting fatigue strength of materials. Mutoh, Satoh and Tsunoda [38] have shown that the introduction of the residual compressive stress is the most significant factor in improving the fretting fatigue behavior of materials.

While working with shot-peened specimens, the profile of the residual compressive stress is very important. Also, the profile of compensatory residual tensile stress, which is unknown, needs to be found. It is possible to find the profile of the compensatory residual tensile stress using an analytical technique described as follows, which was used by Namjoshi, Jain and Mall [6] with 3.81 mm thick shot-peened specimens in the previous study.

$$\int_{0}^{Yo} \sigma_c(y)\, dy = \int_{Yo}^{d/2} \sigma_t(y)\, dy \qquad (35)$$

$$\{ d\sigma_c / dy \}_{-Y0} = \{ d\sigma_t / dy \}_{+Y0} \quad (36)$$

$$[\sigma_t(y)]_{y = d/2} = 0 \quad (37)$$

$$[\sigma_t(y)]_{y = Y0} = 0 \quad (38)$$

where $\sigma_c(y)$ and $\sigma_t(y)$ are the compressive and tensile residual stresses in the specimen as a function of depth (y) respectively (Y-axis is the transverse direction along the thickness of the specimen). Y_0 is the depth at which the residual compressive stress becomes zero and d is the thickness of the specimen. The resulting tensile stress variation then can be expressed as follows

$$\sigma_t(y) = [p\ q\ (M+r)] / [(M+r)^2 + p^2] - s \ : \qquad d/2 > y > Y_0 \quad (39)$$

where $M = y - Y_0$, and the coefficients p, q, r, s can be found after solving the equations (35) through (38) in this analytical solution technique.

After finding the profile of this compensatory residual tensile stress, the value and the depth of the maximum compensatory residual tensile stress becomes important, because it can be used to guess the crack initiation location that causes failure. This assumption was used by Namjoshi, Jain and Mall [6] with 3.81 mm thick shot-peened specimens.

While performing tests in the laboratory, applied stress range can be described as

$$\Delta\sigma = \sigma_{max} - \sigma_{min} \quad (40)$$

Effective stress after considering the stress ratio effect can be shown using the Walker method [21] as

$$\sigma_{eff} = \sigma_{max} (1 - \sigma_{min} / \sigma_{max})^{m} \quad (41)$$

where m was found as 0.45 by Lykins [8] as an accurate value giving good results, so 0.45 is also used in this study. Then, in order to fit the experimental data on a curve, the applied stress range can be described as

$$\Delta\sigma = C_1 (N)^{C2} + C_3 (N)^{C4} \quad (42)$$

where C_1, C_2, C_3, C_4 can be found using a curve fitting technique with Kaleidagraph [39]. Also, effective stress can be described as

$$\sigma_{eff} = C_1 (N)^{C2} + C_3 (N)^{C4} \quad (43)$$

Different C_1, C_2, C_3, C_4 coefficients can also be found for effective stress values.

In their studies with 3.81 mm thickness, Namjoshi, Jain and Mall [6] showed that shot-peening moved the crack initiation location from contact surface to somewhere around 200-300 microns within depth of Ti-6Al-4V. They showed three modes of failure in the shot-peened specimens explained as:

a) "*fatigue-induced failure showing striations with increasing spacing away from the crack initiation site"*,

b) "*the region between the pure fatigue failure and the overload region showing evidence of mixed-mode failure in which both ductile and fatigue-induced failure was present"*, and

c) "*the overload region indicating the plastic deformation*".

They showed that the introduction of residual stresses in the substrate of Ti-6Al-4V

improved the fretting fatigue life of the material when compared to as received specimens test data. They mentioned that in order to realize the beneficial effects of the residual compressive stresses, "*the depth of the compressive zone must be greater than the depth of the region effected by compressive stresses. Therefore, a shot-peening method, which produces a large compressive residual stress at the surface with a rapid fall-off, may not be appropriate to improve the fretting fatigue life. On the other hand, a method that produces a residual stress profile with a smaller gradient, so that the compressive stress goes deeper into the substrate may provide a much better improvement in the fretting fatigue life of the material"*.

As also defined in equation (41), Namjoshi, Jain and Mall [6] used the Walker method [21] to define the effective stress. (It can be obtained when the stress ratio effect is taken into consideration. It should be noted that mean stress may be the same for different stress ratios. So, especially while working with different stress ratios, effective stress should be handled carefully). They showed that either stress range or effective stress plots demonstrated the beneficial effects of shot-peening especially at lower stress levels for 3.81 mm thickness. As a one dimensional approach, they added the effect of maximum compensatory residual tensile stress to the applied axial cyclic stress. They defined the effective stress after incorporating the maximum compensatory residual tensile stress as follows

$$\sigma_{eff} = (\sigma_{max} + \sigma_{ten.res.})[\, 1 - (\sigma_{min} + \sigma_{ten.res}) / (\, \sigma_{max} + \sigma_{ten.res})]^{\,m} \qquad (44)$$

In this study, the residual stresses are assumed to act in both tangential direction (the same direction the applied cyclic stresses act), and transverse direction on the contact

surface and within depth of the material. Namjoshi, Jain and Mall [6] showed that there was a good agreement between life under plain fatigue and life under fretting fatigue with shot-peening when the effect of the residual compensatory tensile stress was included. They also showed that shot-peening eliminated the effect of fretting (due to residual compressive stress), but resulted in plain fatigue like behavior when the effect of the compensatory residual tensile stress was considered. They noticed that the beneficial effects of shot-peening were eliminated when the applied stress exceeded the residual compressive stress.

It should be noted that, for 3.81 mm thickness, any of the fatigue parameters mentioned in this chapter were not evaluated for shot-peened specimens in the previous study. Experimental and Scanning Electron Microscopy (SEM) results were obtained, and an acceptable, logical explanation for crack initiation mechanism was found using the analytical technique described above. Evaluation of the fatigue parameters for 3.81 mm thick specimens will be done by the author of this study.

In Chapter 5, the author will evaluate the mentioned fatigue parameters for both 3.81 mm, and 6.35 mm thicknesses. There will be comparisons between the experimental and predicted results for these two thickness values to show the thickness effects on the shot-peened specimens, and the results found will be discussed in Chapter 6. Also, there will be comparisons between the shot-peened fretting fatigue, as received fretting fatigue, and plain fatigue test data to find accurate explanations for the crack initiation behavior of shot-peened fretting fatigue specimens.

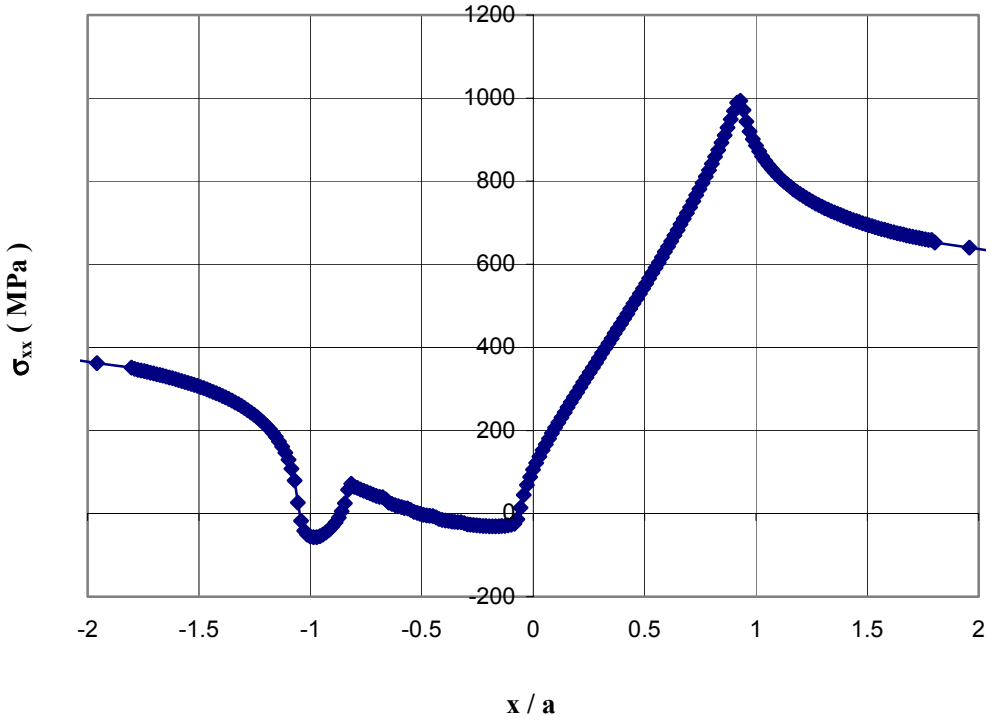

Figure 2.1. Stress Concentration on the Contact Surface (Test # 1)

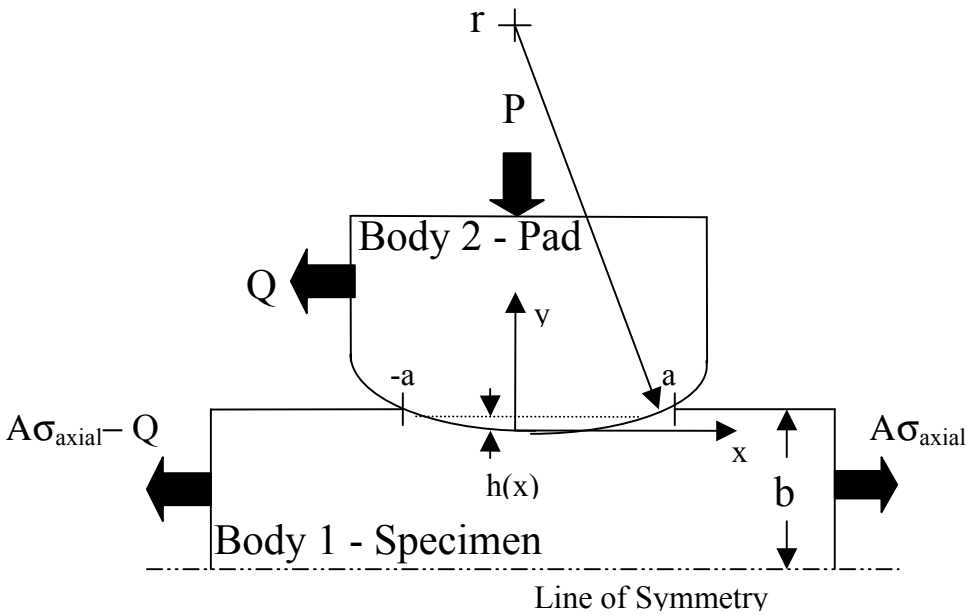

Figure 2.2. Free Body Diagram of Two Bodies Under Fretting Fatigue Loads

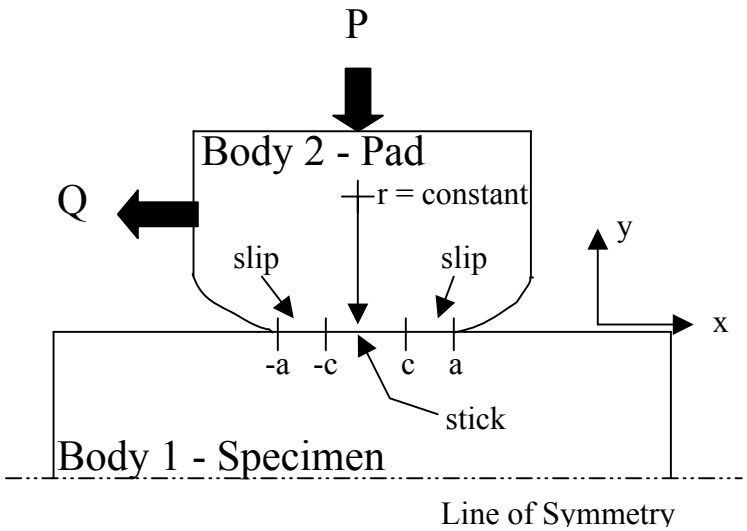

Figure 2.3. Partial Slip Condition For Deformed Bodies

3. Experiments

3.1. Experimental Configuration

As mentioned in Chapter 1, fretting fatigue is a very common problem in aircraft engine turbines. The geometry and loading conditions in a turbine of an aircraft engine are very complex. However, in this study, simplified geometry and loading conditions were used to investigate the effects of shot-peening on high cycle fretting fatigue behavior of titanium alloy, Ti-6Al-4V, which is a very common metal used in aircraft engine turbines.

The fretting fatigue tests were conducted on a servo-hydraulic uniaxial test machine, at room temperature, in a laboratory environment, at cyclic frequencies of 5 Hz and 10 Hz. A cylinder-on-flat configuration was used to introduce the fretting effect. The contacting bodies are the fretting fatigue pads and the fretting fatigue specimen. Two fretting pads, each with cylindrical end radius of 50.8 mm were pressed against the surface of the fretting fatigue specimen using a fretting fixture (Figure 3.1). The contact of the specimen and the pad was supplied by the use of the lateral springs, which applied a constant normal load of 1335 N. Dog-bone shaped shot-peened fatigue specimens with gage section dimensions of 60 mm (length), 6.35 mm (width) and 6.35 mm (thickness) were used (Figure 3.2). In all tests, a normal load (P) of 1335 N was applied, which resulted in a Hertzian peak pressure of 304 MPa, and contact half length of 0.44 mm on the fretting fatigue specimen. This normal load (P) was measured using two load cells on each side of the fretting specimen. Both the fretting specimens and the fretting pads

used in the tests were machined from titanium alloy, Ti-6Al-4V. The modulus of elasticity, E, and the yield stress, σ_y, of Ti-6Al-4V were determined to be 126.5 GPa and 1003 MPa respectively. The specimens were shot-peened based on the SAE Aerospace Materials Specification (AMS) 2432 standard, using a computer controlled equipment with an intensity of 7 Almen. The process was conducted with ASR 110 cast steel shots with 100 % surface coverage.

3.2. Fretting Fatigue Tests and Experimental Results

All fretting fatigue tests of 6.35 mm thick shot-peened specimens were conducted under a tension-tension loading condition at different stress levels, but with the same stress ratio of 0.1. The details of these test data are given in Table 3.1. The coefficient of friction between the fretting specimen and the fretting pads was measured during some of the tests. For this, the specimen was released from the upper grip (Figure 3.1), and then the applied load on the bottom side of the specimen was increased very slowly in displacement control mode till the local sliding between the specimen and fretting pads occurred [40]. This sliding force and the applied normal load provided coefficient of friction, which was found as 0.258 after zero cycles, 0.3 after 5,000 cycles and 0.4583 after 10,000 cycles.

In this study, the applied loads were varied to obtain different cycles data on different logarithmic intervals. After performing 7 tests in the laboratory, the author obtained S-N curves of the 6.35 mm thick shot-peened specimens having the residual compressive stress profile given in Figure 3.3. This profile was obtained before the tests, using X-ray

diffraction technique, by Lambda Research Center, Cincinnati. The compensatory residual tensile stress profile, which was unknown, was assumed to have a rectangular distribution. Figure 3.4 shows the measured residual compressive and assumed compensatory residual tensile stress profiles together. Rectangular distribution assumption for the compensatory residual tensile stress profile will be discussed in Chapter 6. Figure 3.5 shows stress range versus life, and Figure 3.6 shows the effective stress versus life. Effective stress versus life plots are important, especially when different stress ratios are used in the experiments, but it should be repeated that the same stress ratio was used in this study (R = 0.1) for all tests. It can be seen easily from these two charts that shot-peening increases failure life. The trend lines in Figure 3.5 and Figure 3.6 are obtained in Excel after using a curve fitting technique with Kaleidagraph [39]. This technique was also mentioned in Chapter 2. The equations (42) and (43) are used in Excel after the coefficients are calculated by Kaleidagraph [39]. The coefficients C_1, C_2, C_3, C_4 are given in Table 3.2 for both stress range versus life ($\Delta\sigma$ vs. N), and effective stress versus life (σ_{eff} vs. N) charts belonging to 6.35 mm thickness. It should be noted that, these global charts do not include the effects of stress concentration at the trailing edge of contact region and the multiaxial loading effects under fretting condition. Therefore, in Chapter 5, the author will evaluate the fatigue parameters that include the stress concentration and multiaxial loading effects to investigate the crack initiation behavior of Ti-6Al-4V.

The experimental data for 50.8 mm end radius pads and 6.35 mm thick shot-peened specimens are given in Table 3.1. Experimental data for 50.8 mm end radius pads and 3.81 mm thick shot-peened specimens are also shown in Table 3.3. The tests of 3.81 mm

thickness were performed by Namjoshi [6]. In order to make some comparisons between the two different shot-peened specimen groups having two different thicknesses, and two different residual stress profiles, these data need to be shown too. (It should be noted that thickness effects on shot-peened specimens will be discussed in Chapter 6.)

In the experiments, the normal load P was applied first. In this study, the normal load P was constant in all tests and it was 1335 N. Then using 0.1 as the stress ratio value, the cyclic axial load was applied as $\sigma_{axialmax}$ and $\sigma_{axialmin}$ as different values in each test. The corresponding tangential loads Q_{max} and Q_{min} were also found for each test after analyzing the test data. The details for maximum and minimum values of the applied loads, σ_{axial}, and resultant tangential loads, Q, are in Table 3.1. When the test results are analyzed, the author tried to show the maximum and minimum values of the resultant tangential loads after some specific cycles. The aim for this type of analysis was to find the stabilized maximum and minimum Q loads among the whole test duration that would be used in Finite Element Analysis. A typical example for Q_{max} and Q_{min} versus life is given in Figure 3.7. Also the author investigated the changes of the tangential loads Q, versus the applied loads F to find out the hysteresis loops. In the hysteresis loops, it was possible to see the gross sliding, and partial slip conditions. In the gross sliding stage, the Q load was increasing to a local maximum, and then decreasing to the steady state condition. The time of gross sliding in the tests was not very long for the cylindrical pad geometry. In the partial slip stage, Q load was following a stabilized pattern, with a maximum and minimum as stabilized extremums. These stabilized extremum values are important, because these Q_{max} and Q_{min} values are used in the Finite Element input files. In this study, Finite Element Analysis (FEA) is required as also mentioned in Chapter 2,

and it models the actual test configuration to find the axial, transverse and shear stress distributions along the contact surface and within depth of the material. The results of FEA will be used while evaluating the fatigue parameters in Chapter 5. A typical example for Q versus F, found for some specific cycles is also shown in Figure 3.8, where the gross sliding and partial slip stages can be seen easily. Gross sliding stage is the stage where larger loops are seen. Gross sliding stage is happening in the first stages of life. In some of the tests, a sudden drop in Q near the end of the test was noticed and correlated to the rapid growth of a major crack. The failure cycles for these tests were also accurate with the cycles expected according to loading conditions (according to S-N curves). It was observed that the duration of partial slip stage was much longer than gross sliding stage for cylindrical pad geometry.

In the next chapters, using these experimental test results, Finite Element Analysis (FEA) will be conducted for each test, and using the FEA results, fatigue parameters mentioned in Chapter 2 will be evaluated to find possible explanations to Scanning Electron Microscopy (SEM) results. It should be repeated again that SEM was used to find the crack initiation location and initial crack orientation along the contact surface for some of the tests performed.

3.3. Crack Location

An important feature of a fretting fatigue parameter is that it should be able to predict the crack initiation location. In this study, after each fretting fatigue test, it is observed by looking at the fretting scar on the specimen that the failure location was near the trailing

edge of contact where x/a was 1. In Figure 3.9, it can be seen from the fretting fatigue scar that the failure of the fretting specimen belonging to Test # 5 was very near the trailing edge of contact (Trailing edge is the right hand side of the picture). Figure 3.10 shows the fretting scar on the pads used also in Test # 5. The observed contact length was measured as 1.56 mm as it can be seen in Figure 3.10, whereas the analytical result was 0.88 mm (Use equation (25) for the fretting pad having 50.8 mm end radius). Lykins also noticed that, for 50.8 mm end radius pad configuration, the observed contact length was bigger than the analytical result. The values in his case were 1.3 mm, and 0.88 mm respectively for the same geometry. This happened, because when the crack size increased, some changes in the compliance occurred which resulted in larger contact widths than the expected values. For shot-peened specimens, higher coefficient of friction may be the reason for greater experimental contact widths when compared with the values of as received specimens.

Besides the failure location, it is also important to know whether the crack initiation location is on the contact surface or within depth of the material for shot-peened specimens. It is well known that in shot-peened specimens, there is a compressive residual stress on the contact surface, and this compressive stress changes with a profile within depth of the material. The measured residual compressive stress profile along the depth of the specimen for 6.35 mm thickness is shown in Figure 3.3. The measured residual compressive stress becomes zero at a depth of 164 microns in this profile. After this point, the profile of the compensatory residual tensile stress that balances the equilibrium of residual stresses needs to be found. Compensatory residual tensile stress profile is unknown. In this study, for 6.35 mm thickness, the distribution of the

compensatory residual tensile stress was assumed to be rectangular and having the value calculated as 27.95 MPa after the depth of 164 microns from the contact surface (Figure 3.4). In Namjoshi's [6] tests with 3.81 mm thick shot-peened specimens, the distribution of this compensatory residual tensile stress was assumed to have a serpent-like distribution having the peak value of 260 MPa at a depth of 255 microns. The equations for this technique is pointed out in Chapter 2 (Equation (35) through (38)). It must be noted again that in Namjoshi's [6] tests, the thickness used was 3.81 mm. The reasons why it's assumed a rectangular distribution in this study for 6.35 mm thick specimens will be explained in details in Chapter 6.

Under Scanning Electron Microscopy (SEM), for 6.35 mm thick shot-peened specimens, crack initiation location was found to be on the contact surface whereas it was found to be at the depth ranging from 200 to 300 microns for 3.81 mm thick shot-peened specimens. Figure 3.11 through Figure 3.14 show the SEM results of the first and fifth tests performed by the author of this study, using 6.35 mm thick shot-peened specimens. In these figures, it can be seen that the crack initiation location is on the contact surface of the material where there are river patterns and discoloration. Figure 3.11 shows the river patterns clearly. Figure 3.12 shows the tilted position of the specimen which apparently shows the crack initiation location as the corner (Corner shows contact surface). Figure 3.13 shows a very apparent discoloration, and Figure 3.14 shows the discoloration again under higher magnification that indicate the crack initiation location at the contact surface of the specimen. As a result, it can be summarized that for 3.81 mm thick shot-peened specimens, the failure location was near the trailing edge of contact, and crack initiation location was at the depth of the specimen ranging from 200 to 300

microns. For 6.35 mm thick shot-peened specimens, the failure location was near the trailing edge of contact again, but crack initiation location was at the contact surface this time rather than within depth of the material. A possible explanation for the considerable difference in the crack initiation locations between 3.81 mm and 6.35 mm thick specimen groups will be given in Chapter 6. While evaluating the fatigue parameters in Chapter 5, stress relaxation measured on the contact surface using X-ray diffraction technique within base facilities, will be taken into consideration, and the effects of different percentages of stress relaxation on the change of the crack initiation location will be discussed.

3.4. Crack Orientation

Another important feature of a fatigue parameter is that it should be able to predict the initial crack angle at the crack initiation location. The experimentally observed and the predicted angles should match. For 6.35 mm thickness, the initial angle of the primary crack that caused the failure of the specimen was found to be –53.7 degrees for Test # 1. Figure 3.15 shows the initial crack angle for Test # 1. After 8.3 microns, the crack appears to be growing perpendicular to the axial load. The initial crack angle was also found for Test # 4. Figure 3.16 shows that the initial crack angle is –37 degrees, but then it becomes 53.6 degrees. It shows that it is changing its direction by nearly 90 degrees. Lykins [8] also noticed this phenomenon named as orthogonal cracking in his studies. Besides the primary crack that caused the failure of the specimen, secondary crack, which could not grow much, was also found for Test # 5. Figure 3.17 shows the secondary crack found for Test # 5. The initial angle of this secondary crack was found to be –28

degrees.

In Chapter 5 of this thesis, the initial primary crack angles that are found here will be compared with the predicted angles using the fatigue parameters mentioned in Chapter 2. Besides the initial crack angles, the experimentally found crack initiation locations will be compared with the predicted locations. These comparisons will be done for both 3.81 mm and 6.35 mm thickness values.

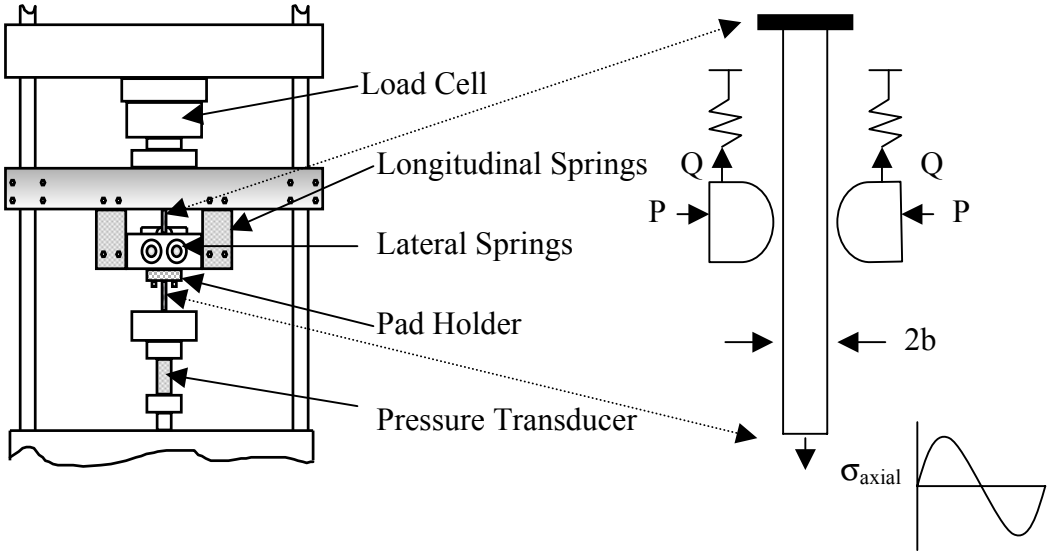

Figure 3.1. Fretting Fatigue Experimental Configuration

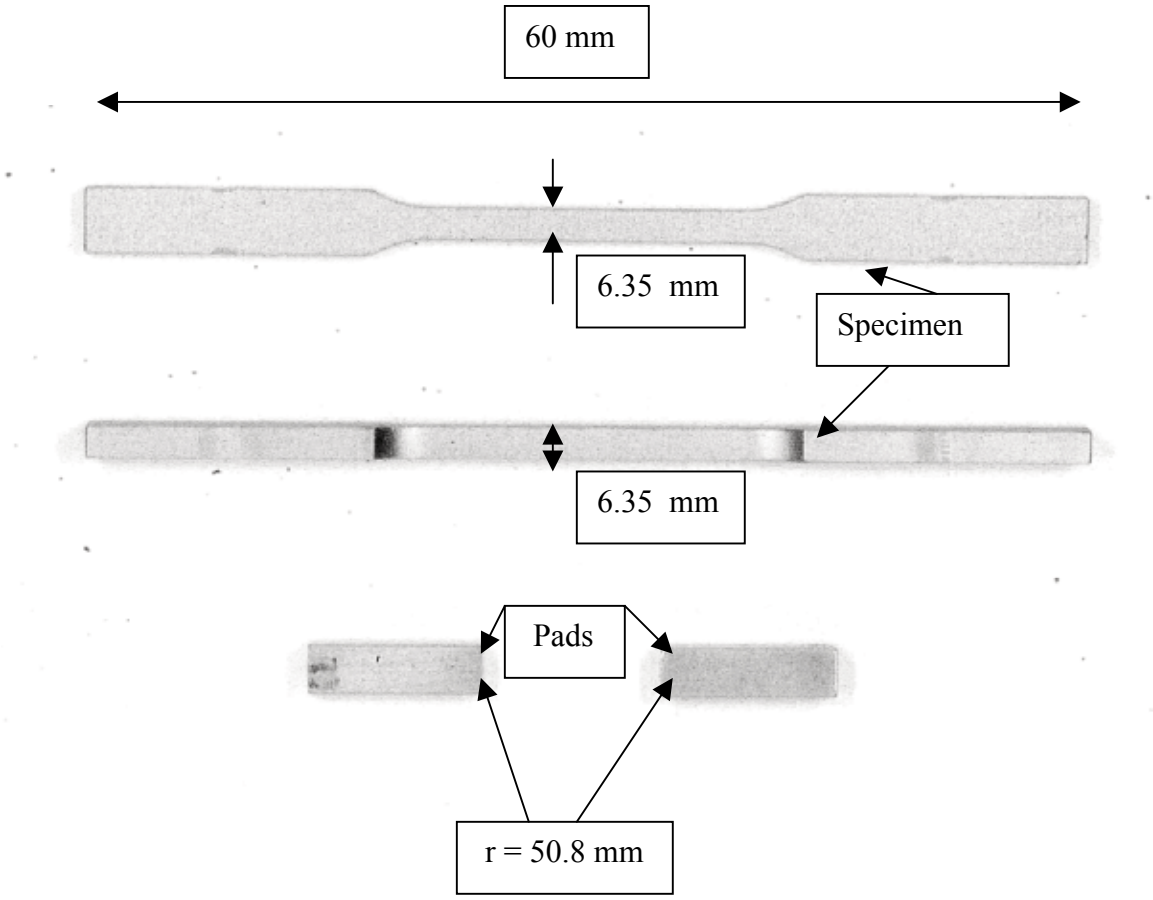

Figure 3.2. Dog-bone shaped specimen and 50.8 mm end radius pad

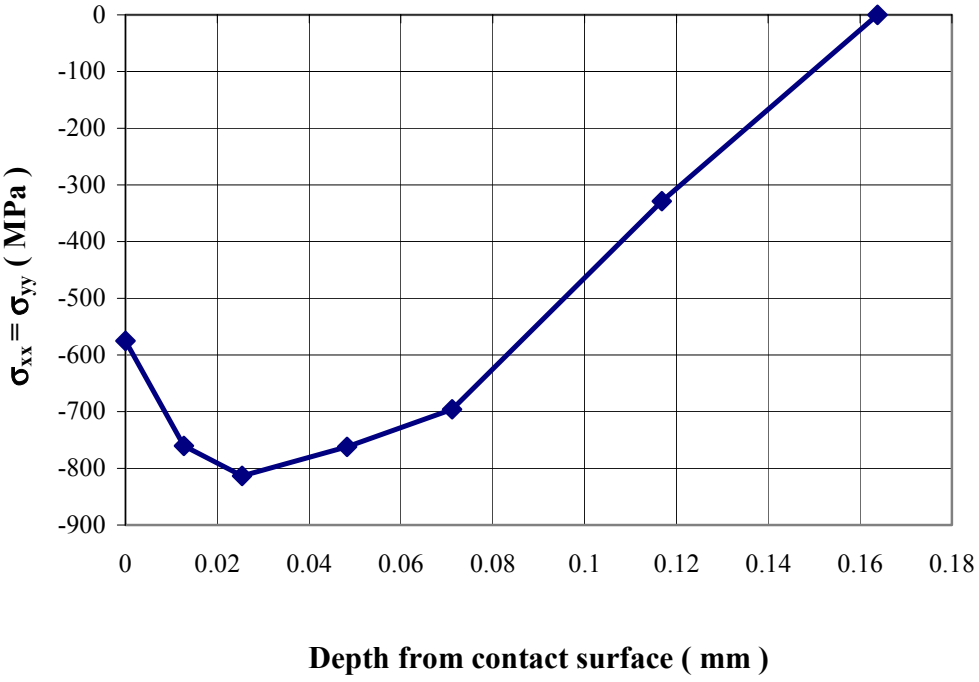

Figure 3.3. Measured Residual Compressive Stress Profile for 6.35 mm thickness (Before tests)

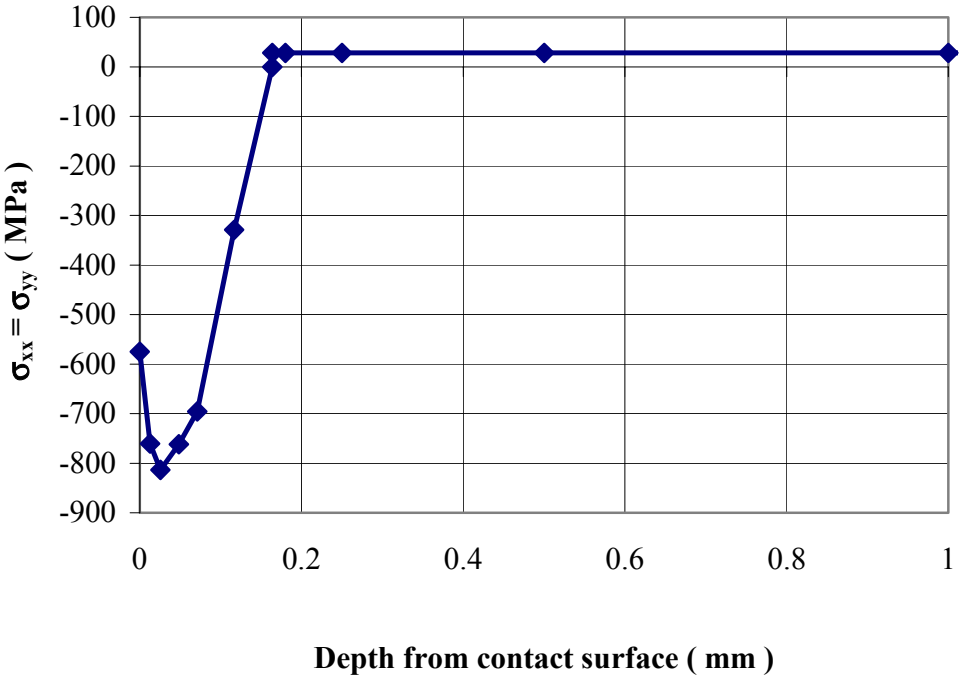

Figure 3.4. Measured Residual Compressive Stress and Assumed Compensatory Residual Tensile Stress Profiles for 6.35 mm thickness

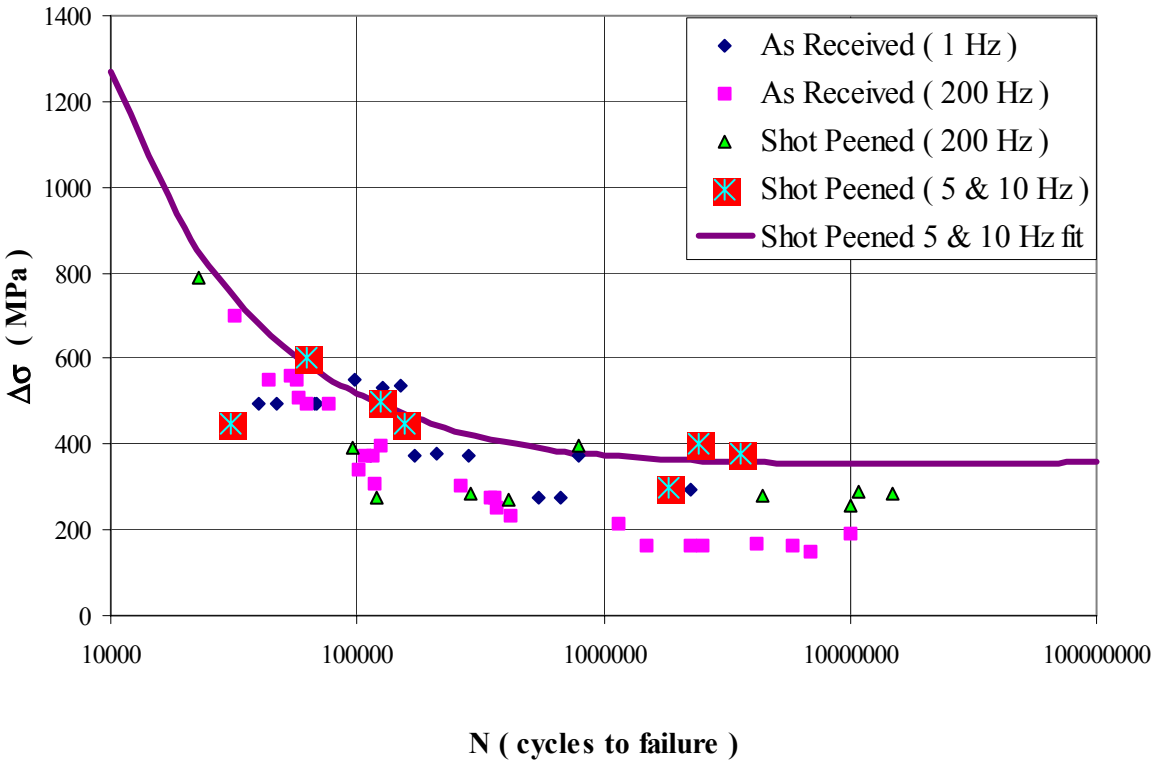

Figure 3.5. Stress Range versus Life ($\Delta\sigma$ vs N)

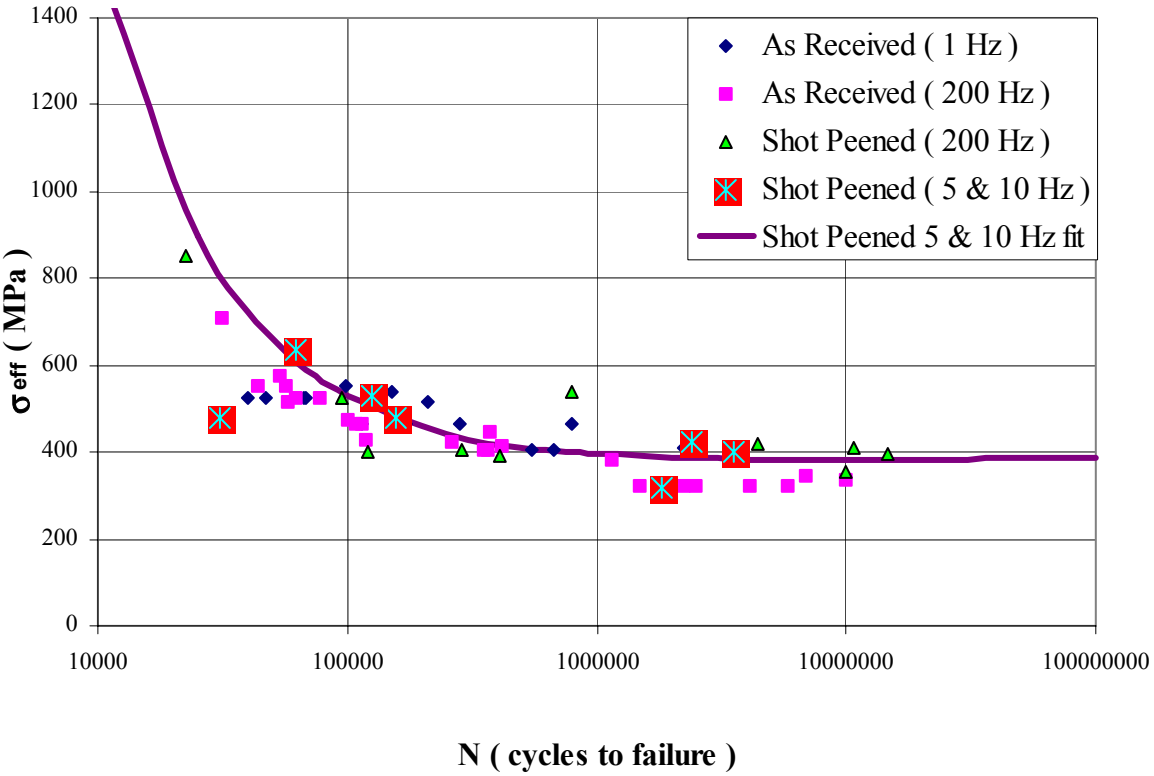

Figure 3.6. Effective Stress versus Life (σ_{eff} vs N)

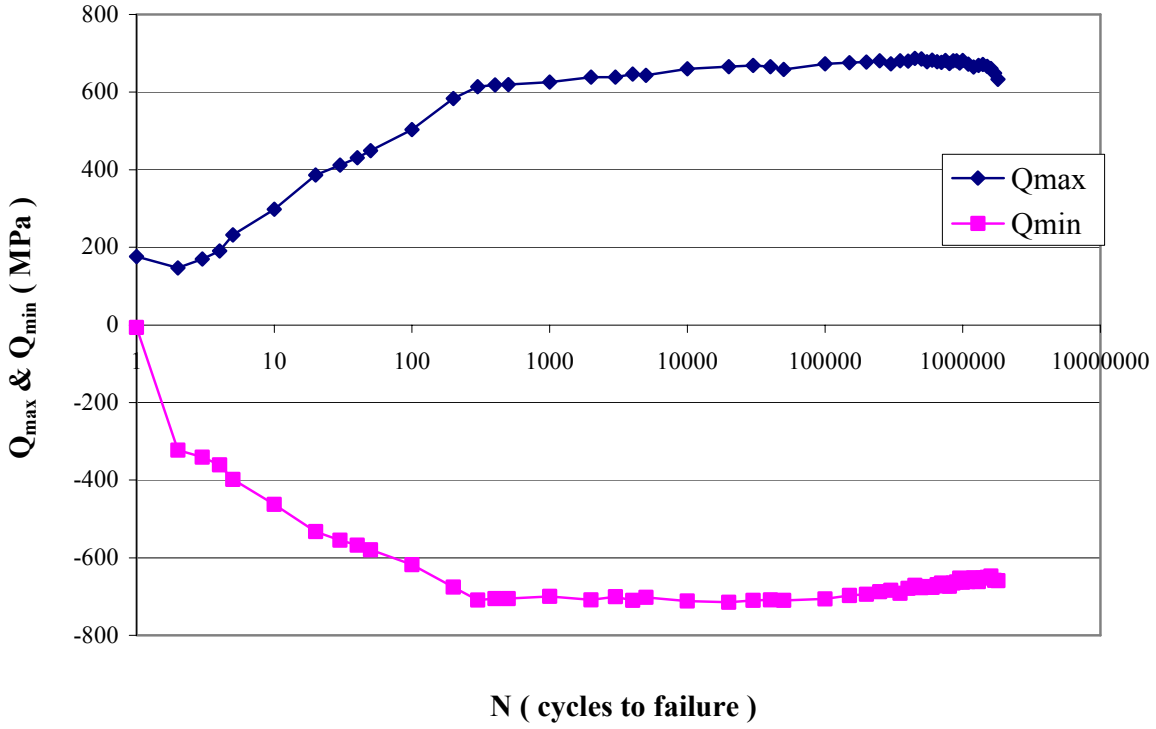

Figure 3.7. Q_{max} & Q_{min} vs N (Test # 2)

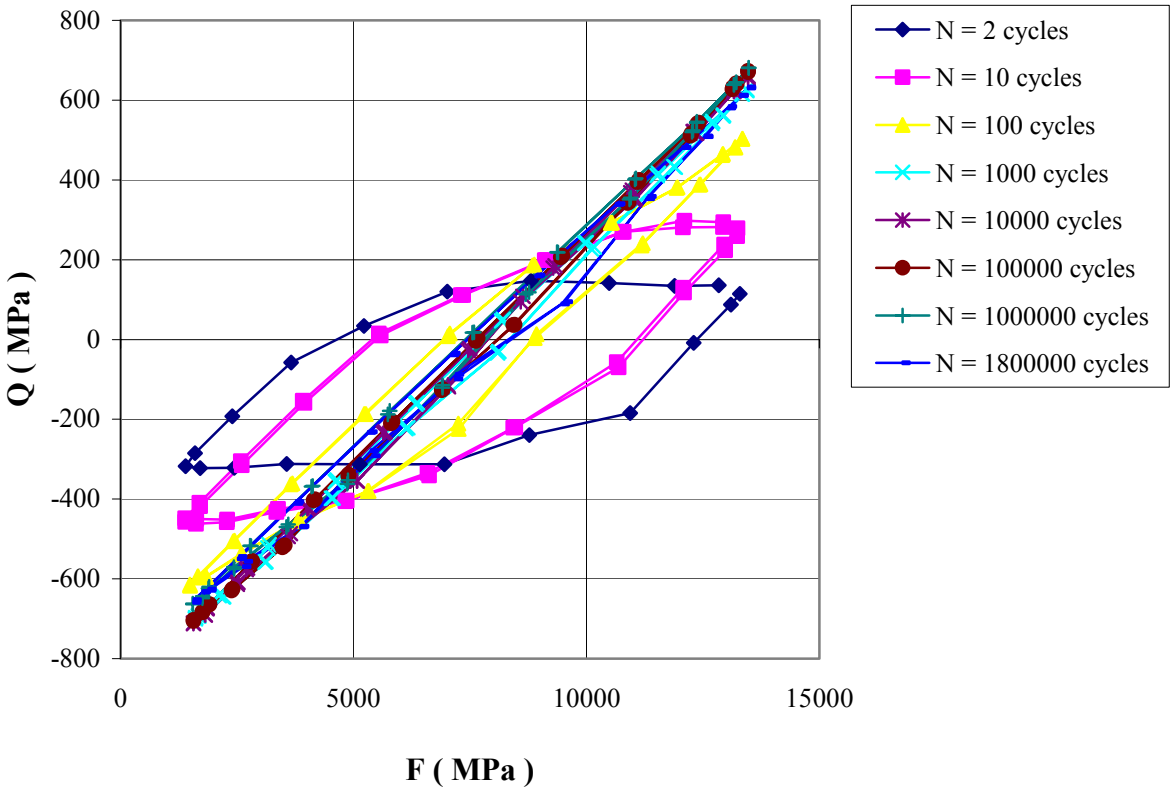

Figure 3.8. Q vs F at different cycles (Test # 2)

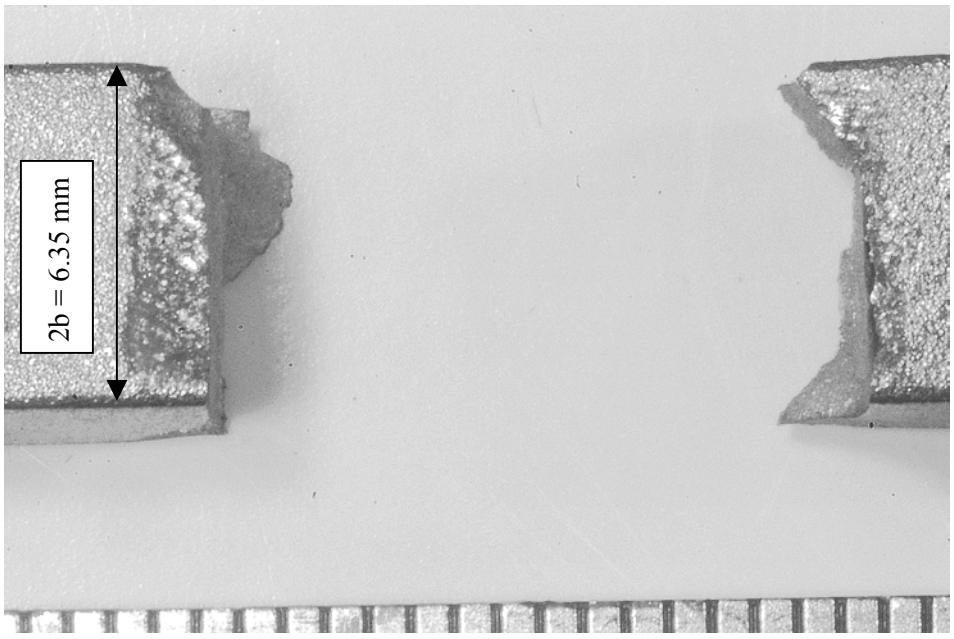

Figure 3.9. Fretting Scar on the Specimen (Test # 5)

Note : Trailing edge of contact is right hand side of the picture.

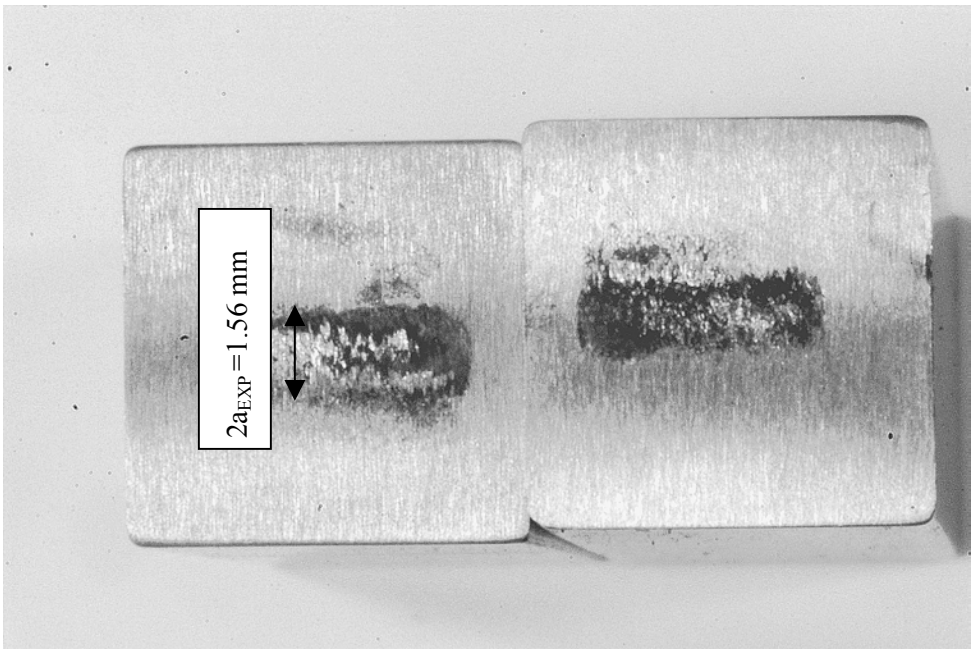

Figure 3.10. Fretting Scar on the Pads (Test # 5)

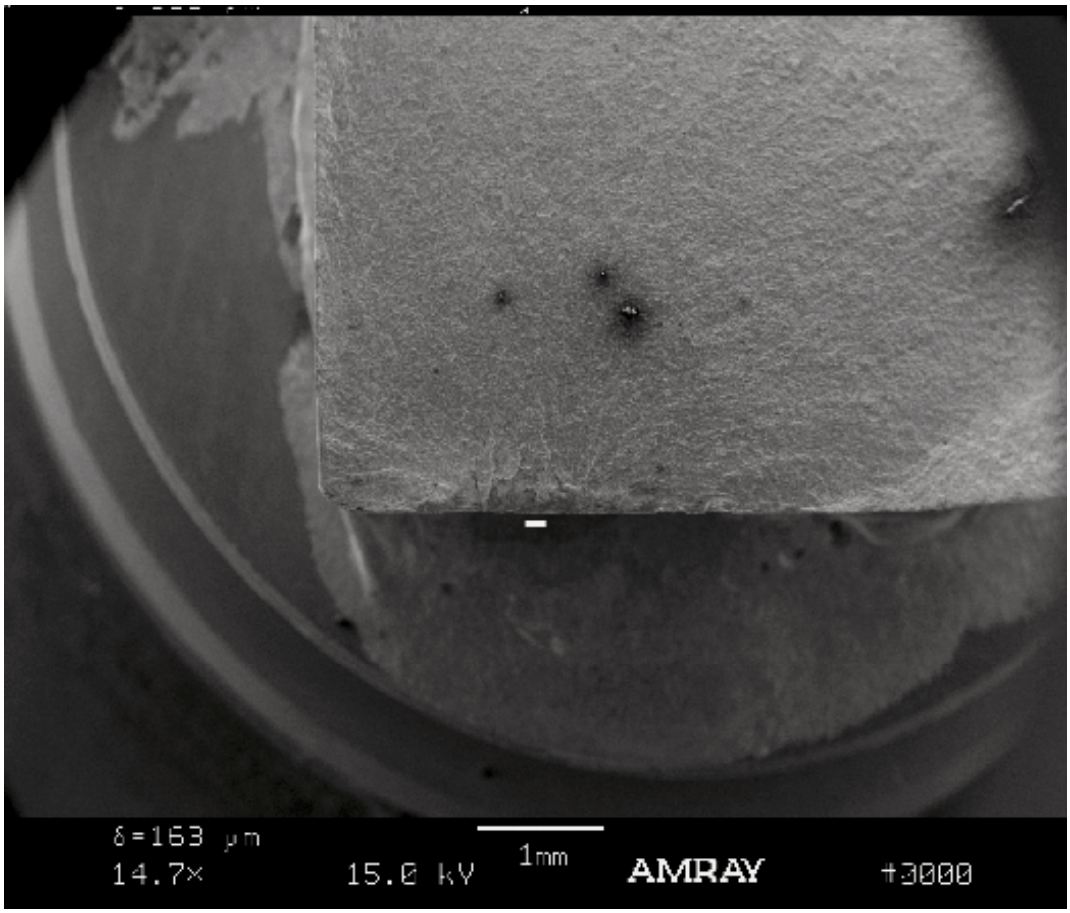

Figure 3.11. Crack Initiation Location (Test # 5)

Crack Initiation Location : Contact Surface

Clue : River Patterns

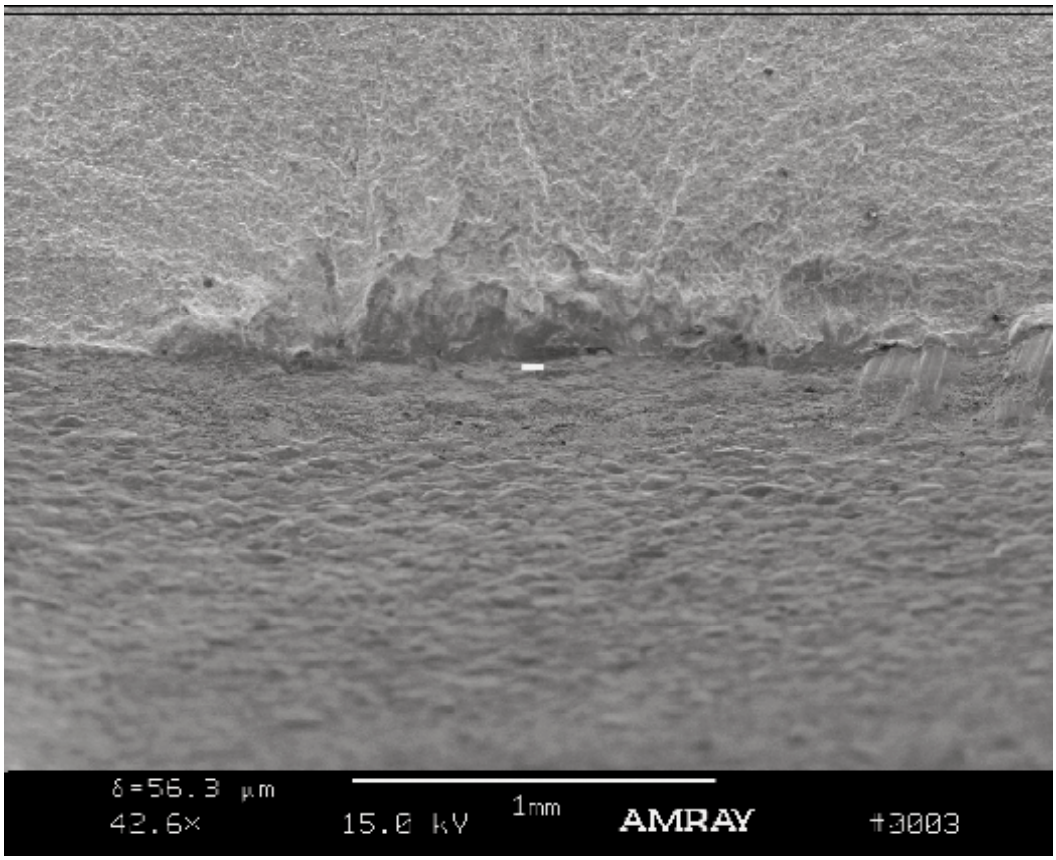

Figure 3.12. Crack Initiation Location (Tilted View of the Specimen) (Test # 5)

Crack Initiation Location : Contact Surface

Clue : River Patterns and Discoloration

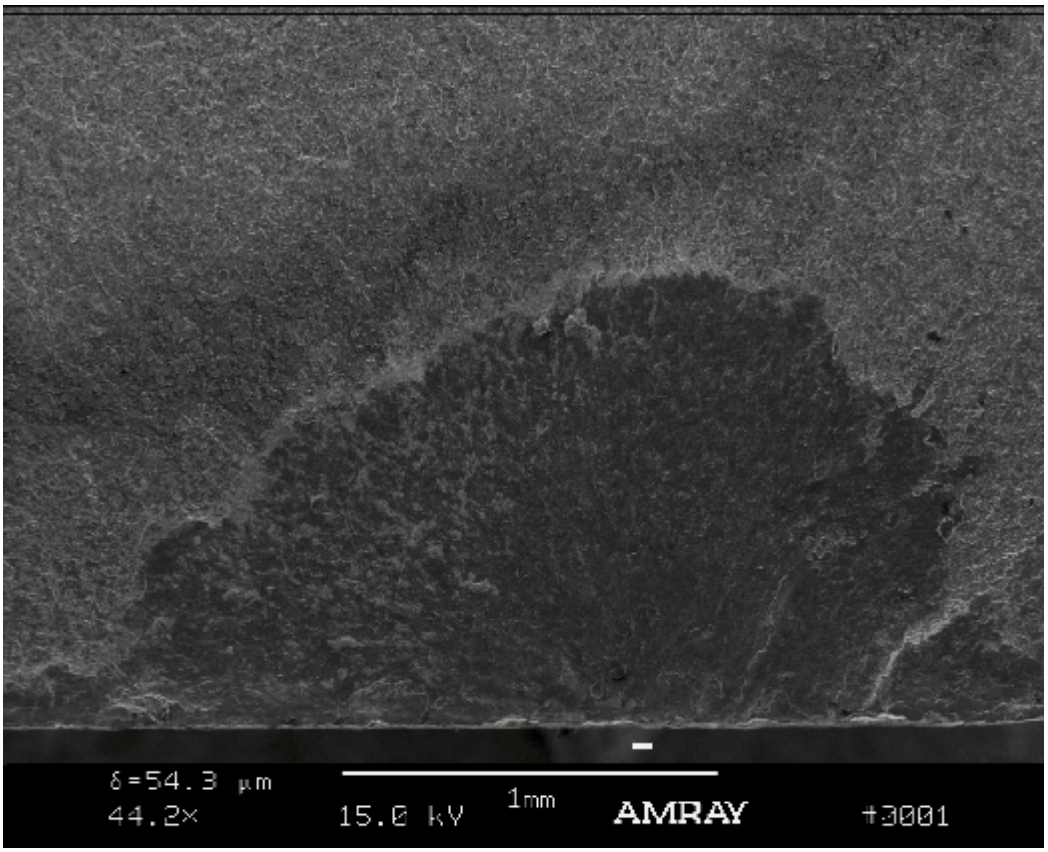

Figure 3.13. Crack Initiation Location (Test # 1)

Crack Initiation Location : Contact Surface

Clue : Discoloration

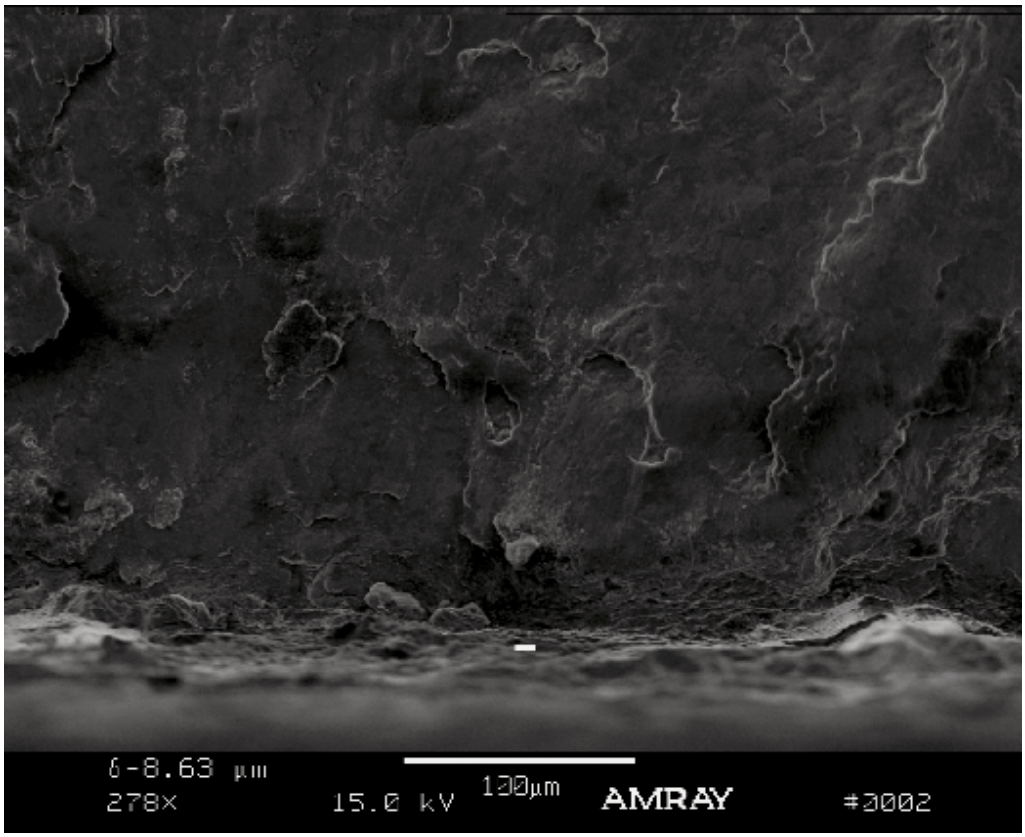

Figure 3.14. Crack Initiation Location (Under Higher Magnification) (Test # 1)

Crack Initiation Location : Contact Surface

Clue : Discoloration

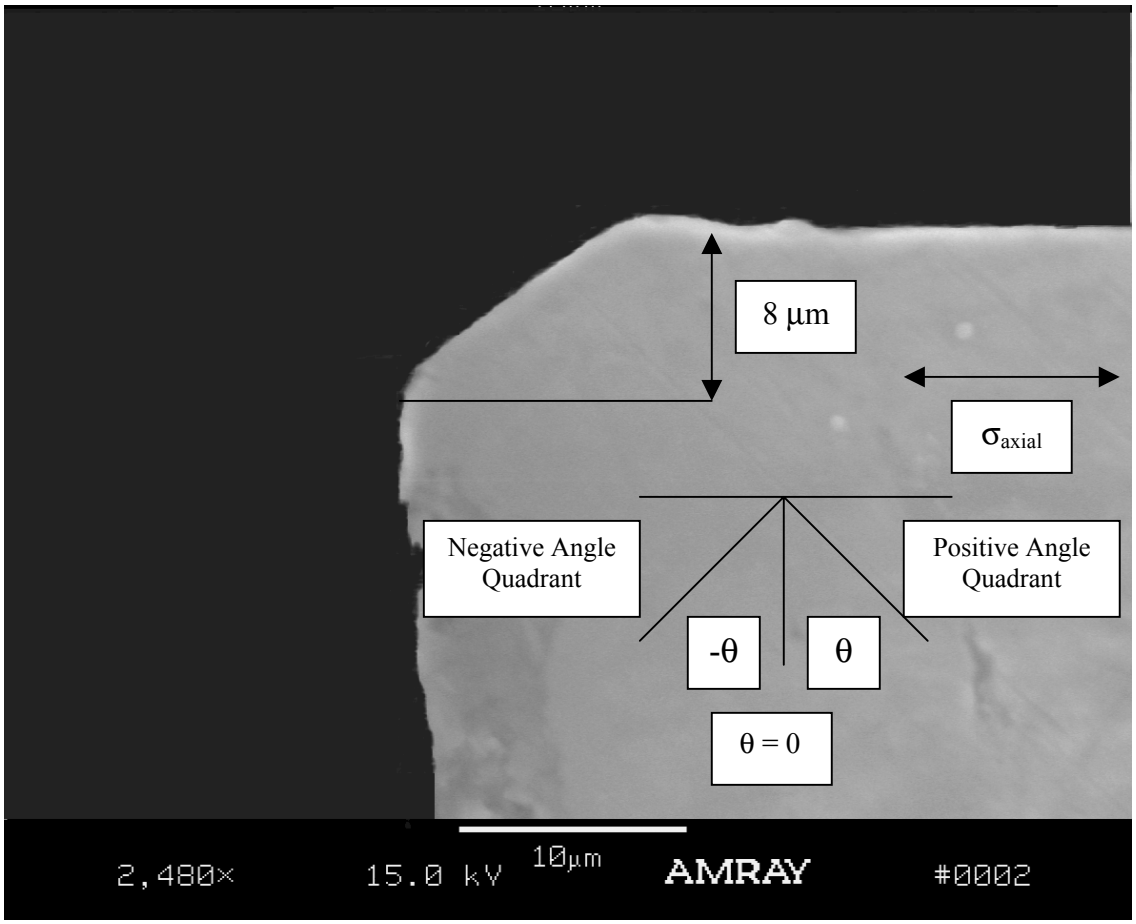

Figure 3.15. Initial Crack Angle (Test # 1)

θ = -53.7 degrees

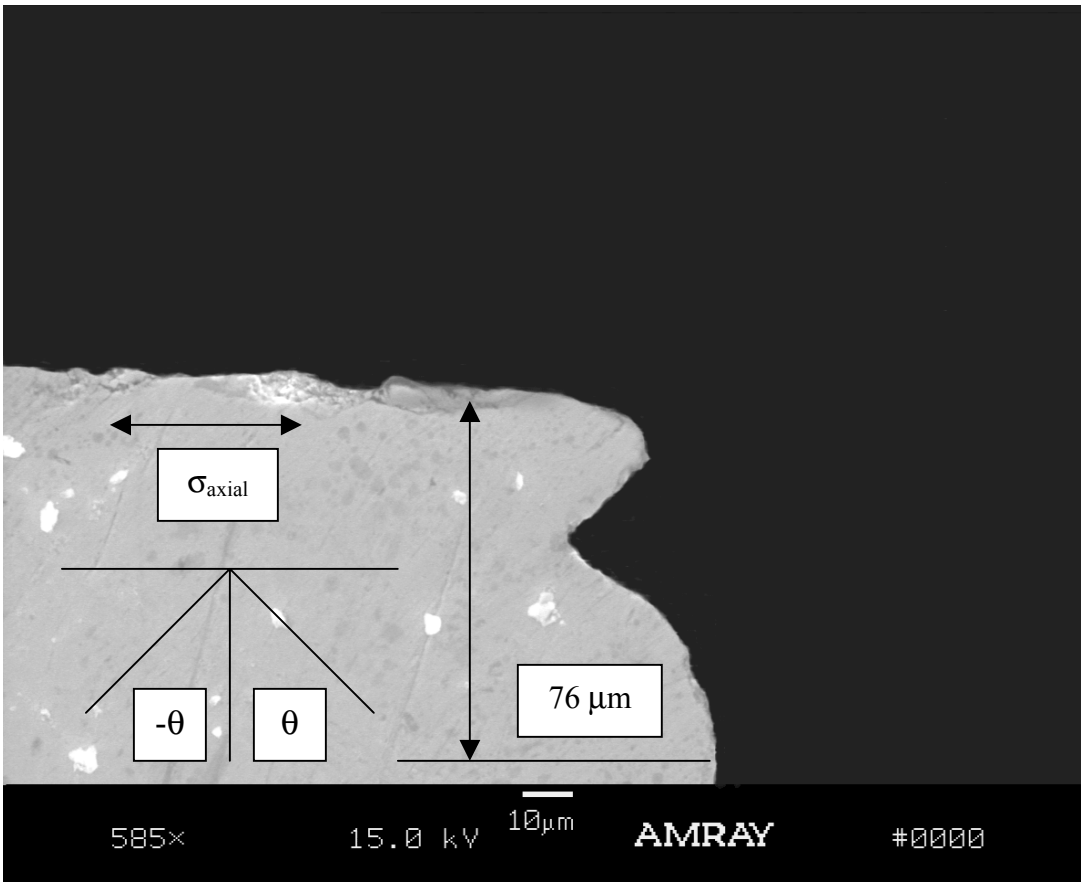

Figure 3.16. Initial Crack Angle (Test # 4)

θ_1 = -37 degrees θ_2 = 53.6 degrees

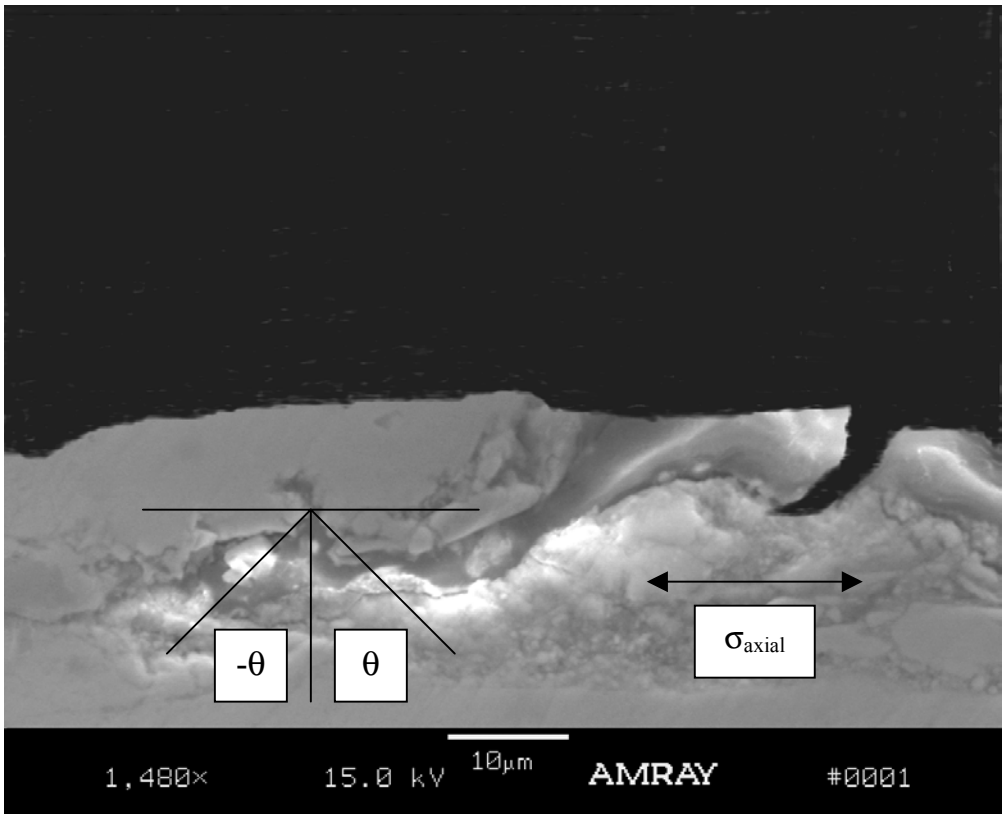

Figure 3.17. Secondary Crack (Test # 5)

$\theta = -28$ degrees

Table 3.1. Test Data For 6.35 mm thick Shot-peened Specimens (This study)

Test #	**σ_{max}**	**σ_{min}**	**R**	**σ_{eff}**	**Q_{max}**	**Q_{min}**	**f**	**N_f**
	(MPa)	(MPa)		(MPa)	(N)	(N)		Cycles
1	500	50	0.1	476.85	1130.64	-969.73	1	30839
2	333.33	33.33	0.1	317.89	687.24	-714.95	1	1189508
3	444.44	44.44	0.1	423.86	631.99	-483.64	1	2415267
4	500	50	0.1	476.85	1482.76	-741	1.2	155545
5	555.55	55.55	0.1	529.83	1643.35	-793.07	1.3	124222
6	422.22	42.22	0.1	402.67	916.52	-577.16	1	3562668
7	666.66	66.66	0.1	635.79	1013.29	-583.06	1	62501

Note : Coefficient of friction, **f** values are the assumed values in FEA.

Table 3.2. C_1, C_2, C_3, C_4 Constants for Equations (42) and (43) for 6.35 mm thickness

Case	**C_1**	**C_2**	**C_3**	**C_4**	**Figure**
$\Delta\sigma$ vs N	640880	-0.70744	289.68	0.011239	Figure 3.5
σ_{eff} vs N	3034300	-0.85304	331.93	0.008337	Figure 3.6

Table 3.3. Test Data For 3.81 mm thickness (Namjoshi's Tests) [6]

Test #	σ_{max}	σ_{min}	**R**	σ_{eff}	Q_{max}	Q_{min}	**f**	N_f
	(MPa)	(MPa)		(MPa)	(N)	(N)		Cycles
16	547.2	272.49	0.4976	401.68	157.8	-224	0.33	4438031
17	621.47	23.71	0.03815	610.68	201	-591.2	0.33	37401
18	631.95	19.86	0.03142	622.94	213	-426.3	0.4	37401
19	649.97	323.97	0.49844	476.47	240	-536	0.5	204504
20	652.73	312.57	0.47887	486.81	223	-79.8	0.33	95149
21	737.86	257.41	0.36887	599.83	250	-93	0.33	59373
22	910.14	119.51	0.13131	854.27	221	-620	0.5	22561

Note : Coefficient of friction, **f** values are the assumed values in FEA.

4. Validation of Finite Element Analysis

4.1. Requirement for Finite Element Analysis

As mentioned in Chapter 2, Finite Element Analysis is required for the configuration of cylindrical pad on a flat specimen in this study, because the configuration has finite boundaries, and the half space assumption is violated, b/a < 10. The thickness of the shot-peened specimens is 6.35 mm, and half of the thickness is 3.175 mm. Analytical solution gives the value of contact half width as 0.44 mm. Contact half width, a, can be found using equations (18), (24), and (25) of Chapter 2. Then b/a ratio is found to be 7.2159, which is smaller than 10. This ratio can be found as (3.175 / 0.44) = 7.2159. So, half space assumption is violated, b/a < 10, and Finite Element Analysis (FEA) is required to get accurate data confirming the experimental results.

4.2. Finite Element Model of Fretting Fatigue Configuration

Finite Element Analysis in this thesis was conducted using commercially available code ABAQUS [7]. Finite Element Model of the fretting fatigue specimen and cylindrical pads was created using 4-noded, plane strain elements along with master-slave contact algorithm on the contact surface between the fretting pad and the specimen. The 4-noded elements (bilinear) were chosen instead of 8-noded elements (serendipity), because the mid side node in the 8-noded element introduces an oscillation in the stress state along the contact interface as also mentioned by Lykins [8]. The first step in defining contact between the pad and the specimen was to create contact surfaces. This

was accomplished using contact elements which established a relationship between the slave nodes (nodes on the specimen) and the master surface (surface of the pad). This determined which segments on the master surface interact with which slave nodes and established the contact algorithm for the transfer of the loads between the two contacting bodies. The master-slave contact algorithm uses the same type of formulation as the gap element technique.

FEA Model of the pad having end radius, r = 50.8 mm, and specimen having the thickness, 2b = 6.35 mm is shown in Figure 4.1. In this model, there are three bodies. The first body is the fretting specimen, the second body is the fretting pad, and the third body is the lateral spring pad (rigid body constraint). The fretting pad and the fretting specimen have the same material properties. The Elasticity Modulus is 126 GPa, and Poisson's ratio is 0.32. The lateral spring pad (rigid body constraint) has different material properties. The Elasticity Modulus is 34.475 KPa, and Poisson's ratio is 0.3.

In the FEA mesh generated, half length of the specimen is 19.05 mm, half thickness of the specimen is 3.175 mm, width of the specimen is 6.35 mm, width of the pad is 9.525 mm, cylindrical end radius of the pad is 50.8 mm, and contact width between the pad and the specimen is 6.35 mm. On the contact surface, the element length of the contacting elements is 6.2011 μm, and the element height of the contacting elements is 7.9375 μm. (These values were close to the converged values Lykins [8] used in his studies. After mesh refinement studies, he found element length as 6.2 μm and element height as 6.2 μm). These dimensions are gradually increasing in the regions away from the contact zone.

The load and boundary conditions on the fretting fatigue configuration are shown in

Figure 4.2. The fretting pad was constrained in X-direction by a rigid body constraint. Also a multi-point constraint (MPC) was applied at the top of the pad to prevent it from rotating due to the application of loads. These top nodes of the pad were forced to move in unison in Y-direction. The specimen was constraint in X and Y directions by providing constraints on the left and at the bottom of the specimen respectively. Also there were multi-point constraints (MPC) between the border elements where element sizes changed. This was used to prevent free nodes of the smaller elements penetrate the bigger elements.

The loads were applied in three steps. The normal load P, was applied first on top of the pad as a distributed load. P load was constant in all tests (1335 N), and the applied P value as a distributed load was 22.064 MPa. The contact half length was calculated as 0.44028 mm after this first step, and the Hertzian Peak Pressure was 303.44 MPa. The analytical solution results for contact half length and Hertzian Peak Pressure were calculated as 0.44 mm, and 304 MPa respectively using the technique described in Chapter 2 (Use equations (18), (24), (25) for contact half length, and (23) for Hertzian Peak Pressure). In the second step, the maximum tangential load Q_{max}, and the maximum axial stress $\sigma_{axial,max}$ were applied to match the experimental maximum cyclic loading condition. In the third step, the minimum tangential load Q_{min}, and the minimum axial stress $\sigma_{axial,min}$ were applied to match the experimental minimum cyclic loading condition. Tangential load Q was applied on the left hand side of the fretting pad, and axial stress, σ_{axial}, was applied on the right hand side of the fretting specimen as it can be seen in Figure 4.1 and Figure 4.2. It should be repeated that Q_{max} and Q_{min} values used in FEA input files were found after analyzing the test data for each specific test as also mentioned

in Chapter 3. It should also be noted that computations in FEA were conducted over one cycle, just for the maximum and minimum loading conditions.

Coefficient of friction was different for each test. In each FEA input file, coefficient of friction, f, was calculated using the criterion $Q \leq f P$, where P is the applied normal load (1335 N), and Q is the tangential load found after analyzing the test data for each test. The data for Q_{max}, Q_{min} and f values used in this study for 6.35 mm thickness is given in Table 3.1. The data for coefficient of friction given in Table 3.1 were assumed appropriate and used for each test of 6.35 mm thickness. The same assumptions were made for 3.81 mm thickness by Namjoshi [6]. The data of the assumed coefficient of friction for 3.81 mm thickness is also given in Table 3.3.

4.3. Comparisons for Validation

Figure 4.3 shows the variation of σ_{xx} in X-direction along the contact surface. It shows the FEA result and Chan Lee solution [35] together. For Test # 1, FEA solution gives $\sigma_{xx,max}$ = 993.2937 MPa as a peak value at x/a = 0.9295, and Chan Lee solution gives $\sigma_{xx,max}$ = 1000 MPa at x/a = 0.96 as the peak value. The difference between FEA and Chan Lee solutions is less than 1 % when the peak stress values are compared, and less than 4 % when the locations of the peak stresses are compared. Alternative analytical technique, Ruiz program (Chan Lee solution) gives the half contact length as 0.4398 mm, and peak pressure as 304.2 MPa.

As a summary, the contact half length and the peak pressure values for the solutions of Nowell and Hills [33] (analytical-contact mechanics), FEA, and RUIZ (Chan Lee

solution [35]) will be as below:

$a_{analytical}$ = 0.44 mm, a_{FEA} = 0.44028 mm, a_{RUIZ} = 0.4398 mm, and

$p_{0,analytical}$ = 304 MPa, $p_{0,FEA}$ = 303.44 MPa, $p_{0,RUIZ}$ = 304.2 MPa.

Based on these results, FEA models used in this thesis are considered accurate, and the results of FEA are used while evaluating the fatigue parameters in Chapter 5.

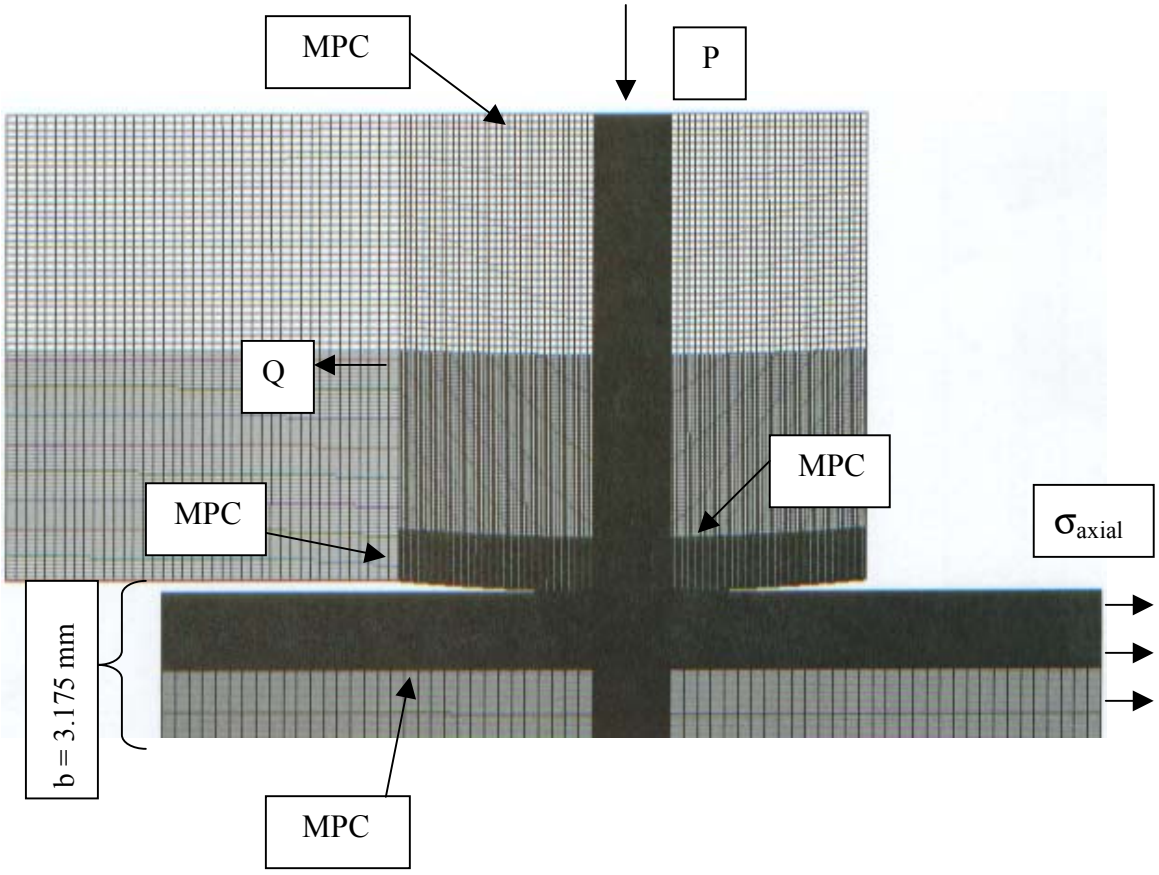

Figure 4.1. FEA Model of 6.35 mm thickness (specimen),
and 50.8 mm end radius (pad)

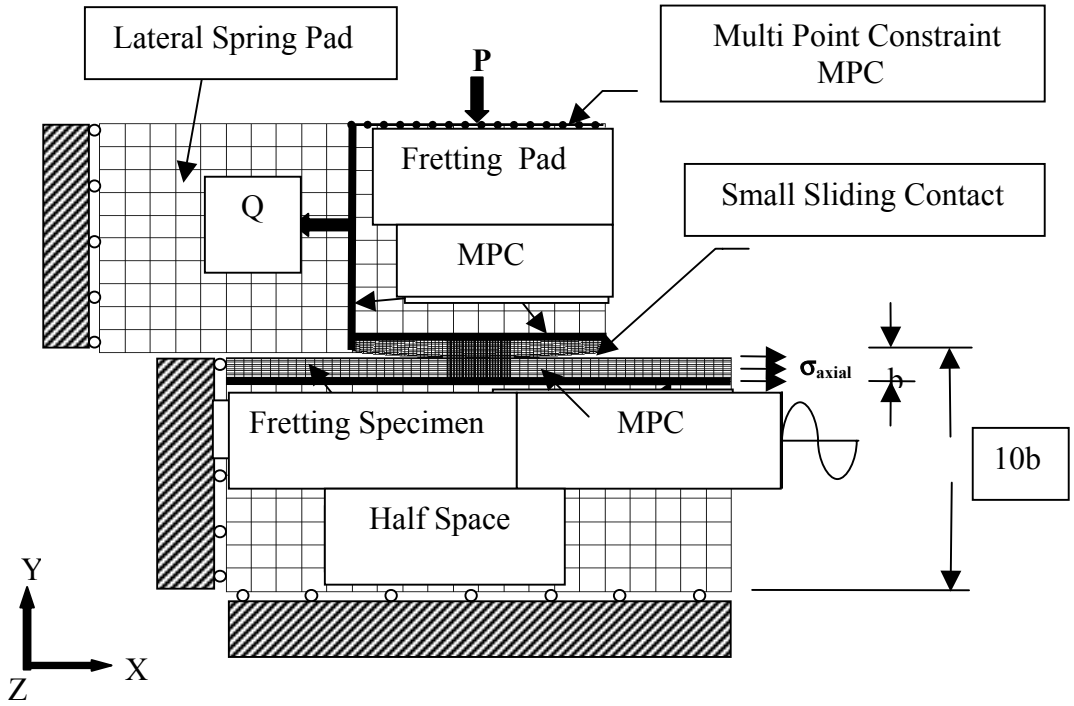

Figure 4.2. Load And Boundary Conditions on a Fretting Fatigue Configuration

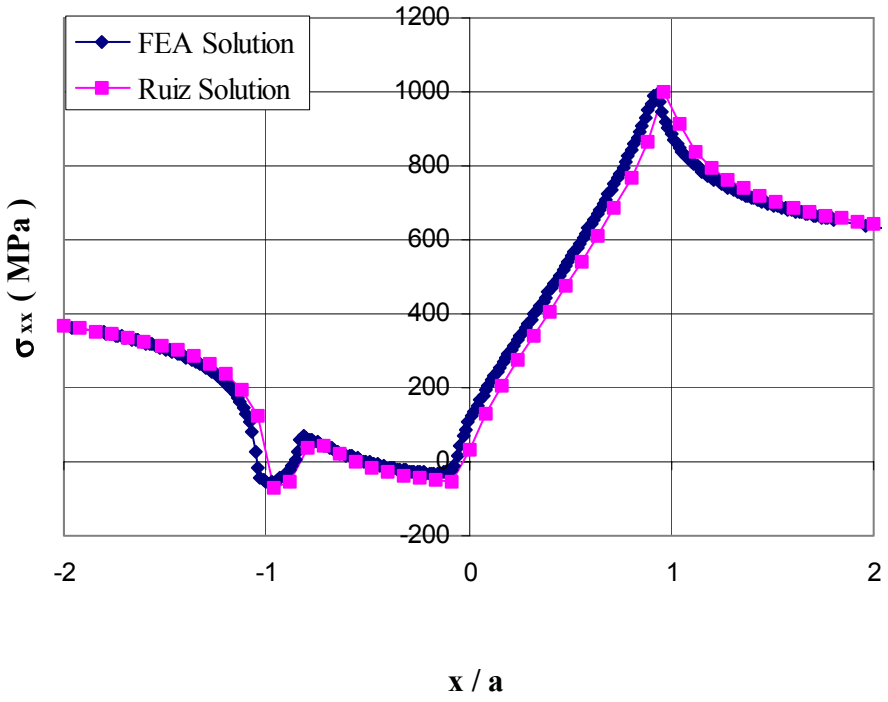

Figure 4.3. σ_{xx} Along X-axis on the Contact Surface (Test # 1)

5. Fatigue Parameter Evaluations and Results

5.1. General

In this chapter, some of the fatigue parameters mentioned in Chapter 2 will be evaluated to investigate the crack initiation behavior of shot-peened fretting fatigue specimens. These parameters will be Smith-Watson-Topper parameter, Findley parameter, Shear Stress Range parameter (SSR), and Modified Shear Stress Range Parameter (MSSR). As also mentioned in Chapter 3, evaluation of these fatigue parameters are important, because by means of these fatigue parameters, the stress concentration on the trailing edge of contact, and multiaxial loading effects are taken into consideration, as it should be the case in fretting fatigue.

For all of the fatigue parameters that are evaluated in this chapter, Finite Element Analysis (FEA) was conducted for each specific test, and then axial, transverse and shear stresses of the FEA output data were used in parameter programs written in Fortran.

In the first part, all these fatigue parameters were evaluated for three different cases, for both 3.81 mm and 6.35 mm thickness values. In the first case, stresses in the residual stress profiles were not added to FEA stress results, just like the case for as received fretting specimens (100 % Stress Relaxation Case). In the second case, stresses in the residual stress profiles were added to FEA stress values, and fatigue parameters were evaluated using the resultant stresses obtained after incorporating the residual stresses (0 % Stress Relaxation Case). It should be noted that residual stresses were assumed biaxial and equal to each other as axial and transverse stresses in this study ($\sigma_{xx} = \sigma_{yy}$).

In the third case, parameters were evaluated for 60 % stress relaxation (60 % was chosen, because after failure, X-ray diffraction, which was performed within base facilities, showed around 60 % stress relaxation on the contact surface for Test # 1).

After the tests, some of the failed specimens were sent to X-ray diffraction to get the new profile of the residual stresses after failure. The aim was to find out how much stress relaxation occurred on the specimens. Figure 5.1 shows the profile of residual stresses obtained in the base facilities for Test # 1. This profile was obtained just on the contact surface of the specimen after failure. The X-ray diffraction technique within base facilities was not capable of finding the profile of the residual stresses within depth of the material. So, the same percentage of stress relaxation (60 % for this specific case) was assumed to have occurred within depth of the specimen at each specific depth layer. Based on this assumption, fatigue parameter evaluations are repeated for different percentages of stress relaxation.

Smith-Watson-Topper, Findley and Shear Stress Range parameters were evaluated for three cases mentioned above (100 %, 0 %, 60 % Stress Relaxation Cases) (Figure 5.2.a through Figure 5.5.c). Modified Shear Stress Range parameter (MSSR) was also evaluated for these three cases like the other parameters in the first part. Later, MSSR parameter was evaluated for three more cases to do more analyses about stress relaxation. Besides 100 %, 0 % and 60 % stress relaxation cases, MSSR parameter was also evaluated for 20 %, 40 % and 80 % stress relaxation cases (Figure 5.6.a through Figure 5.6.f). The reasons for more analyses of MSSR parameter with different percentages of stress relaxation will be discussed at the end of this chapter.

All fatigue parameters were evaluated at all planes ranging from $-90° \leq \theta \leq 90°$ in

increments of 0.1°, which provided the parameters' maximum value, location and critical plane orientation (critical plane is the plane where parameters have maximum values). For all the parameter evaluations, normal and shear stresses were computed as follows

$$\sigma = (\sigma_{xx}+\sigma_{yy}) / 2 + ((\sigma_{xx} - \sigma_{yy}) / 2) * cos (2\theta) + \tau_{xy} * cos (2\theta) \quad (45)$$

$$\tau = -((\sigma_{xx} - \sigma_{yy}) / 2) * sin (2\theta) + \tau_{xy} * cos (2\theta) \quad (46)$$

where θ was changing between –90 degrees and 90 degrees with 0.1 increments. Along longitudinal direction, evaluations were performed in the interval where $-7 < x/a < 7$ on the FEA mesh. The measured fretting fatigue life data were then plotted as a function of these fatigue parameters with their maximum values. While evaluating all the fatigue parameters, the location where the maximum value of the parameter was computed, was accepted as the crack initiation location and the plane where the maximum value of the parameter was computed, was accepted as the initial crack orientation.

In this chapter, fatigue parameter evaluation results will be compared with the experimental results found in Chapter 3, and then these results will be discussed in Chapter 6. The appropriate fatigue parameter for shot-peened specimens will be determined through the comparison of experimental results found in the laboratory, and the parameter results found after evaluations.

In the Figures 5.2.a through 5.10, R = 2 inch show the as received fretting fatigue data obtained with pads having 50.8 mm end radius, R = 4 inch show the as received fretting fatigue data obtained with pads having 101.6 mm end radius, R = 12 inch show the as received fretting fatigue data obtained with pads having 304.8 mm end radius. Flat Pad 1

and Flat Pad 2 show the as received fretting fatigue data obtained with flat pads having edge radii of 50.8 mm and 101.6 mm respectively.

5.2. Smith-Watson-Topper Parameter (SWT)

SWT parameter was evaluated for two different versions. The first version was the product of the maximum principal stress and the principal strain amplitude, ($\sigma_{max}*\varepsilon_a$), and the second version was the maximum of the product of principal stress and principal strain amplitude [max($\sigma*\varepsilon_a$)]. Figure 5.2.a, Figure 5.2.b, and Figure 5.2.c show the results found for the first version, and Figure 5.3.a, Figure 5.3.b, and Figure 5.3.c show the results found for the second version of SWT parameter obtained for three cases, for both 3.81 mm, and 6.35 mm thickness values.

As also mentioned in Chapter 3, a good fatigue parameter should be able to predict the cycles to crack initiation, crack initiation location, and initial crack orientation. The results of both versions of SWT parameter according to these criteria, for both thickness values are as follows:

5.2.1. For 6.35 mm thickness.

5.2.1.1. CASE 1: 100 % Stress Relaxation. Maximum value of both versions of the SWT parameter showed the crack initiation location at the contact surface near the trailing edge (around x/a = 0.93). Both versions of SWT parameter could not predict the cycles to crack initiation well for this thickness (Figure 5.2.a for the first version, and Figure 5.3.a for the second version). Initial crack angle was around -2 degrees, which was not in good agreement with the experimental counterparts, and was slightly different

for both versions of SWT parameter.

5.2.1.2. CASE 2: 0 % Stress Relaxation. The first version of SWT parameter showed the crack initiation location at the contact surface near the trailing edge (around x/a = 0.93), which matched the experimental results, but the second version showed at the depth of 24 μm inside the specimen at around x/a = (0.732 ~ 0.817). The first version of SWT parameter predicted the cycles to crack initiation better than the second version, because the values of the first version were closer to plain fatigue data (Figure 5.2.b for the first version, and Figure 5.3.b for the second version). Initial crack angle was around -2 degrees for the first version, and around 81 degrees for the second version, which were not in agreement with experimental results.

5.2.1.3. CASE 3: 60 % Stress Relaxation. Maximum value of both versions of the SWT parameter showed the crack initiation location at the contact surface near the trailing edge (around x/a = 0.93), which again matched the experimental results. Both versions of SWT parameter could not predict the cycles to crack initiation well (Figure 5.2.c for the first version, and Figure 5.3.c for the second version). Initial crack angle was around -2 degrees, which was not in good agreement with the experimental counterparts, and it was slightly different for both versions.

5.2.2. For 3.81 mm thickness.

5.2.2.1. CASE 1: 100 % Stress Relaxation. Maximum value of both versions of the SWT parameter showed the crack initiation location at the contact surface near the trailing edge (around x/a = 0.95). Both versions of SWT parameter predicted the cycles to crack initiation well, because the parameter values were following a path close to the curve of the plain fatigue fit (Figure 5.2.a for the first version, and Figure 5.3.a for the

second version). Initial crack angle was around –0.5 degrees, which was not in good agreement with the experimental results, and it was slightly different for both versions.

5.2.2.2. CASE 2: 0 % Stress Relaxation. The first version of SWT parameter showed the crack initiation location at the depth of 260 μm (around x/a =0.97), which matched the experimental results, but the second version showed contact surface (around x/a = (0.423 ~ 0.832)), which was not the case for 3.81 mm thickness. The second version of SWT parameter predicted the cycles to crack initiation better than the first version, because the values of the second version were following nearly the same curve of the plain fatigue fit (Figure 5.2.b for the first version, and Figure 5.3.b for the second version). Initial crack angle was around 0 (zero) degree for the first version, and around 85 degrees for the second version, which were not in good agreement with the experimental results.

5.2.2.3. CASE 3: 60 % Stress Relaxation. Most of the results for the first version of SWT parameter showed the crack initiation location at the depth of 260 μm (around x/a = 0.97), which again matched the experimental results, but most of the results for the second version showed the contact surface (around x/a = (0.423 ~ 1.8)), which was not correct for 3.81 mm thickness. Both versions of SWT parameter predicted the cycles to crack initiation well, but not as well as the second case (Figure 5.2.c for the first version, and Figure 5.3.c for the second version). Initial crack angle was around 0 (zero) degree for the first version, and around -1 degrees for the second version, which were not in good agreement with the experimental results.

In summary, it can be said that SWT parameter could not meet all the required conditions for both thickness values at the same time. Both versions of SWT parameter

were effective in predicting the number of cycles to crack initiation for 3.81 mm thickness, but they were not effective for 6.35 mm thickness (Figure 5.2.a through Figure 5.3.c). Especially, the first version of SWT parameter was more effective than the second version in predicting the crack initiation location (at the contact surface for 6.35 mm, and at the depth of 260 μm for 3.81 mm thickness), and (near the trailing edge of contact where x/a = 1). Neither versions of SWT parameter was effective in predicting the initial crack angle, neither for 6.35 mm, nor 3.81 mm thickness values.

5.3. Findley Parameter

Multiaxial loading effects should be taken into consideration in fretting fatigue as also mentioned in Chapter 2. Findley parameter explicitly includes the effects of the normal stresses besides the shear stresses. In this approach, crack initiation is assumed to be governed by both the maximum shear stress amplitude, $\tau_a = (\tau_{max} - \tau_{min}) / 2$, and maximum stress normal to the orientation of the maximum shear multiplied by an influence factor, k (k is an empirical constant which is 0.35 here), shown as follows

$$FP = \tau_a + k\, \sigma_{max} \tag{47}$$

Figure 5.4.a, Figure 5.4.b, and Figure 5.4.c show the measured fretting fatigue life data as a function of Findley parameter obtained for three cases, for both thicknesses. The results of Findley parameter found for the three cases, for both thickness values are as follows:

5.3.1. For 6.35 mm thickness.

For all of the cases below, maximum value of Findley parameter showed the crack initiation location at the contact surface and near the trailing edge (around x/a = 0.92), which matched the experimental results. Initial crack angle was around 24 degrees, which was not in good agreement with the experimental counterparts.

5.3.1.1. CASE 1: 100 % Stress Relaxation. Findley parameter could not predict the cycles to crack initiation well for this thickness, because the parameter values were too high when compared to plain fatigue and as received fretting fatigue data (Figure 5.4.a).

5.3.1.2. CASE 2: 0 % Stress Relaxation. Findley parameter predicted the cycles to crack initiation better than the first case, because the parameter values were closer to plain fatigue data (Figure 5.4.b).

5.3.1.3. CASE 3: 60 % Stress Relaxation. Findley parameter could not predict the cycles to crack initiation well, because the parameter values were higher than the plain fatigue and as received fretting fatigue data like the first case (Figure 5.4.c).

5.3.2. For 3.81 mm thickness.

For all of the cases below, maximum value of Findley parameter showed the crack initiation location near the trailing edge (around x/a = 0.96), which matched the experimental results.

5.3.2.1. CASE 1: 100 % Stress Relaxation. Maximum value of Findley parameter showed the crack initiation location at the contact surface which did not match the experimental results. It predicted the cycles to crack initiation very well, because the parameter values were following a very similar curve to the plain fatigue fit data (Figure

5.4.a). Initial crack angle was around 26 degrees, which was not in good agreement with the experimental counterparts.

5.3.2.2. CASE 2: 0 % Stress Relaxation. Maximum value of Findley parameter showed the crack initiation location at the depth of 260 μm inside the specimen, which was in agreement with the experimental results. It predicted the cycles to crack initiation very well, because the parameter values were following nearly the same curve of the plain fatigue fit data (Figure 5.4.b). Initial crack angle was around 23 degrees, which was not in good agreement with the experimental results.

5.3.2.3. CASE 3: 60 % Stress Relaxation. Maximum value of Findley parameter showed the crack initiation location at the depth of 260 μm inside the specimen, which again matched the experimental results. It predicted the cycles to crack initiation well, but not as well as the first two cases (Figure 5.4.c). Initial crack angle was around 23 degrees, which was not in good agreement with the experimental counterparts.

In summary, it can be said that Findley parameter could not meet all the required conditions for both thickness values at the same time. It was effective in predicting the number of cycles to crack initiation, especially for 3.81 mm thickness. It should be noted that it was not very effective for 6.35 mm thickness, except for 0 % Stress Relaxation case (Figure 5.4.a through Figure 5.4.c). It was also effective in predicting the crack initiation location (at the contact surface for 6.35 mm, and at the depth of 260 μm for 3.81 mm thickness), and (near trailing edge of contact where x/a = 1). It was not effective in predicting the initial crack angle, neither for 6.35 mm, nor 3.81 mm thickness.

5.4. Shear Stress Range Parameter

In this section, while evaluating the Shear Stress Range (SSR) parameter, the maximum and minimum shear stresses were computed on all planes ranging from $-90° \leq \theta \leq 90°$ in increments of 0.1°, using the results of FEA. Then, maximum shear stress range was obtained ($\Delta\tau_{crit} = \tau_{max} - \tau_{min}$). Using the Walker method [21], effective shear stress range was obtained in the next step. The Shear Stress Range parameter is then defined as follows

$$SSR = \Delta\tau_{crit,effective} = \tau_{max}(1-R_\tau)^m \tag{48}$$

where R_τ is the shear stress ratio on the critical plane, and m is a fitting parameter, which was determined to be 0.45 by Lykins [8], as also mentioned in the previous chapters. Figure 5.5.a, Figure 5.5.b, and Figure 5.5.c show the measured fretting fatigue life data as a function of Shear Stress Range parameter ($SSR = \Delta\tau_{crit,effective}$), obtained for three cases, for both 3.81 mm, and 6.35 mm thickness values.

SSR parameter showed the same results for all the three cases (100 %, 0 % and 60 % Stress Relaxation Cases), and for each thickness separately. The maximum shear stresses remained the same whereas the normal stresses changed. This can be explained by using Mohr's circle. The difference between the first, second, and the third cases is basically the amount of the residual stresses added to the system. As the residual stresses are assumed biaxial ($\sigma_{xx} = \sigma_{yy}$), the result of the maximum shear stress on Mohr's circle remains same in all three cases (Maximum shear stress is the diameter of Mohr's circle). It should be noted that Modified Shear Stress Range parameter (MSSR) includes the

effect of the normal stresses besides the shear stresses unlike SSR parameter, and the difference in the normal stresses will be helpful while evaluating the MSSR parameter. Also, it should be repeated that the normal stresses are found while evaluating SSR parameter as well as shear stresses. The results of SSR parameter found separately for each thickness are as follows

5.4.1. For 6.35 mm thickness.

For all three cases (100 %, 0 %, 60 % Stress Relaxation Cases), maximum value of Shear Stress Range parameter showed the crack initiation location at the contact surface and near the trailing edge (around x/a = 0.91), which matched the experimental results. It could not predict the cycles to crack initiation well, because the parameter values were too high when compared to plain fatigue and as received fretting fatigue data (Figure 5.5.a through Figure 5.5.c). In Figure 5.5.a, Figure 5.5.b, and Figure 5.5.c, it can be seen that the value of SSR parameter is same for all three cases, for 6.35 mm thickness value. Initial crack angle was around 36 degrees, which was in good agreement with the experimental counterparts.

5.4.2. For 3.81 mm thickness.

For all three cases (100 %, 0 %, 60 % Stress Relaxation Cases), maximum value of Shear Stress Range parameter showed the crack initiation location at the contact surface and near the trailing edge (around x/a =0.95), which did not match the experimental results. It predicted the cycles to crack initiation well, because the parameter values were following a very similar path, like the curve of the plain fatigue fit data (Figure 5.5.a through Figure 5.5.c). In Figure 5.5.a, Figure 5.5.b, and Figure 5.5.c, it can also be seen that the value of SSR parameter is same for all three cases, for 3.81 mm thickness

value. Initial crack angle was around 42 degrees, which was also in good agreement with the experimental counterparts.

In summary, it can be said that Shear Stress Range parameter (SSR = $\Delta\tau_{crit,effective}$) could not meet all the required conditions for both 6.35 mm and 3.81 mm thick specimens at the same time. It was very effective in predicting the number of cycles to crack initiation for 3.81 mm thickness, but it was not effective for 6.35 mm thick specimens (Figure 5.5.a through Figure 5.5.c). It predicted the crack initiation location at the contact surface and near the trailing edge (around x/a = 0.91 for 6.35 mm, around x/a = 0.95 mm for 3.81 mm), which was correct for 6.35 mm, but wrong for 3.81 mm thickness. It should be repeated that crack initiation location for 3.81 mm thick specimens was not at the contact surface. In addition, SSR parameter predicted the initial crack angle effectively for both 6.35 mm and 3.81 mm thickness values, unlike Smith-Watson-Topper (SWT), and Findley (FP) parameters.

5.5. Modified Shear Stress Range Parameter

As mentioned in Chapter 2, Mall, Jain, Namjoshi, and Lykins [26] proposed Modified Shear Stress Range (MSSR) parameter to overcome the shortcoming of Findley parameter in predicting the crack initiation cycles, and the initial crack orientation. Shear Stress Range (SSR) parameter was modified in the form of Findley parameter to include the normal stresses that act in crack opening mode besides the shear stresses, as it should be the case in multiaxial fatigue loading. As also shown with equation (15), this modified version of Shear Stress Range critical plane parameter,

MSSR is expressed as follows

$$MSSR = A.\Delta\tau_{crit,eff}^{B} + C.\sigma_{max}^{D} \quad (49)$$

where $\Delta\tau_{crit,eff}$ is the same as in equation (48), and σ_{max} is the maximum normal stress on the critical plane. As noted before, σ_{max} is evaluated with SSR parameter. A, B, C, D constants were obtained by a curve fitting technique as 0.75, 0.5, 0.75, and 0.5 respectively by Mall, Jain, Namjoshi, and Lykins [26].

It should be noted that for MSSR parameter, crack initiation location, and initial crack angle results for surface and for each layer within depth are the same results of SSR parameter. The difference is the value of MSSR parameter, as it's evaluated by using both shear and normal stresses, unlike SSR parameter. Both parameters are evaluated at each Y value. (Y-axis is along the thickness, through the depth of specimen). After MSSR parameter is evaluated, the maximum value of MSSR parameter should be checked to see where it's predicting the crack initiation location (whether on the contact surface or inside the specimen), and how much that maximum value is. The results found for MSSR parameter for three cases (100 %, 0 %, 60 % Stress Relaxation Cases) for both thickness values are as follows:

5.5.1. For 6.35 mm thickness.

For all the three cases (100 %, 0 %, 60 % Stress Relaxation Cases), crack initiation location and initial crack angle results were the same results of SSR parameter. Crack initiation location was near the trailing edge (around x/a = 0.91), and initial crack angle was around 36 degrees, which matched the experimental results.

5.5.1.1. CASE 1: 100 % Stress Relaxation. Maximum value of the MSSR parameter showed the crack initiation location at the contact surface which matched the experimental results. It could not predict the cycles to crack initiation well, because the parameter values were too high when compared to plain fatigue and as received fretting fatigue data (Figure 5.6.a).

5.5.1.2. CASE 2: 0 % Stress Relaxation. Maximum value of the MSSR parameter showed the crack initiation location at the depth of 156-206 μm inside the specimen, which did not match the experimental results. It could not predict the cycles to crack initiation well, because the parameter values were again high when compared to plain fatigue and as received fretting fatigue data (Figure 5.6.f).

5.5.1.3. CASE 3: 60 % Stress Relaxation. Maximum value of the MSSR parameter showed the crack initiation location at the contact surface, which again matched the experimental results. It could not predict the cycles to crack initiation well, because the parameter values were again high when compared to plain fatigue and as received fretting fatigue data (Figure 5.6.c).

5.5.2. For 3.81 mm thickness.

For all the three cases (100 %, 0 %, 60 % Stress Relaxation Cases), crack initiation location and initial crack angle results were the same results of SSR parameter. Crack initiation location was near the trailing edge (around x/a =0.95), and initial crack angle was around 42 degrees, which matched the experimental results.

5.5.2.1. CASE 1: 100 % Stress Relaxation. Most of the data of maximum value of the MSSR parameter showed the crack initiation location at the contact surface which did not match the experimental results. It could not predict the cycles to crack initiation well,

because the parameter values were high when compared to plain fatigue and as received fretting fatigue data, but it should be noted that the results for this thickness, 3.81 mm, were closer to plain fatigue data than the results of the 6.35 mm thickness (Figure 5.6.a).

5.5.2.2. CASE 2: 0 % Stress Relaxation. Maximum value of the MSSR parameter showed the crack initiation location at the depth of 260 μm inside the specimen, which matched the experimental results for this thickness. It could not predict the cycles to crack initiation well, because the parameter values were high when compared to plain fatigue and as received fretting fatigue data (Figure 5.6.f).

5.5.2.3. CASE 3: 60 % Stress Relaxation. Maximum value of the MSSR parameter showed the crack initiation location at the depth of 260 μm inside the specimen, which again matched the experimental results. It could not predict the cycles to crack initiation well, because the parameter values were again high when compared to plain fatigue and as received fretting fatigue data (Figure 5.6.c).

In summary, it can be said that MSSR parameter could not meet all the required conditions for both 6.35 mm and 3.81 mm thickness values at the same time. Except for 100 %, and 0 % stress relaxation cases, it predicted the crack initiation location effectively (at the contact surface for 6.35 mm, and at the depth of 260 μm for 3.81 mm thickness), and near the trailing edge of contact ($x/a = 0.91$ for 6.35 mm, $x/a = 0.95$ for 3.81 mm). In addition, it predicted the initial crack angle effectively for both thicknesses. It was not effective in predicting the number of cycles to crack initiation for both thickness values (Figure 5.6.a, Figure 5.6.f, and Figure 5.6.c).

Up to this point, it is seen that none of the fatigue parameters met all the three requirements at the same time under these evaluation conditions. Smith-Watson-Topper

(SWT), Findley and Shear Stress Range (SSR) parameters could not meet all the required conditions for shot-peened fretting specimens at the same time. For these three parameters, changes in the residual stress profile didn't help collapsing the data of both thickness values on a single curve, and it won't help when the same analyses are performed again for different percentages of stress relaxation, because the results for 6.35 mm thickness will be always higher than the results of 3.81 mm (see Figure 5.2.a through Figure 5.5.c)

It should be noted that for 0 % Stress Relaxation case, results of MSSR parameter for 3.81 mm were higher than the results of 6.35 mm thickness for the first time in the whole process of parameter evaluations (see Figure 5.6.f). This lead us to do more evaluations of MSSR parameter for different percentages of stress relaxation to help collapse the data of both thickness values. The evaluation of MSSR showed that the results would collapse when more evaluations were performed for different percentages of stress relaxation between 0 % and 100 % (see the changes in Figure 5.6.a through Figure 5.6.f).

MSSR parameter is good at predicting the crack initiation location, and the initial crack orientation for both thickness values. For MSSR parameter, the problem is in predicting the cycles to crack initiation, in other words, collapsing the data of both thickness values on a single curve. In Figure 5.1, the profile of the residual stresses for Test # 1, measured after failure of the specimen is shown (for 6.35 mm thickness). This profile is just an example showing stress relaxation (60 % for this specific test), and it is measured just on the contact surface of the specimen. The X-ray diffraction technique was not able to measure the profile also for the depth of the material, as it was performed within the base facilities. So, the same percentage of stress relaxation was assumed to

have occurred within depth of the specimen for each layer. Based on this assumption, for different percentages of stress relaxation, MSSR parameter is evaluated for both 3.81mm, and 6.35 mm thickness values. Figure 5.6.a through Figure 5.6.f show the measured fretting fatigue life data as a function of MSSR parameter, obtained for six cases. These are 100 %, 80 %, 60 %, 40 %, 20 %, and 0 % Stress Relaxation cases. The aim is collapsing the data of both thickness values on a single curve using these figures.

When the parameters that are evaluated for these six cases are analyzed carefully, it will be possible to collapse the data of both thickness values as shown in Figure 5.7 and Figure 5.8. The best fit for these collapsed data can be obtained in Excel as shown in Figure 5.9 and Figure 5.10 after finding C_1, C_2, C_3, C_4 coefficients using a curve fitting technique in Kaleidagraph [39]. The same technique was used while obtaining the fits for Figure 3.5 and Figure 3.6 (see Chapter 3). C_1, C_2, C_3, C_4 coefficients for the best fits are given in Table 5.1and Table 5.2. It should be noted that, for 100 % and 0 % stress relaxation cases, the changes in the value of MSSR parameter were very small for 3.81 mm thickness when compared with the changes of MSSR parameter for 6.35 mm thickness (see Figure 5.6.a and Figure 5.6.f). In other words, MSSR parameter was more sensitive in thicker specimens. So, while assuming stress relaxation to obtain the collapsed data, the author analyzed the results very carefully, especially for 6.35 mm thickness. The most important criterion here is that at the assumed percentages of stress relaxation, the maximum value of MSSR parameter should predict the correct crack initiation location for each thickness (at contact surface for 6.35 mm, and at the depth ranging from 200 to 300 microns for 3.81 mm). The assumed percentages of stress relaxation, and the maximum values of MSSR parameter predicting the correct crack

initiation location at the assumed percentages are shown in Table 5.3 and Table 5.4 for each thickness separately. As also mentioned previously, for 3.81 mm thickness, the changes in the values of MSSR parameter were very small when compared with the changes of 6.35 mm thickness for 100 % and 0 % stress relaxation cases (see Figure 5.6.a and Figure 5.6.f). Also, MSSR parameter was predicting the correct crack initiation location for 5 of the 6 cases for 3.81 mm thickness (Except for 100 % stress relaxation case). The difference in the maximum values of MSSR parameter between 80 % and 0 % stress relaxation cases was at most 3 MPa for each test of 3.81 mm thickness. As it is a small number, while assuming stress relaxation, there won't be a big mistake if any percentage between 80 % and 0 % of stress relaxation is accepted.

In this study, the author tried two different approaches based on two assumptions about stress relaxation while collapsing the data of shot-peened specimens that would be used to estimate cycles to crack initiation. The approaches were consistent, because the same assumptions were made for both thicknesses at the same time.

In the first approach, more stress relaxation was assumed to have occurred in High Cycle Regime based on the assumption that higher cycles were leading to more stress relaxation. A consistent pattern was followed for both thicknesses as follows

20 % Stress Relaxation in Low Cycle Regime (up to 100,000 cycles)

20 % Stress Relaxation between Low Cycle and High Cycle Regimes

(between 100,000 and 1,000,000 cycles)

40 % Stress Relaxation in High Cycle regime (after 1,000,000 cycles)

Based on this assumption, the data would be collapsed as shown in Figure 5.7 and the trend line of the collapsed data was provided as shown in Figure 5.9.

In the second approach, more stress relaxation was assumed to have occurred in both Low Cycle and High Cycle Regimes based on the assumption that higher cycles and higher applied stress levels were leading to more stress relaxation. Similarly, another consistent pattern was followed for both thicknesses as follows

40 % Stress Relaxation in Low Cycle Regime (up to 100,000 cycles)

20 % Stress Relaxation between Low Cycle and High Cycle Regimes

(between 100,000 and 1,000,000 cycles)

40 % Stress Relaxation in High Cycle regime (after 1,000,000 cycles)

Based on this assumption, the data would be collapsed as shown in Figure 5.8 and the trend line of this collapsed data was provided in the same manner as shown in Figure 5.10.

As a result, based on the two assumptions made up to here, the data found in Figures 5.7, 5.8, 5.9 and 5.10 were accepted as accurate, and these data will be used to estimate the crack initiation cycles of shot-peened fretting fatigue specimens (Chapter 6).

Under these conditions, among all the parameters that are evaluated in this thesis, the most appropriate parameter was found to be MSSR parameter, and it was the only fatigue crack initiation parameter that could meet all the requirements at the same time for shot-peened fretting fatigue specimens having two different thickness values.

In the next chapter, all the results found up to here will be summarized and discussed. There will be more explanations for the thickness effects on the fretting behavior of shot-peened specimens. There will also be suggestions for future studies based on the constraints and restrictions experienced in this thesis.

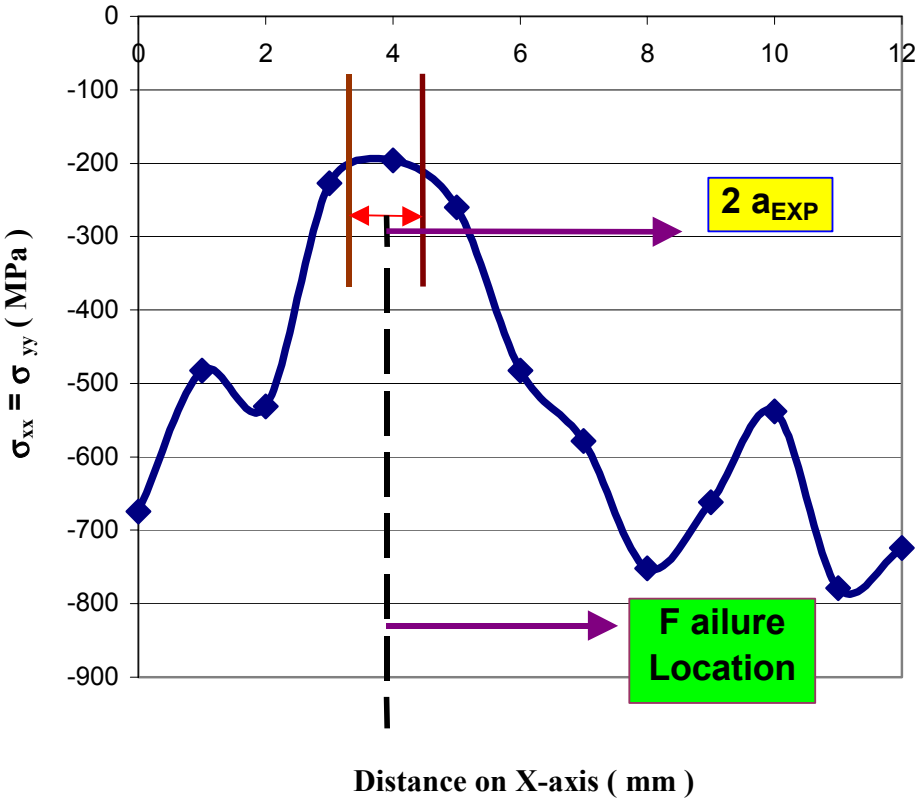

Figure 5.1. Measured Residual Stress Profile on contact surface after failure
(Test # 1) (6.35 mm)

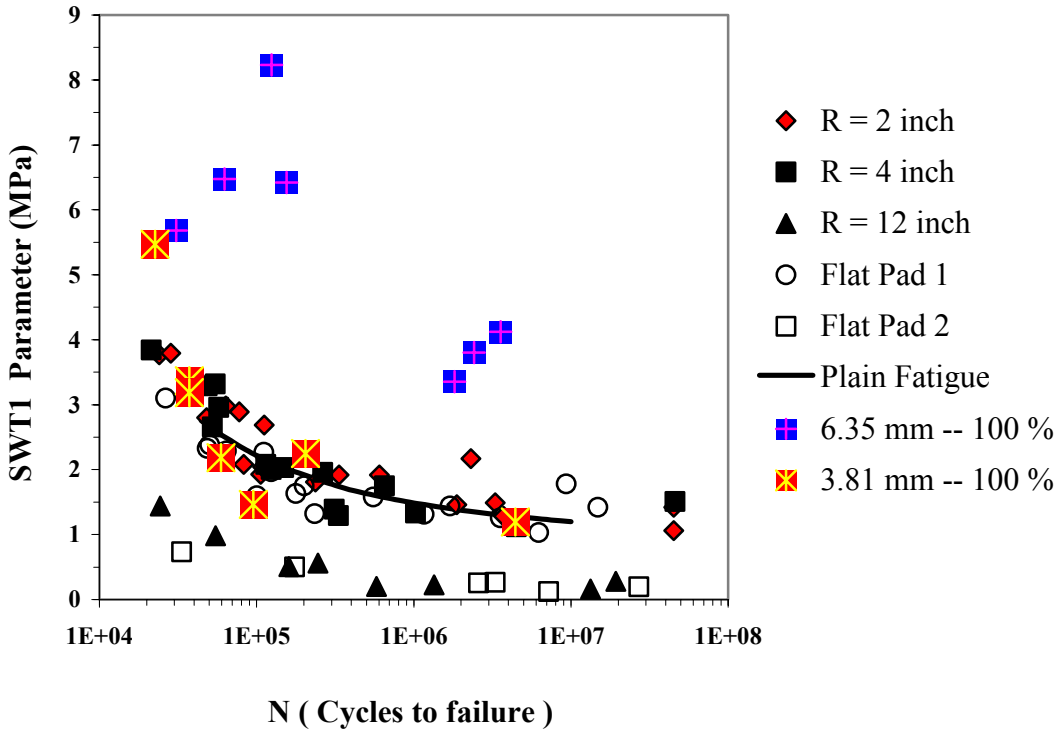

Figure 5.2.a. SWT 1 Parameter versus Life (100 % Stress Relaxation)
(Shown as 100 %)

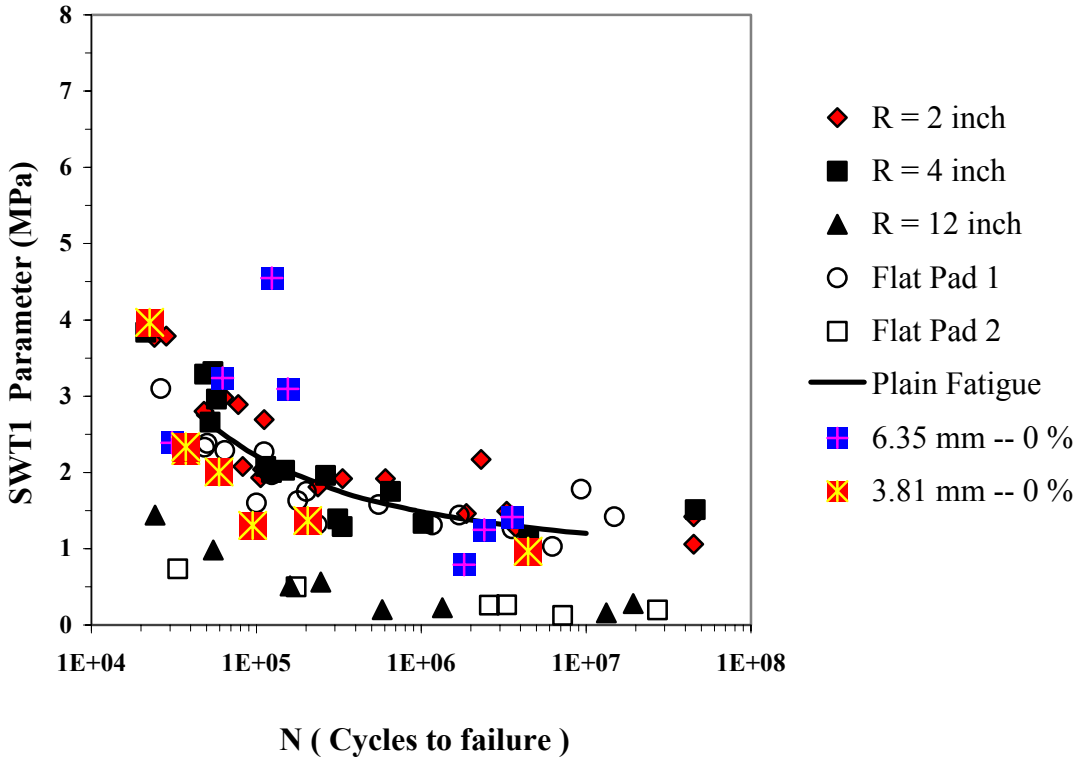

Figure 5.2.b. SWT 1 Parameter versus Life (0 % Stress Relaxation)
(Shown as 0 %)

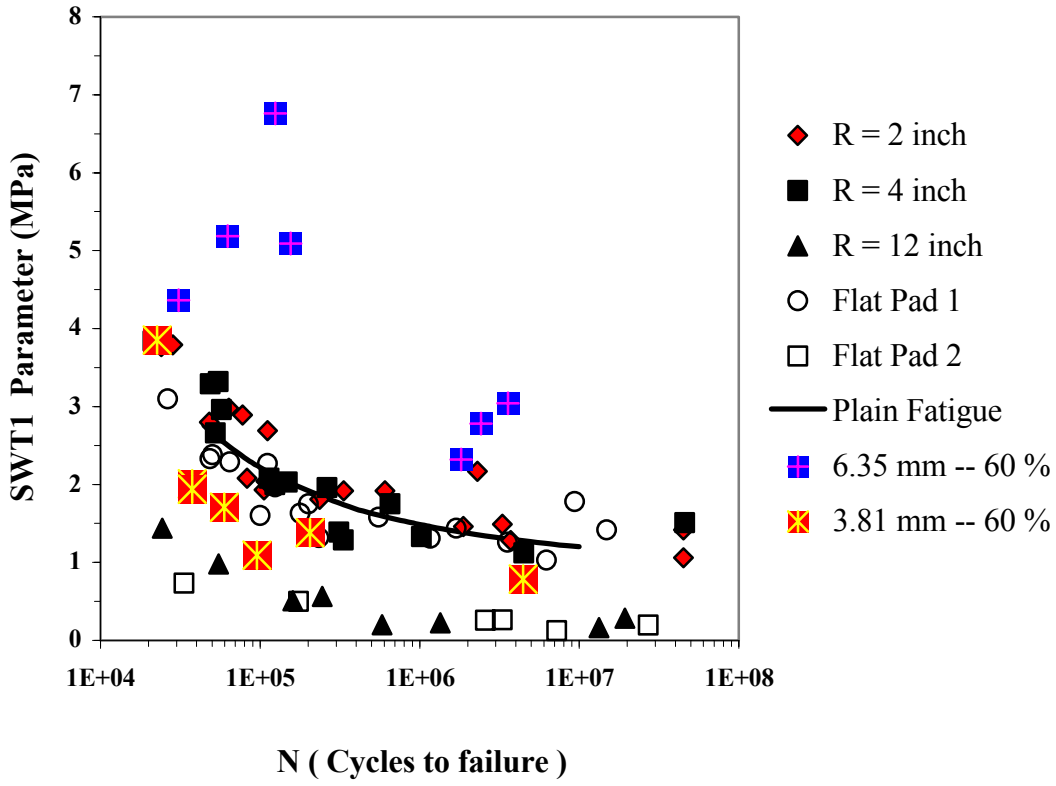

Figure 5.2.c. SWT 1 Parameter versus Life (60 % Stress Relaxation)
(Shown as 60 %)

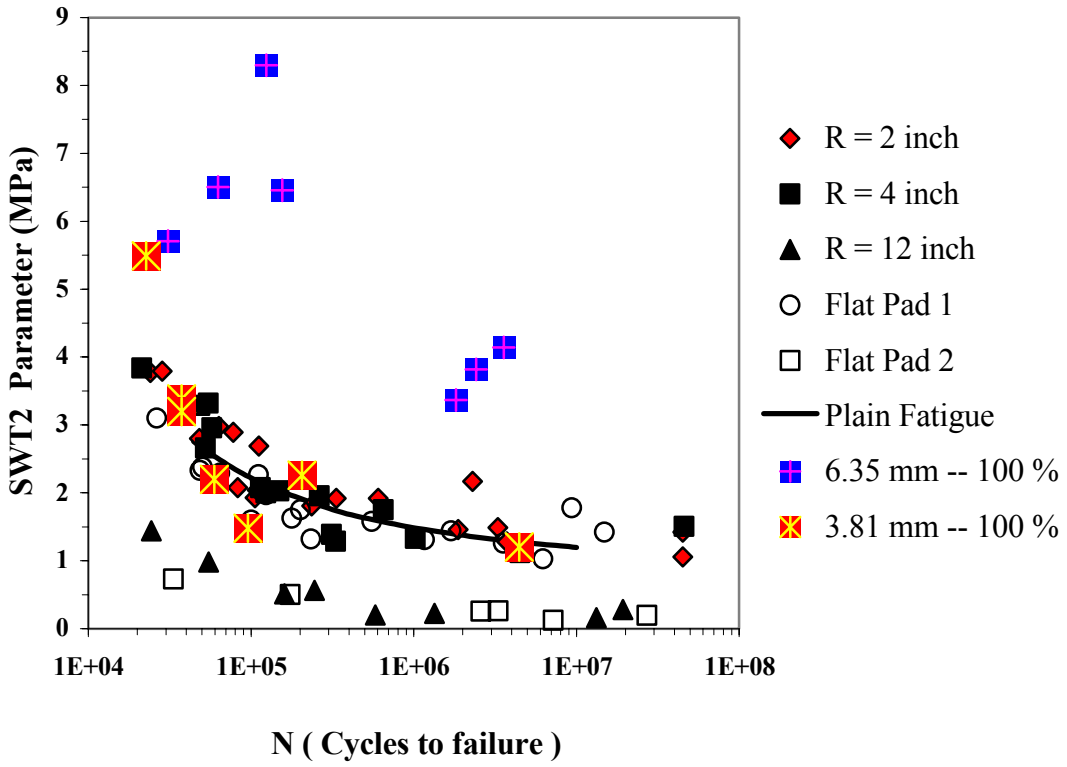

Figure 5.3.a. SWT 2 Parameter versus Life (100 % Stress Relaxation)
(Shown as 100 %)

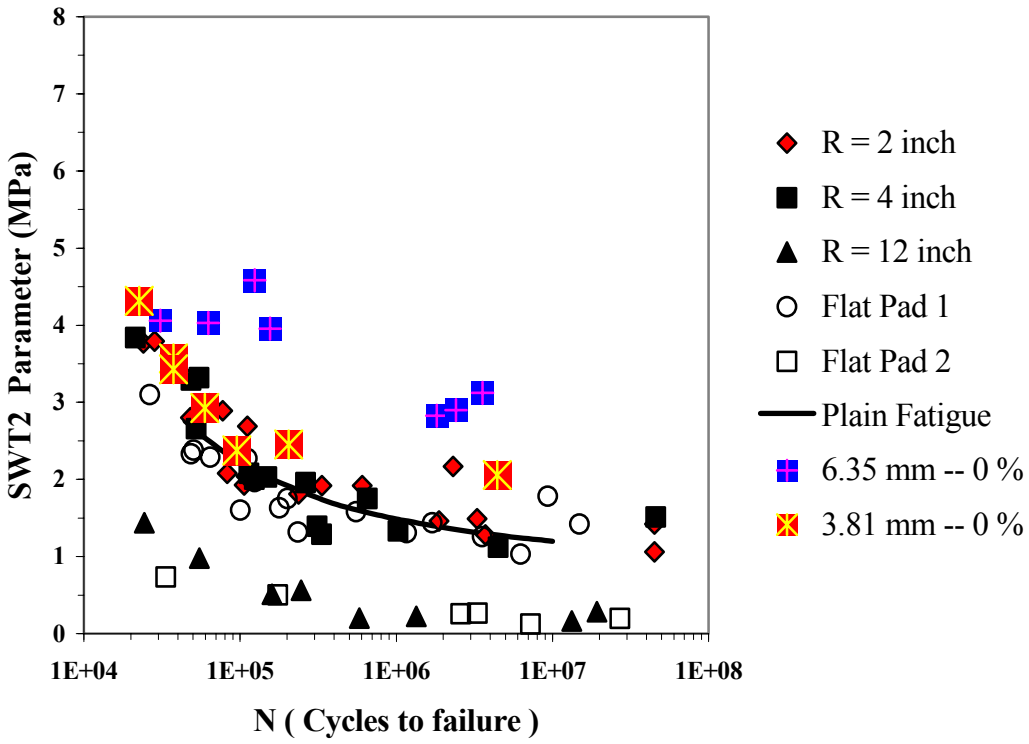

Figure 5.3.b. SWT 2 Parameter versus Life (0 % Stress Relaxation)
(Shown as 0 %)

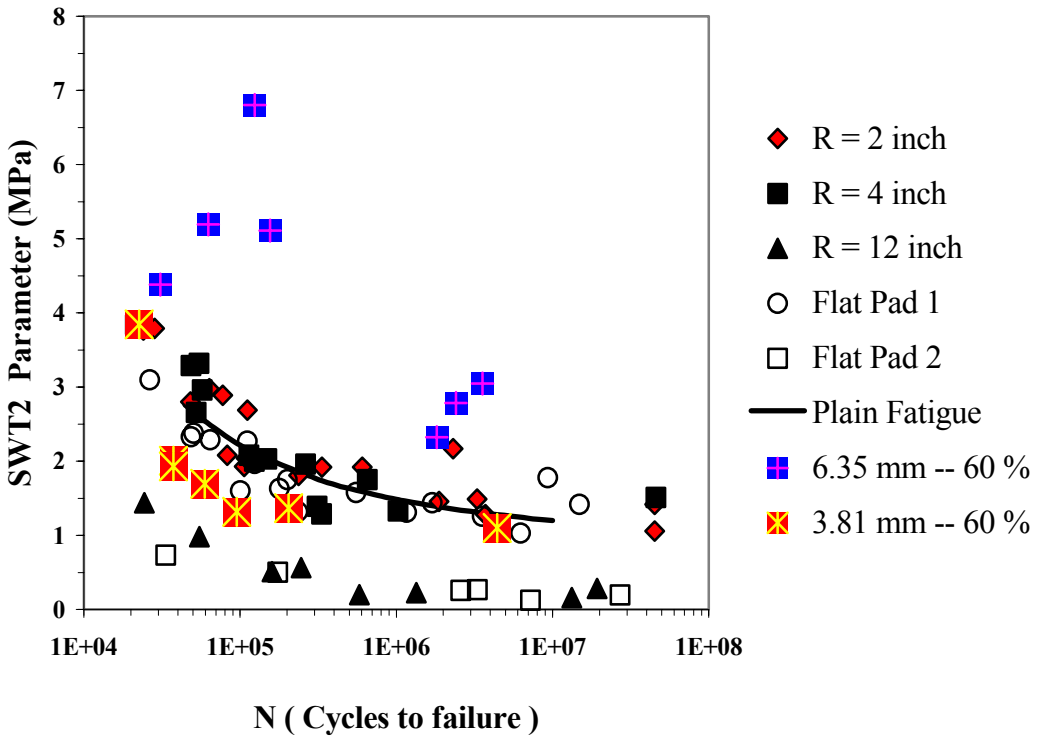

Figure 5.3.c. SWT 2 Parameter versus Life (60 % Stress Relaxation)
(Shown as 60 %)

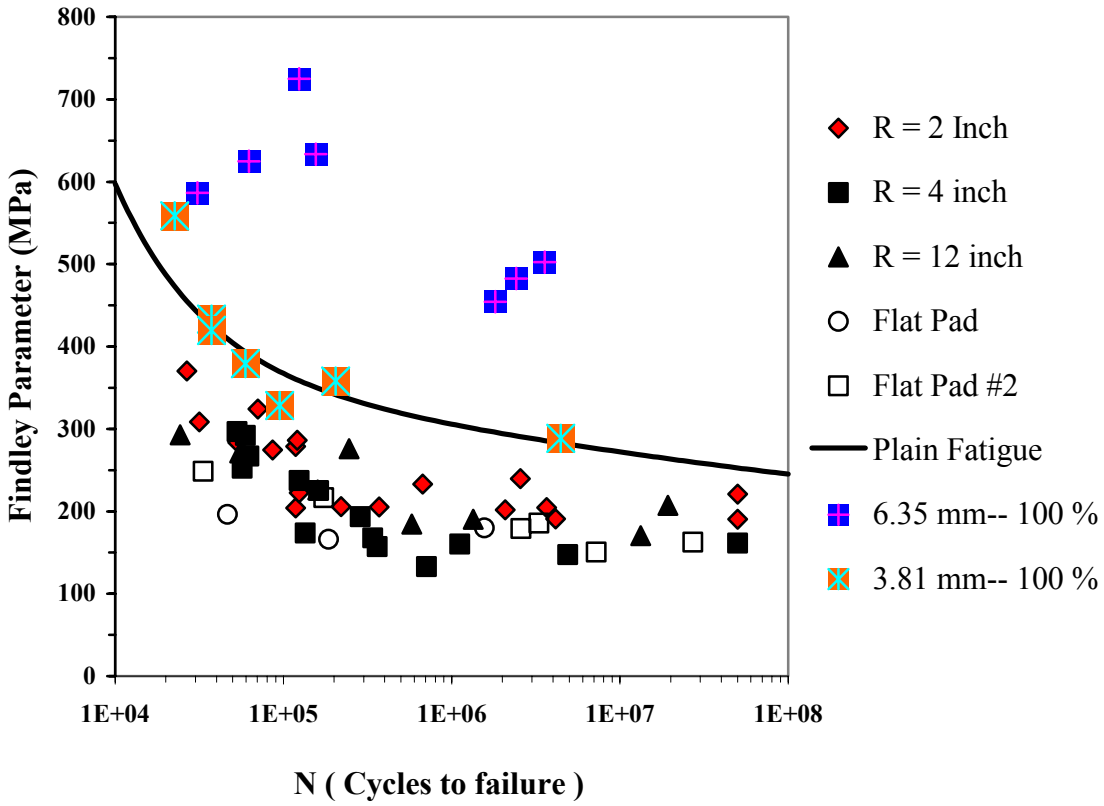

Figure 5.4.a. Findley Parameter versus Life (100 % Stress Relaxation)
(Shown as 100 %)

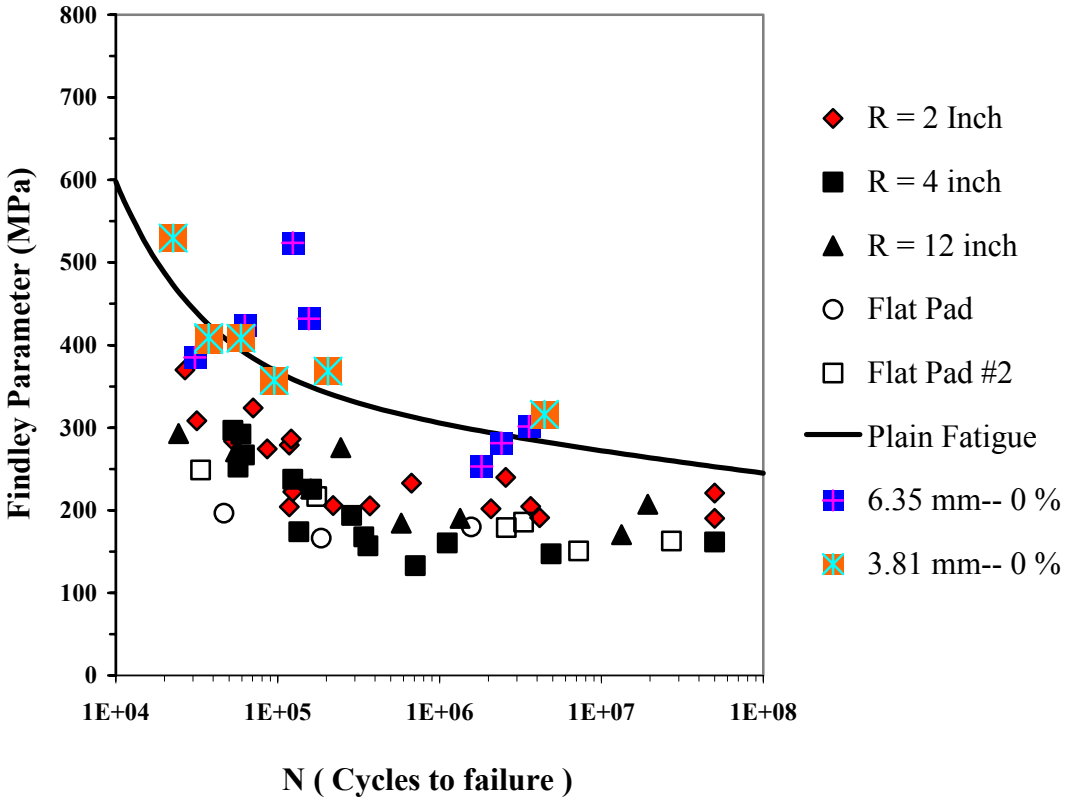

Figure 5.4.b. Findley Parameter versus Life (0 % Stress Relaxation)
(Shown as 0 %)

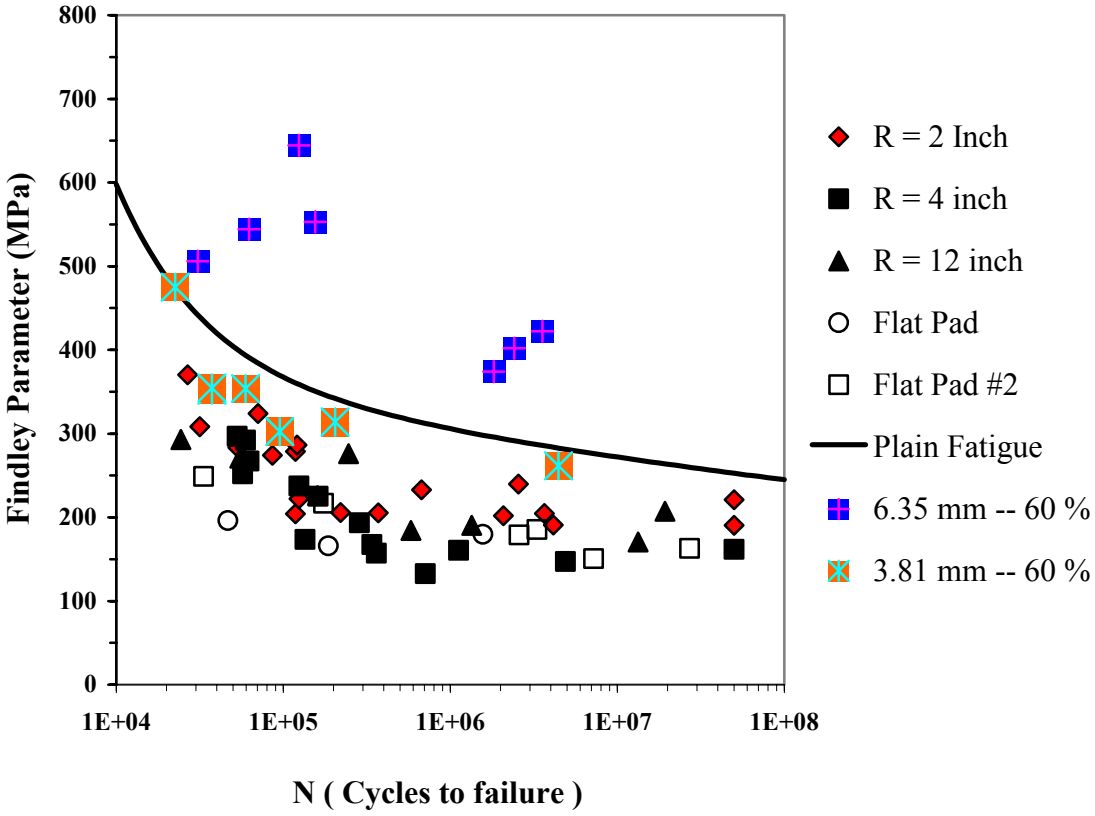

Figure 5.4.c. Findley Parameter versus Life (60 % Stress Relaxation)
(Shown as 60 %)

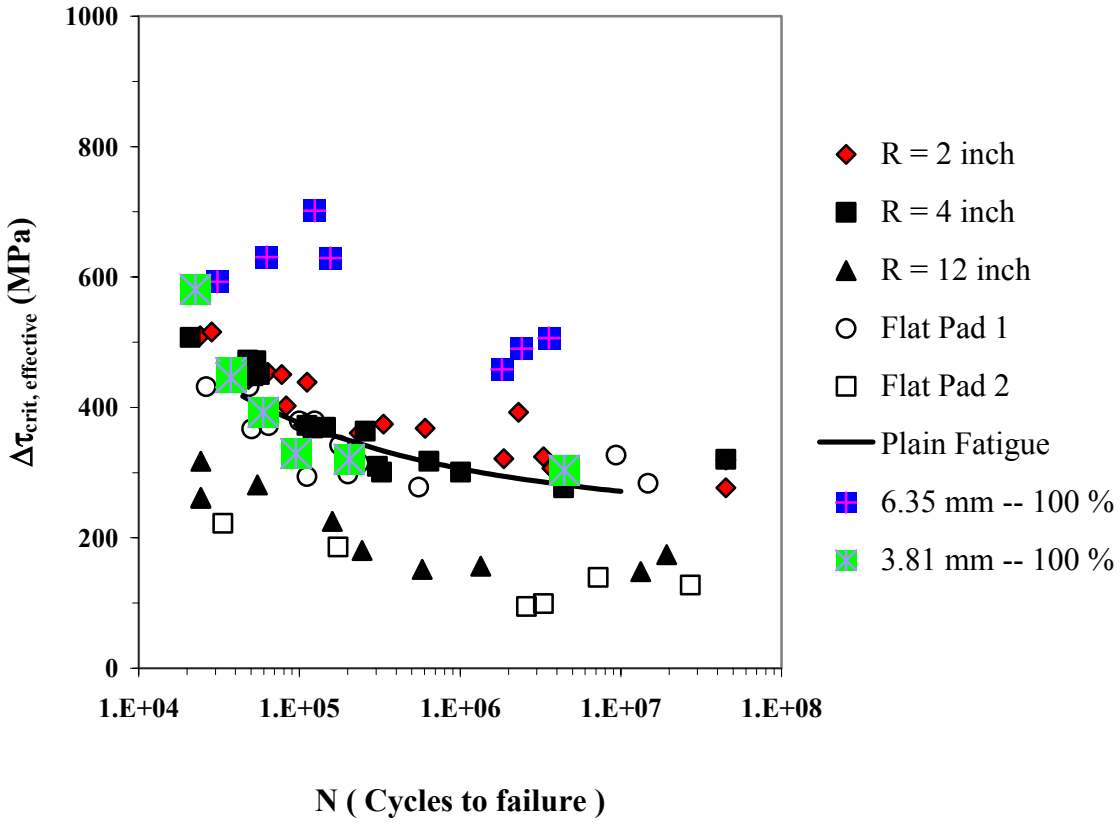

Figure 5.5.a. SSR Parameter versus Life (100 % Stress Relaxation)
(Shown as 100 %)

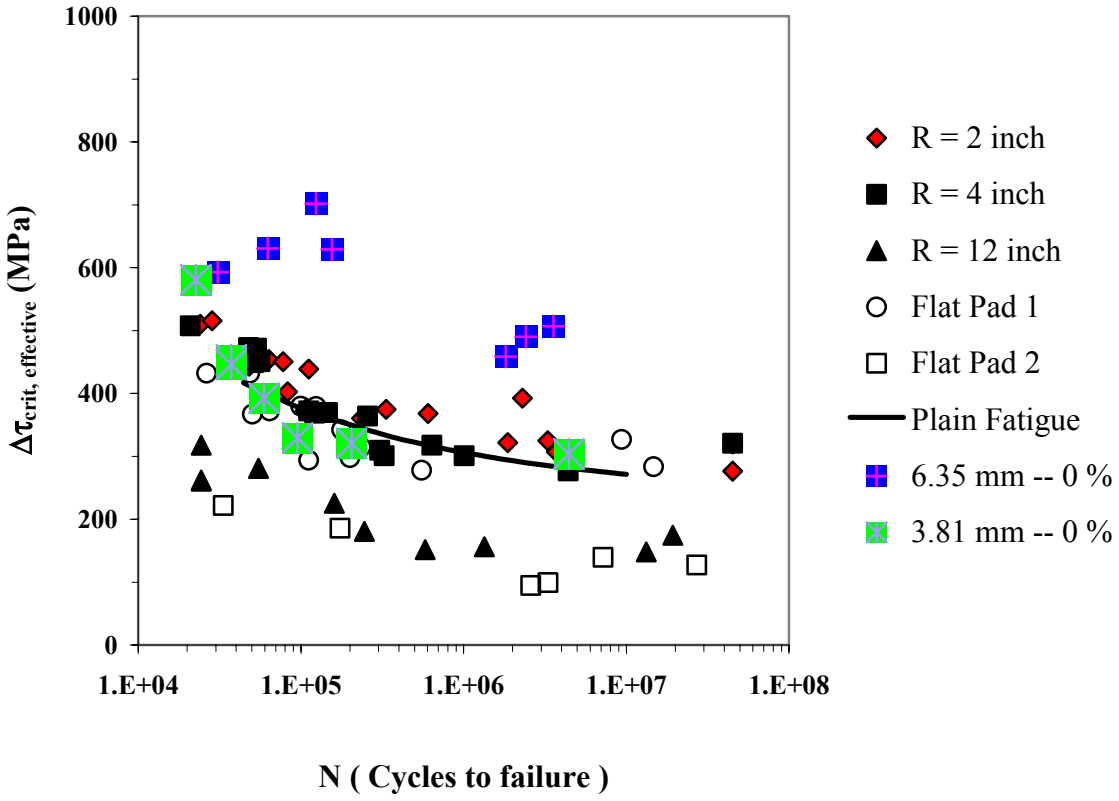

Figure 5.5.b. SSR Parameter versus Life (0 % Stress Relaxation)
(Shown as 0 %)

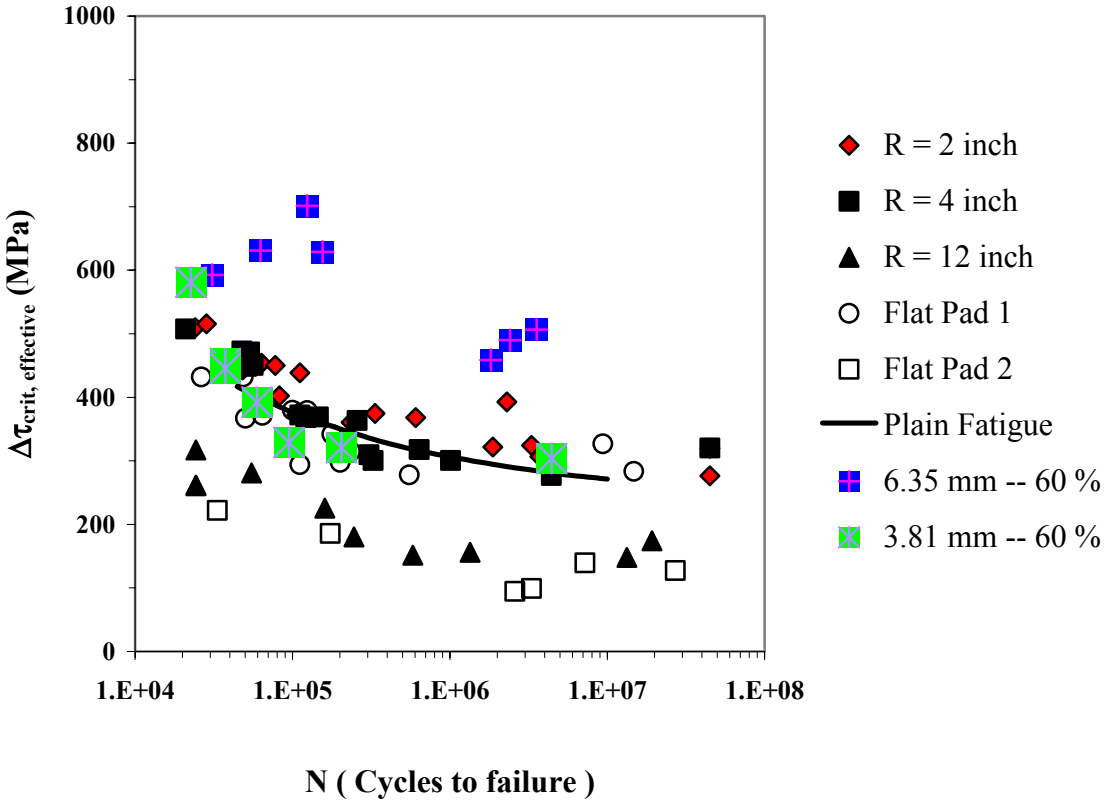

Figure 5.5.c. SSR Parameter versus Life (60 % Stress Relaxation)
(Shown as 60 %)

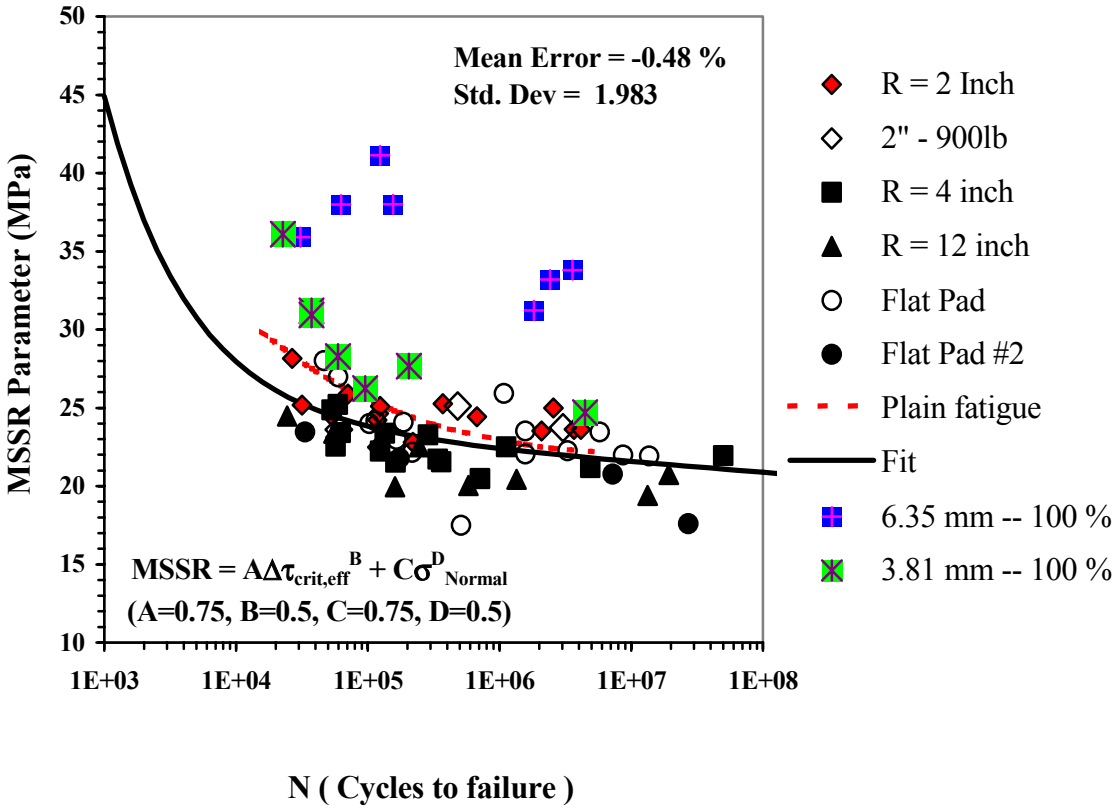

Figure 5.6.a. MSSR Parameter versus Life (100 % Stress Relaxation)
(Shown as 100 %)

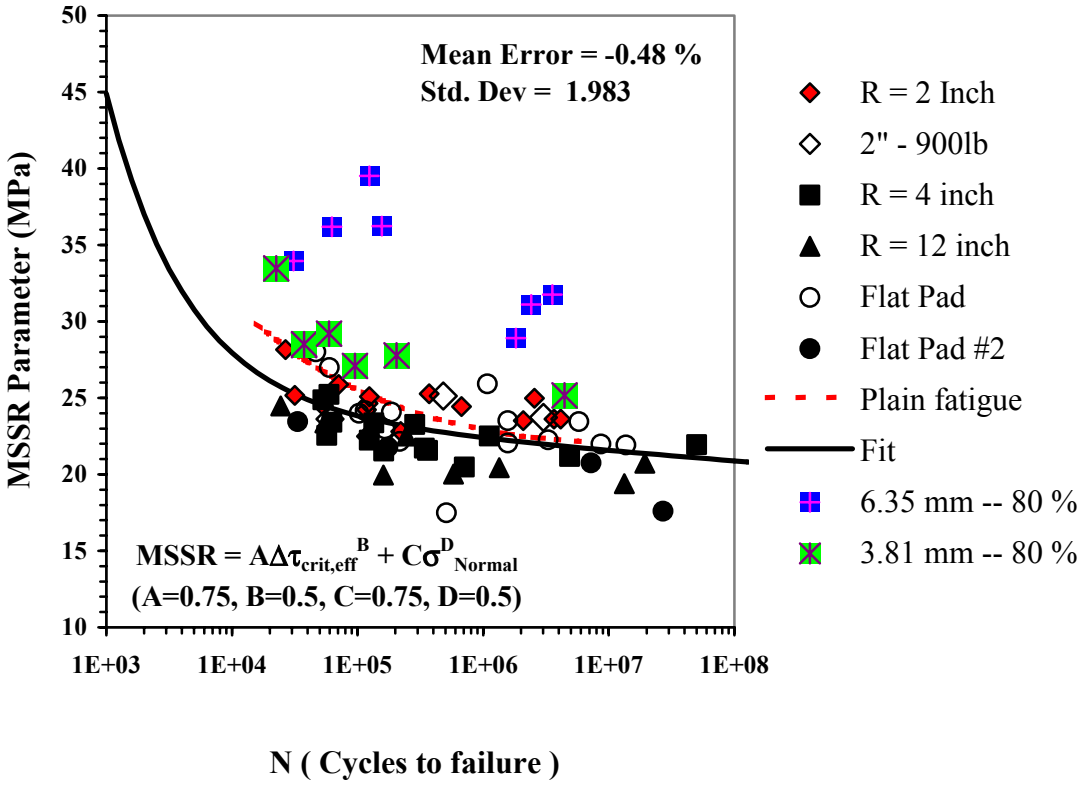

Figure 5.6.b. MSSR Parameter versus Life (80 % Stress Relaxation)
(Shown as 80 %)

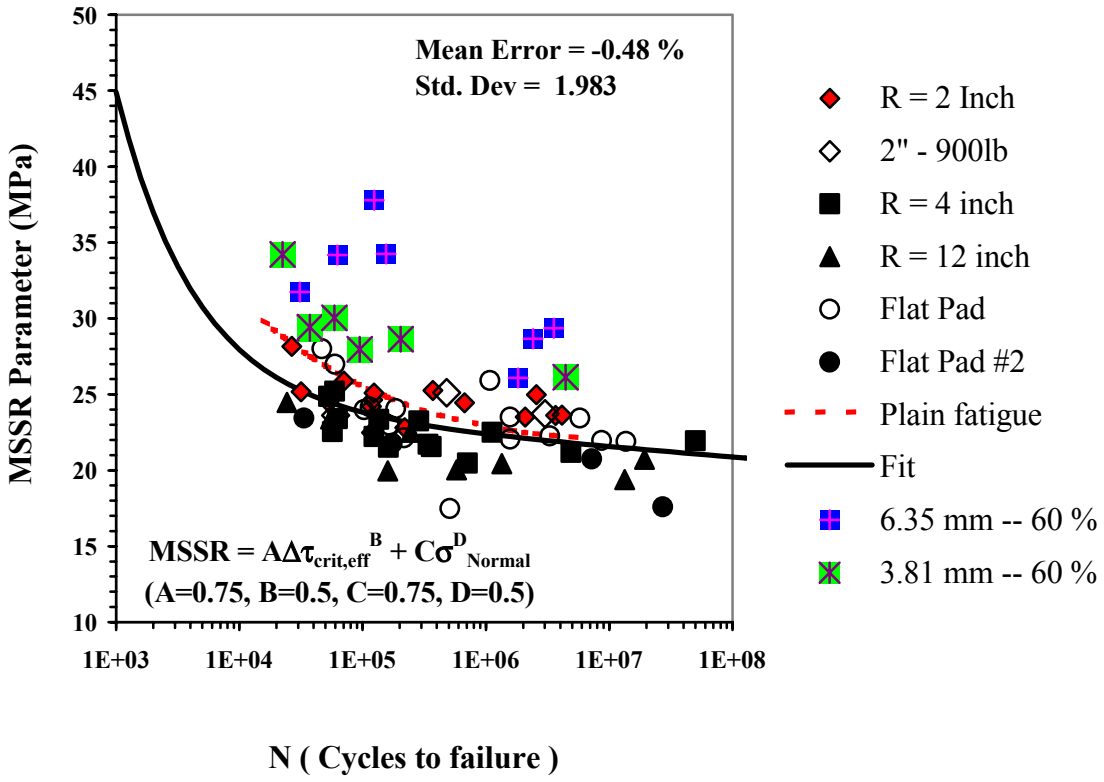

Figure 5.6.c. MSSR Parameter versus Life (60 % Stress Relaxation)
(Shown as 60 %)

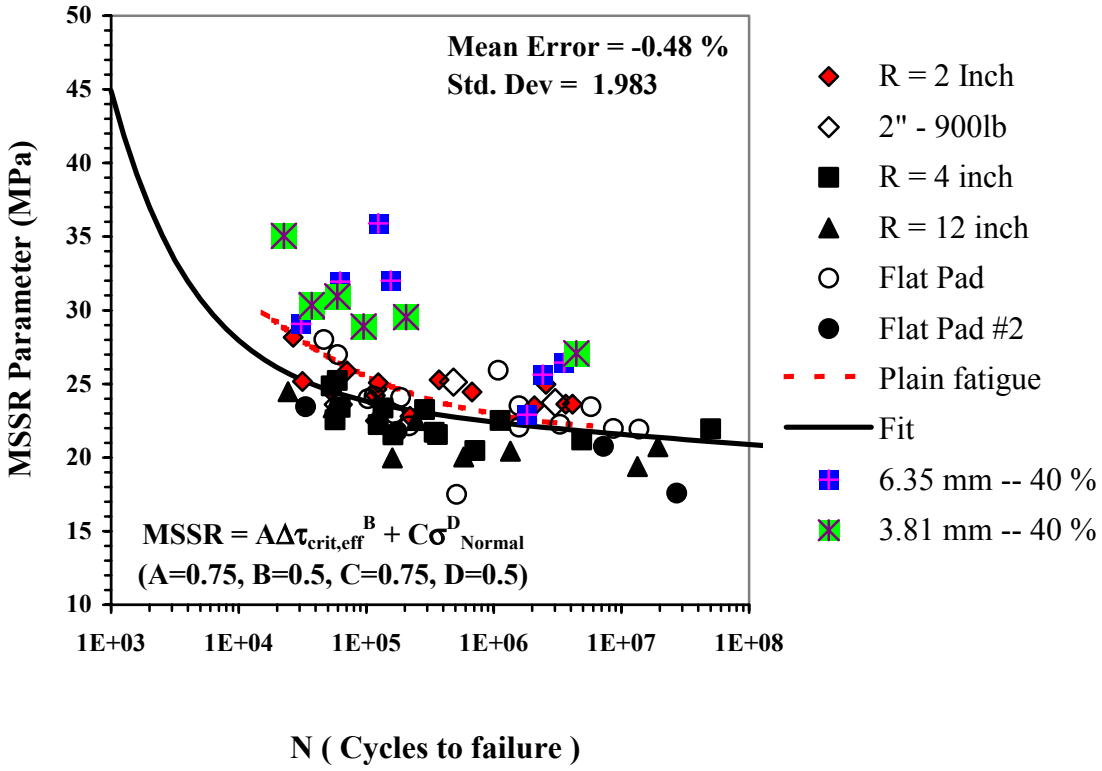

Figure 5.6.d. MSSR Parameter versus Life (40 % Stress Relaxation)
(Shown as 40 %)

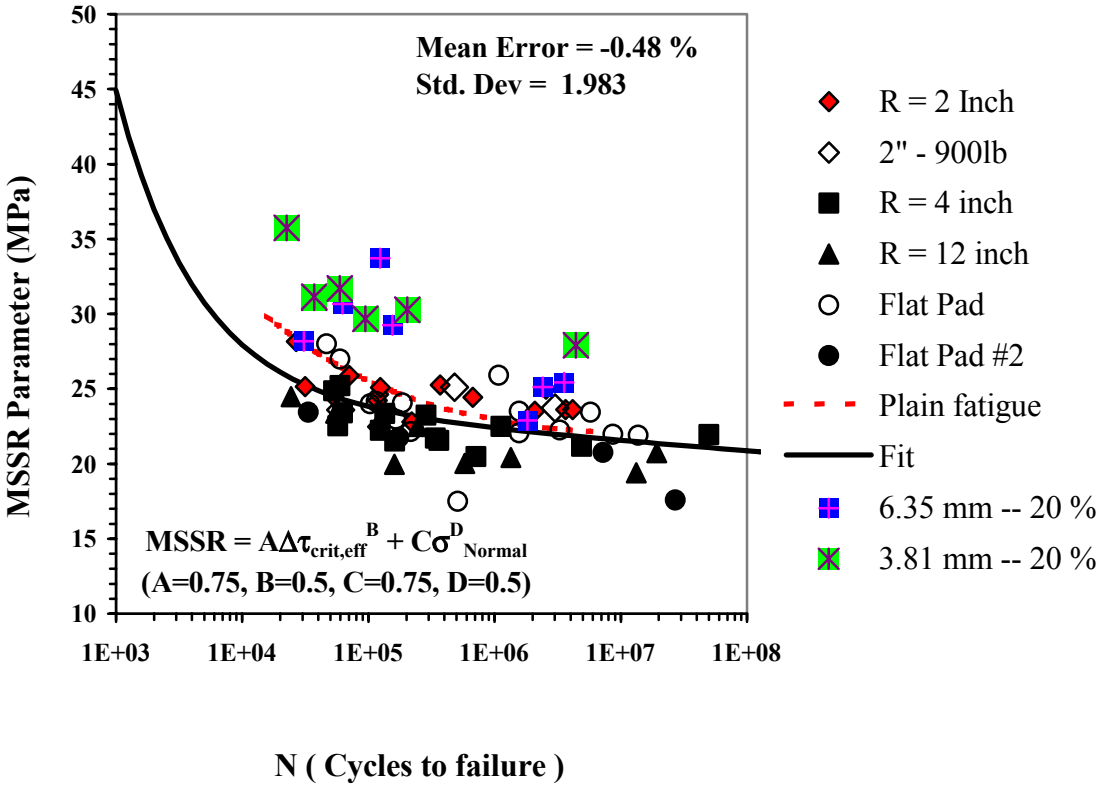

Figure 5.6.e. MSSR Parameter versus Life (20 % Stress Relaxation)
(Shown as 20 %)

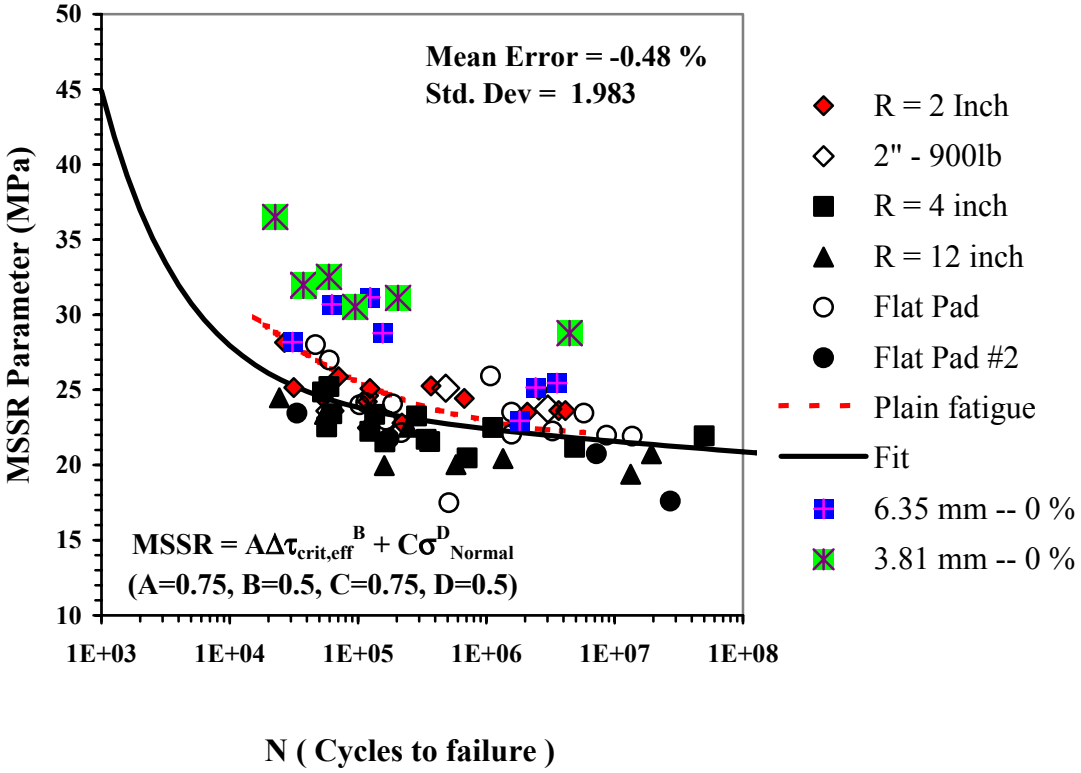

Figure 5.6.f. MSSR Parameter versus Life (0 % Stress Relaxation)
(Shown as 0 %)

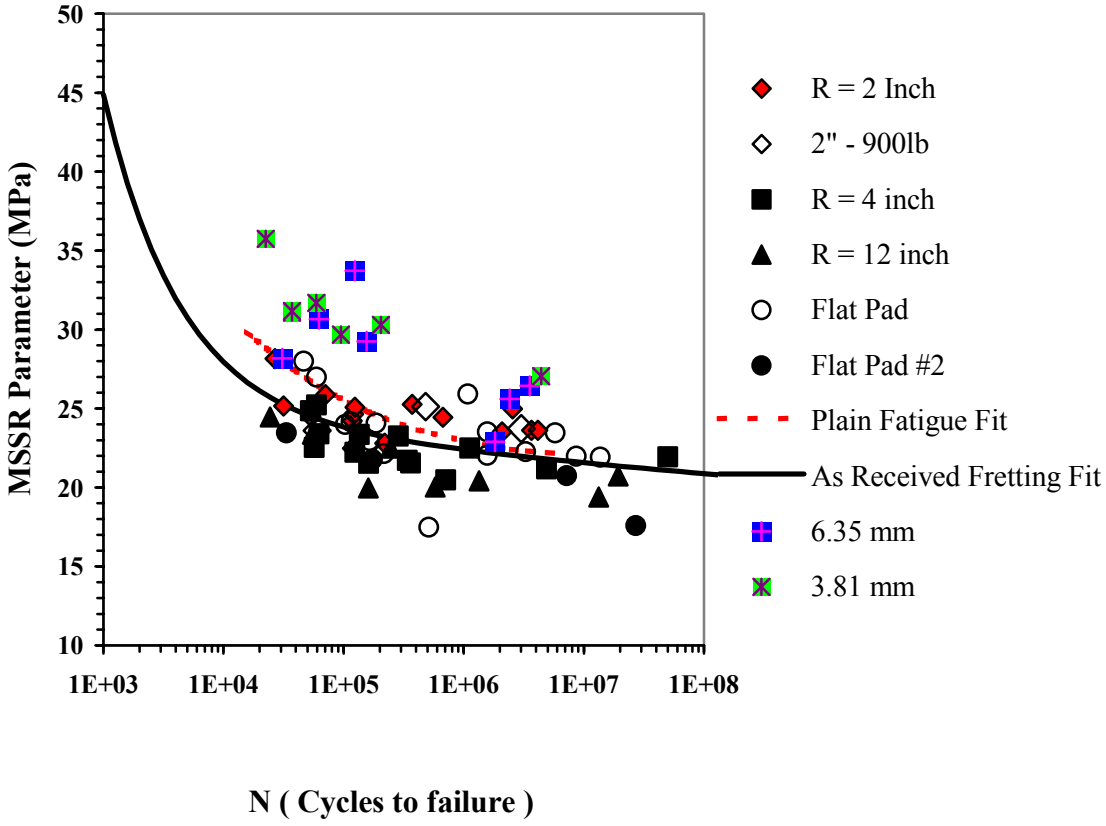

Figure 5.7. Consistent Data of Shot-peened Specimens (Approach 1)
Assumed percentages of stress relaxation are shown below (Same for each thickness)

20 % for Low Cycle Regime (Up to 100,000 cycles)
20 % between Low and High Cycle Regimes (Between 100,000 and 1,000,000 cycles)
40 % for High Cycle Regime (After 1,000,000 cycles)

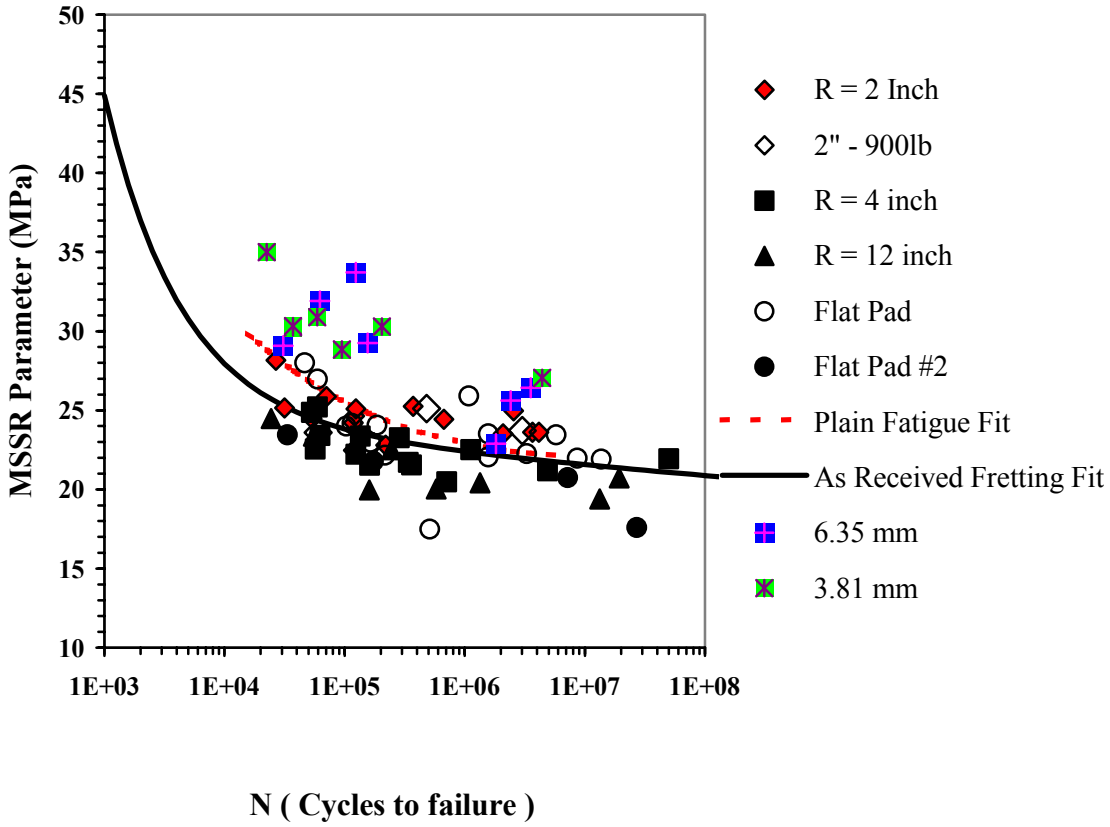

Figure 5.8. Consistent Data of Shot-peened Specimens (Approach 2)
Assumed percentages of stress relaxation are shown below (Same for each thickness)

40 % for Low Cycle Regime (Up to 100,000 cycles)
20 % between Low and High Cycle Regimes (Between 100,000 and 1,000,000 cycles)
40 % for High Cycle Regime (After 1,000,000 cycles)

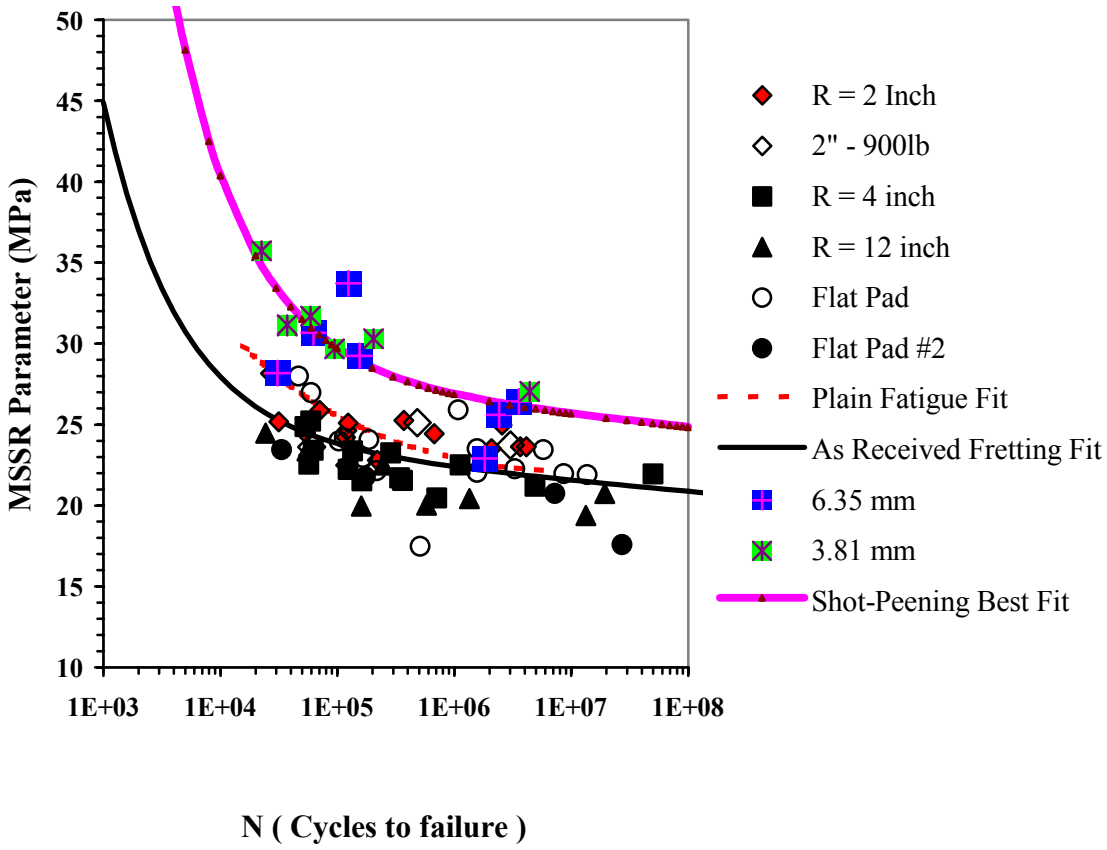

Figure 5.9. Best Fit of Consistent Data (Approach 1)
(See Figure 5.7. for assumed percentages of stress relaxation)

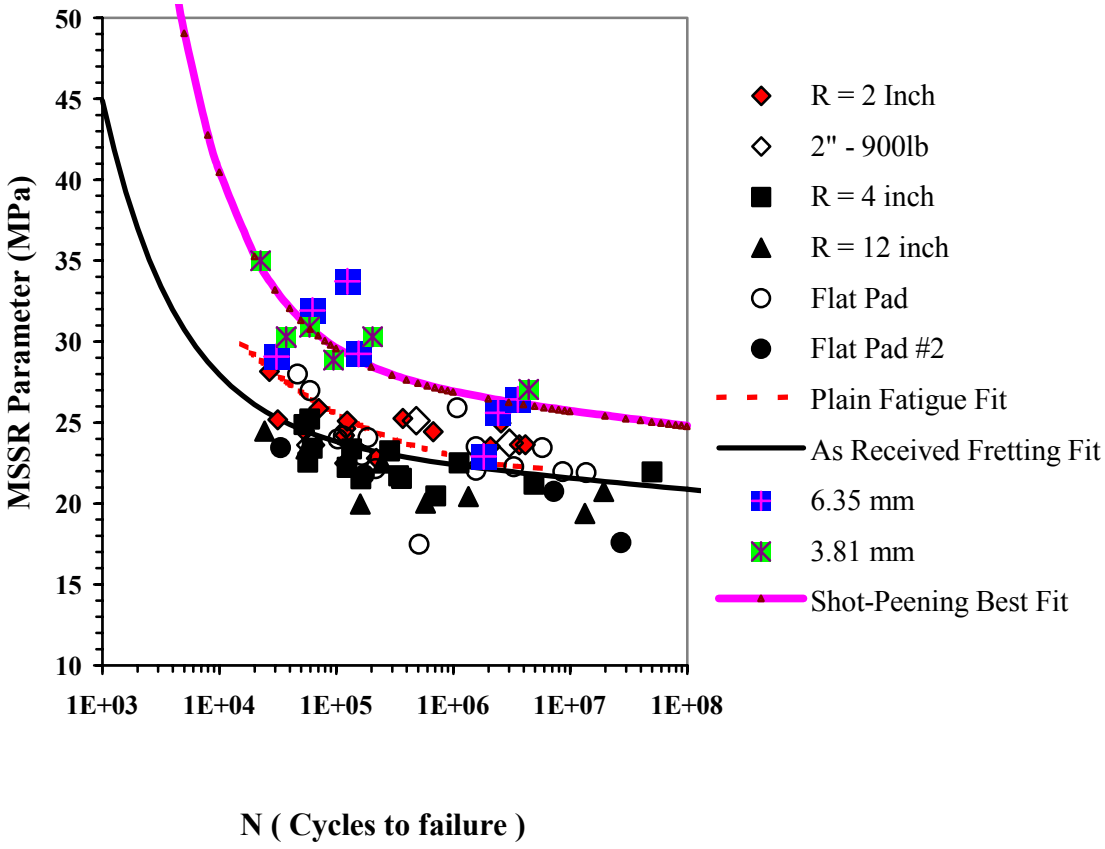

Figure 5.10. Best Fit of Consistent Data (Approach 2)
(See Figure 5.8. for assumed percentages of stress relaxation)

Table 5.1. C_1, C_2, C_3, C_4 Constants for Best Fit of Collapsed Data (Approach 1)

Case	C_1	C_2	C_3	C_4	Figure
Approach 1	31.458	-0.012787	6566.2	-0. 6804	5.9

Table 5.2. C_1, C_2, C_3, C_4 Constants for Best Fit of Collapsed Data (Approach 2)

Case	C_1	C_2	C_3	C_4	Figure
Approach 2	32.685	-0.014982	12774	-0. 75648	5.10

Table 5.3. Assumed Percentages of Stress Relaxation, and Maximum Values of MSSR Parameter for Approach 1 (Data of Figure 5.7)

6.35 mm thickness

Test #	1	7	5	4	2	3	6
Failure Cycles	30839	62501	124222	155545	1819508	2415267	3562668
Assumed Percentage of Stress Relaxation	20%	20%	20%	20%	40%	40%	40%
Max. Value of MSSR	28.176	30.697	33.739	29.265	22.910	25.618	26.455

3.81 mm thickness

Test #	22	18	17	21	20	19	16
Failure Cycles	22561	37352	37401	59373	95149	204604	4438031
Assumed Percentage of Stress Relaxation	20%	20%	20%	20%	20%	20%	40%
Max. Value of MSSR	35.794	31.193	31.117	31.743	29.729	30.333	27.074

Note : At the assumed percentages of stress relaxation, maximum value of MSSR is predicting the correct crack initiation location for each thickness and for each test. (contact surface for 6.35 mm, at the depth ranging from 200 to 300 microns for 3.81 mm)

Table 5.4. Assumed Percentages of Stress Relaxation, and Maximum Values of MSSR Parameter for Approach 2 (Data of Figure 5.8)

6.35 mm thickness

Test #	1	7	5	4	2	3	6
Failure Cycles	30839	62501	124222	155545	1819508	2415267	3562668
Assumed Percentage of Stress Relaxation	40%	40%	20%	20%	40%	40%	40%
Max. Value of MSSR	29.079	31.939	33.739	29.265	22.910	25.618	26.455

3.81 mm thickness

Test #	22	18	17	21	20	19	16
Failure Cycles	22561	37352	37401	59373	95149	204604	4438031
Assumed Percentage of Stress Relaxation	40%	40%	40%	40%	40%	20%	40%
Max. Value of MSSR	35.052	30.35	30.275	30.935	28.892	30.333	27.074

Note : At the assumed percentages of stress relaxation, maximum value of MSSR is predicting the correct crack initiation location for each thickness and for each test. (contact surface for 6.35 mm, at the depth ranging from 200 to 300 microns for 3.81 mm)

6. Summary, Conclusions, Discussion and Suggestions for Future Studies

6.1. Summary

In this study, 7 tests under different loading conditions were performed in order to find the effects of shot-peening on high cycle fretting fatigue behavior of Ti-6Al-4V. S-N curves of 6.35 mm thick shot-peened specimens were obtained as shown in Figures 3.5 and 3.6. Besides 6.35 mm, test results of 3.81 mm thickness were also analyzed and used in this study to investigate the effects of thickness on shot-peened specimens. It should be repeated that the tests of 3.81 mm thickness were performed by Namjoshi, Jain, and Mall [6]. Based on the applied stress, Figure 6.1 shows the test results of both thickness values together on the same graph. It demonstrates the change of total life under different loading conditions for different stress ratios. Figure 6.1 clearly shows the benefits of shot-peening for both thickness values. It is seen in this figure that shot-peening increased the total life of fatigue specimens when compared with as received fretting fatigue data.

The experimental observations showed that for both thickness values, the specimens failed near the trailing edge of contact.

The next step in this study was to analyze the test data of both thickness values. After the tests were completed, the changes in maximum and minimum tangential loads were analyzed over the whole test duration to find the stabilized maximum and minimum tangential loads (Q loads). Then these stabilized extremum values were used in Finite Element Analysis models. Finite Element Analysis model was validated by using an

analytical solution technique (see Pages 61 & 62, and Figure 4.3). After validation, the results of FEA were accepted as accurate, and the axial, transverse and shear stress distributions along the contact surface and within depth of the specimen were used while evaluating the fatigue crack initiation parameters.

Scanning Electron Microscopy (SEM) was done to find the crack initiation location, and initial crack orientations of shot-peened fretting fatigue specimens. SEM showed that for thick specimens (6.35 mm), the crack initiation location was at the contact surface whereas it was found at the depth ranging from 200 to 300 microns for thin specimens (3.81 mm) by Namjoshi, Jain, and Mall [6]. For thick specimens, the initial crack orientation was around -37 and ± 53 degrees, and for thin specimens it was around 42 degrees.

Smith-Watson-Topper (SWT), Findley (FP), Shear Stress Range (SSR), and Modified Shear Stress Range (MSSR) parameters were evaluated for different percentages of stress relaxation. It was seen that Smith-Watson-Topper, Findley, and Shear Stress Range parameters could not meet all the required conditions at the same time for shot-peened specimens no matter what percentages of stress relaxation were assumed to have occurred.

Modified Shear Stress Range (MSSR) parameter was evaluated for 6 different percentages of stress relaxation. Based on two different assumptions about stress relaxation, it was possible to collapse the data of shot-peened specimens having two different thickness values (Figures 5.7 and 5.8). While assuming the different percentages of stress relaxation given in Tables 5.3 and 5.4, the most important criterion was that the maximum value of MSSR parameter should have been able to predict the

correct crack initiation location for each thickness and for each test specifically.

Finally, collapsed data of shot-peened fretting fatigue specimens, which are given in Figures 5.7 and 5.8 were accepted as accurate under the assumptions made in Chapter 5. After the collapsed data were obtained, the curves in Figures 5.9 and 5.10 were found. Using either of these curves, it could be possible to predict the crack initiation cycles of shot-peened fretting fatigue specimens. Figure 6.2 shows that there is almost no difference between the trend lines that were obtained in Figures 5.9 and 5.10. So, it was found that for low cycle regime (up to 75,000 cycles), crack initiation of shot-peened specimens was occurring at around 35 % of total life, between low cycle and high cycle regimes (between 75,000 and 1,000,000 cycles), it was occurring at around 22 % of total life, and for high cycle regime (after 1,000,000 cycles), it was occurring at around 5 % of total life.

6.2. Conclusions

Based on the results found in this study, the following conclusions can be made:

1. Shot-peening improves the life of Ti-6Al-4V under fretting fatigue conditions. This improvement in life is more in lower stress levels (see Figure 3.5, Figure 3.6 and Figure 6.1).
2. Failure of specimens occur near the trailing edge (at around x/a = 1), where there is a stress concentration on the contact interface. (see Figure 2.1 and Figure 4.3).
3. Different thickness values of shot-peened specimens lead to changes in crack initiation locations. In thinner specimens (3.81 mm), there will be a big peak value

in the compensatory residual tensile stress profile. Based on this peak value, the crack initiation location will be inside the specimen, even when the stress relaxation goes up to 80 %. In thicker specimens (6.35 mm), there won't be a big peak value in the compensatory residual tensile stress profile, because after the compressive zone, the remaining thickness for the tensile zone will be much greater, which will lead to a smaller maximum value for the compensatory residual tensile stress. (Therefore, the distribution of the compensatory residual tensile stress was assumed rectangular for 6.35 mm thickness. The areas under the compressive and the tensile zones had to be same to keep the equilibrium of residual stresses, and that requirement was satisfied in this study). In addition, it is found that thicker specimens are more sensitive to stress relaxation. So, different percentages of stress relaxation may change the crack initiation location of thicker specimens relatively easier than the thinner specimens. The crack initiation location of thicker specimens will be at the contact surface if the stress relaxation is more than 40 %. There may be a scatter in the crack initiation locations if the stress relaxation is between 20 % and 40 %. So, results of each test should be analyzed very carefully in this interval (Maximum value of the parameter should predict the correct initiation location). If the stress relaxation is less than 20 %, the crack initiation location may move towards the depth of the material to somewhere around 150 to 200 microns. In other words, for small percentages of stress relaxation, thicker specimens may behave like the thinner specimens.

4. Initial crack orientation of thinner specimens will be closer to ± 45 degrees (plane of maximum shear stress) when compared to the initial crack orientation of thicker specimens. It can be said that crack initiation under fretting conditions is dominantly

dependent on shear stresses.

5. Smith-Watson-Topper, Findley, and Shear Stress Range parameters were not able to meet all the requirements for shot-peened specimens.

6. Based on the two assumptions made in Chapter 5, Modified Shear Stress Range (MSSR) parameter was found to be the only parameter that could be used to predict the number of cycles to crack initiation (Figure 5.9 and Figure 5.10), the crack initiation location, and the initial crack orientation of shot-peened fretting fatigue specimens. Therefore, MSSR parameter was determined to be an appropriate fatigue crack initiation parameter while investigating the crack initiation behavior of Ti-6Al-4V on shot-peened specimens under high cycle fretting fatigue conditions.

6.3. Discussion, and Suggestions for Future Studies

In this study, the residual stresses were assumed to be biaxial ($\sigma_{xx} = \sigma_{yy}$). So, the residual stresses were added to σ_{xx} and σ_{yy} values of FEA output data equally to get the resultant stresses in each layer of depth through Y-axis (along thickness). Because of this reason, SSR parameter showed the same values, but for different percentages of stress relaxation, the normal stresses acting in crack opening mode changed (see Pages 75 & 76 for explanations). Residual stress profiles showing stress relaxation were obtained just on the contact surface of the material (Figure 5.1), and there had to be some assumptions for the amount of stress relaxation along the depth of the material. So, the same percentage of stress relaxation was assumed to have occurred within depth at each layer and evaluations were repeated for different percentages of stress relaxation. In

order to find the actual profiles of residual stresses within depth of the material, either X-ray diffraction techniques within the base facilities should be improved or the failed specimens should be sent to Lambda Research Center, Cincinnati, just like they were sent before the tests. More analyses with the actual profiles of residual stresses after failure will help understanding the crack initiation behavior of Ti-6Al-4V better.

In this study, coefficient of friction was found to be higher for thicker specimens than the thinner specimens. For different loading conditions, the dynamic coefficient of friction always changed. Some tests were performed to find the changes of coefficient of friction, but it was too difficult to find the stabilized coefficient of friction. So, in the future, changes in the dynamic coefficient of friction would be analyzed in another study in more details. For different thickness values, reasons for the changing dynamic coefficient of friction would be investigated, especially with a third thickness. If the same tests and analyses are performed with a third thickness, it will be helpful in confirming the results found in this study. Test results of the third thickness can be used to confirm the collapsed data obtained in Figures 5.7 and 5.8. Tests with a third thickness will also help understanding the thickness effects on dynamic coefficient of friction, and on MSSR parameter better. Figure 6.3 shows the change of MSSR parameter along the depth of the material. It is seen that in thicker specimens, the crack initiation location will be more probably on the contact surface for most of the percentages of stress relaxation. However, Figure 6.4 shows that in thinner specimens, crack initiation location will be inside the material at the depth ranging from 200 to 300 microns, even when the stress relaxation goes up to 80 %. Tests with a third thickness will contribute to a better understanding of the thickness effects on crack initiation behavior of shot-peened specimens.

It is known that crack initiation occurs at around 50 % to 90 % of the total fatigue life under high cycle fretting fatigue conditions. In this study, it is found that crack initiation of shot-peened specimens is occurring at about 5 % to 35 % of the total fatigue life. The surface roughness of the shot-peened specimens may be the reason leading to crack initiations in the early stages of life, but probably, these cracks are not able to grow easily because of the compressive zone induced by shot-peeenig. It is more likely for the cracks to grow when stress relaxation occurs, and the residual compressive stresses become less. So, finding the actual stress relaxation percentages at low cycle and high cycle regimes is very important at this point, which will be helpful in future studies.

In order to understand the beneficial effects of shot-peening better, the specimens should be sent to re-shot-peening. Using the S-N curves in Figure 3.5 and Figure 3.6 (or Figure 6.1), two or more different stress levels can be selected. These tests would be run until the chosen percentages of total life at each stress level. Then the tests would be stopped and the specimens would be sent to re-shot-peeening. When the specimens come back from re-shot-peening, the tests would be continued until failure. The final results would be seen on the S-N curves to find out whether re-shot-peening is increasing total life or not. Also, the same type of analyses would be performed for the re-shot-peened specimens to understand the stress relaxation phenomenon better. These future studies will definitely contribute to a better understanding of the behavior of shot-peened specimens under high cycle fretting fatigue conditions.

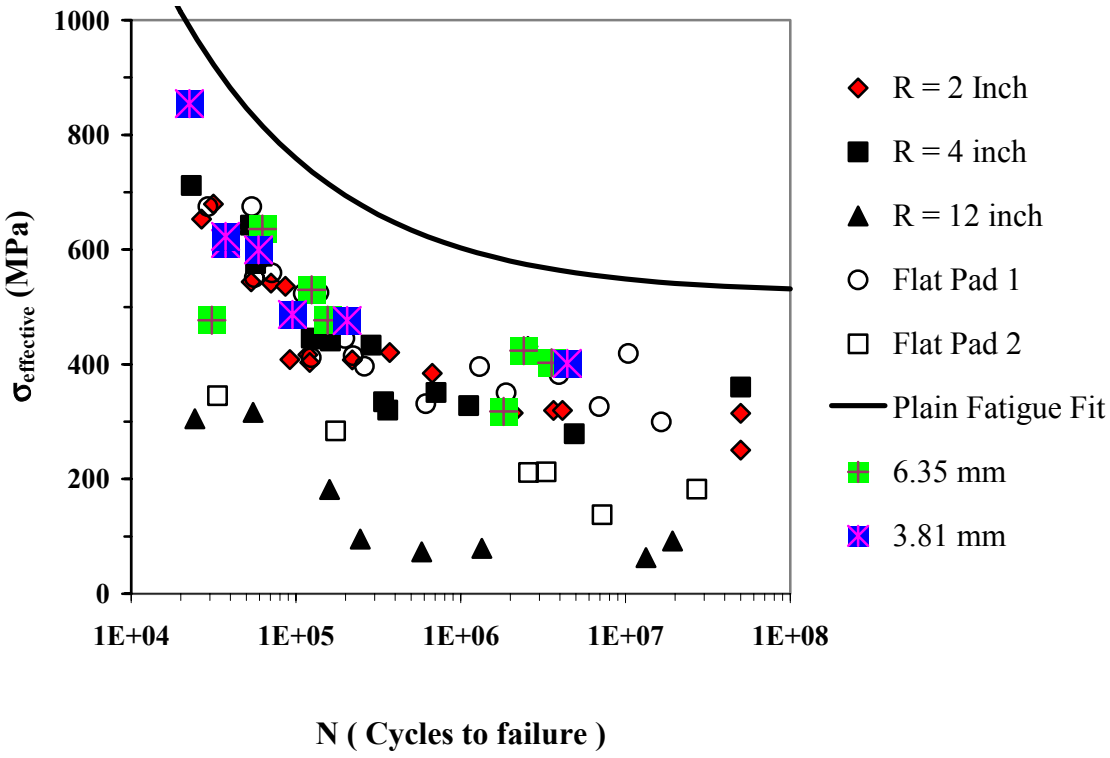

Figure 6.1. Global Chart for Fretting Fatigue Data including Shot-Peened Fretting Fatigue Data of 6.35 mm and 3.81 mm thickness values

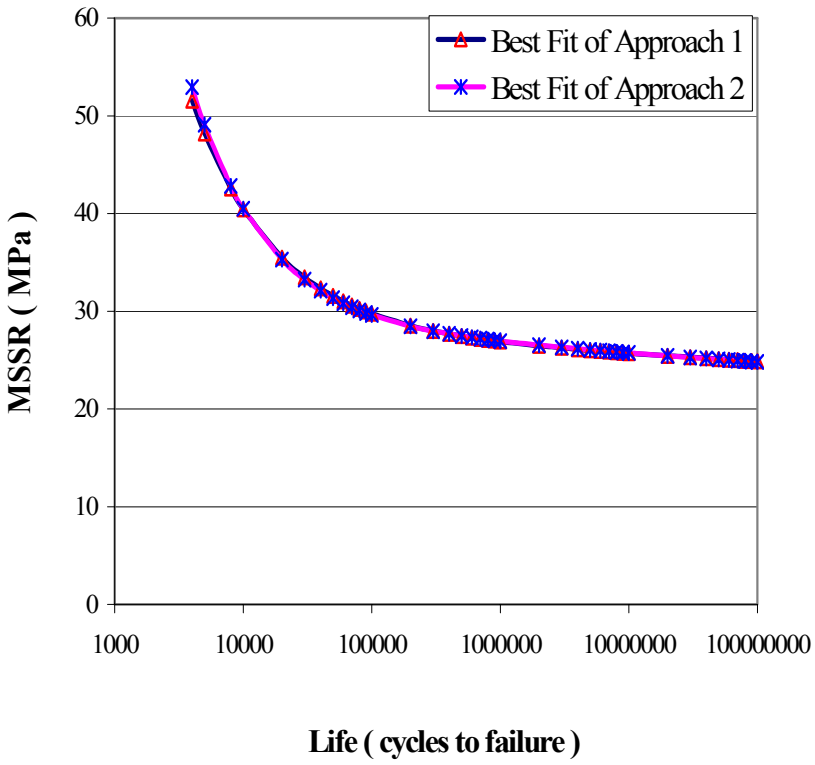

Figure 6.2. Difference between best fits of two different approaches

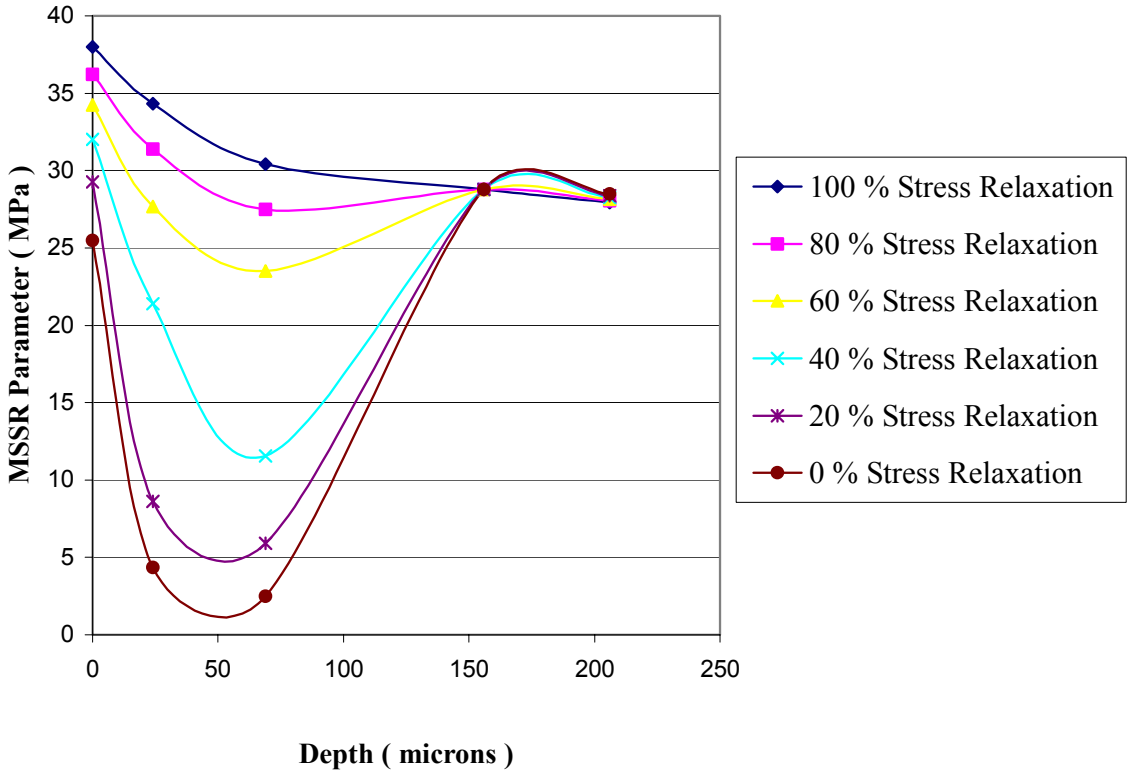

Figure 6.3. MSSR Parameter versus Depth for 6.35 mm thickness (Test # 4)

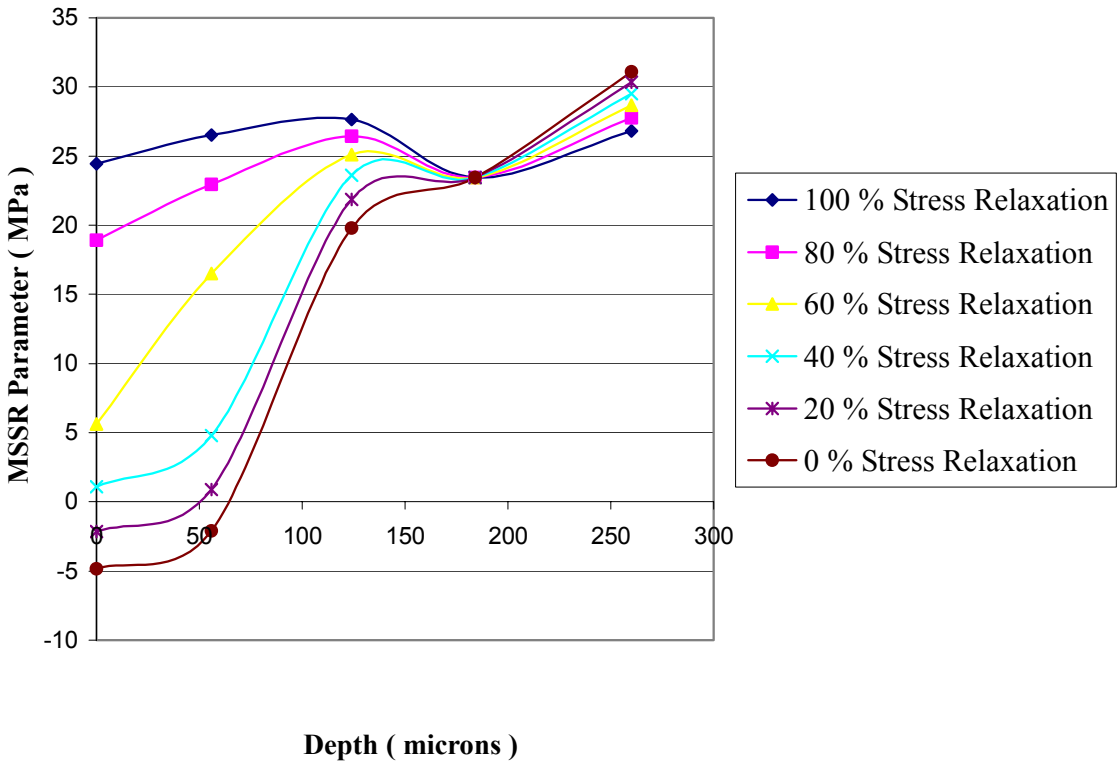

Figure 6.4. MSSR Parameter versus Depth for 3.81 mm thickness (Test # 19)

Bibliography

1. R. B. Waterhouse, *Avoidance of Fretting Fatigue Failures,* Fretting Fatigue, Applied Science Publishers, London, pp 221-240, 1981.

2. G. Leadbeater, B. Noble, and R. B. Waterhouse, *The Fatigue of an Aluminum Alloy Produced by Fretting on Shot Peened Surfaces,* Proceedings of 6th Int. Con. On Fracture, India, Vol. 3, pp 2125-2132, 1984.

3. M. K. Gabel, and J. J. Bethk, *Coatings for Fretting Prevention,* Wear, Vol. 46, pp 81-96, 1979.

4. R. G. Vardiman, D. Creighton, et al, *Effect of Ion Implantation on Fretting Fatigue in Ti-6Al-4V Alloy,* ASTM STP 780, American Society for Testing and Materials, Philadelphia, pp, 138-149, 1982.

5. K. Tanaka, Y. Mutoh, and S. Sakoda, *Effect of Contact Materials on Fretting Fatigue in a Spring Steel,* Transactions on Japan Soc. Mech. Engrs (A), Vol 51, No. 464, pp 1200-1207, 1985.

6. S. Namjoshi, V. K. Jain, S. Mall, *Effects of Shot-peening on Fretting Fatigue Behavior of Ti-6Al-4V*. (in press)

7. ABAQUS Standard User's Manual Vol 2., Hibbit, Karlsson and Sorensen, Inc. 1995.

8. C. D. Lykins, *An Investigation of Fretting Fatigue Crack Initiation Behavior on the Titanium Alloy Ti-6Al-4V*, Dissertation.

9. Harris W.J., *The Influence of Fretting on Fatigue*, AGARD Advisory Group for Aerospace Research and Development, Advisory Report 8, 1967.

10. D. Hoeppner and G. Goss, *A Fretting Fatigue Damage Threshold Concept*, Wear, Vol. 27, 1974, 61-70.

11. K. Endo and H. Goto, *Initiation and Propagation of Fretting Fatigue Cracks*, Wear, Vol. 125, 1988, 129-146.

12. T. Lindley and K. Nix, *The Role of Fretting in the Initiation and Early Growth of Fatigue Cracks in Turbo Generator Materials*, Multiaxial Fatigue, ASTM, 1985, 340-360.

13. K. Nix, and T. Lindley, *The Application of Fracture Mechanics to Fretting Fatigue*, Fatigue and Fracture of Engineering Materials and Structures, 1985,

Vol. 8, No. 2,143-160.

14. C. Ruiz, P. Boddington and K. Chen, *An Investigation of Fatigue and Fretting in a Dovetail Joint*, Experimental Mechanics, 1984, Vol. 24, No. 3, 208-217.

15. C. D. Lykins, S. Mall, and V. K. Jain, *An Evaluation of Parameters for Predicting Fretting Fatigue Crack Initiation*, International Journal of Fatigue, Vol. 22, pp 703-716, 2000.

16. A. Elkholy, *Fretting Fatigue in Elastic Contacts due to Tangential Micromotion*, Tribology International, 1996, Vol. 29, No. 4, 265-273.

17. S. Fouvry, P. Kapsa and L. Vincent, *Analysis of Sliding Behavior for Fretting Loadings: Determination of Transition Criteria*, 1995, Wear, Vol. 185, 35-46.

18. L. Coffin, Jr., *A Study of the Effects of Cyclic Thermal Stresses on a Ductile Metal*, Trans. ASME, 1954, Vol. 76, 931-950.

19. S. Manson, *Behavior of Materials Under Conditions of Thermal Stress*, NACA Technical Report TN 2933, 1953.

20. O. Basquin, *The exponential Law of Endurance Tests*, Am. Soc. Test. Mater. Proc., 1910, Vol. 10, 625-630.

21. K. Walker, *The Effect of Stress Relaxation During Crack Propagation and Fatigue for 2024-T3 and 7075-T6 Aluminum*, Presented to Subcommittee E-9V Winter Meeting, Feb 1969.

22. D. Socie, *Multiaxial Fatigue Damage Models*, Journal of Engineering Materials and Technology, Oct 1987 Vol. 109, 293-298.

23. K. Nishioka and K. Hirakawa, *Fundamental Investigations into Fretting fatigue*, Part 3, Bulletin of JSME, 1969, Vol. 12, No. 51, 397-407.

24. K. Nishioka and K. Hirakawa, *Fundamental Investigations into Fretting fatigue*, Part 2, Bulletin of JSME, 1969, Vol. 12, No. 50, 180-187.

25. K. Smith, P. Watson and T. Topper, *A Stress Strain Function for the Fatigue of Metals*, Journal of Materials, JMLSA, 1970, Vol. 5, No 4, 767-778.

26. S. Mall, V. K. Jain, S. Namjoshi, C. D. Lykins, *Fretting Fatigue Crack Initiation Behavior of Ti-6Al-4V*. (in press)

27. M. Szolwinski, and T. Farris, *Mechanics of Fretting Fatigue Crack Formation*, 1996, Wear, 93-107.

28. A. Fatemi and D. Socie, *A Critical Plane Approach to Multiaxial Fatigue Damage Including Out of Phase Loading*, Fatigue and Fracture of Engineering Materials and Structures, 1988 Vol. 11, 149-165.

29. R. Neu, J. Pape, D. Swalla-Michaud, *Methodologies for Linking Nucleation and Propagation Approaches for Predicting Life Under Fretting Fatigue*, Fretting Fatigue: Current Technology and Practices, ASTM 1367, D. Hoeppner, V. Chandrasekaran and C. Elliot, Eds. American Society for Testing and Materials, 1999.

30. G. Lundberg and A. Palmgren, *Dynamic Capacity of Rolling Bearings*, Acta Polytechnica-Mech Eng. Series 1, 1947, Vol 1., No. 3, 4-51.

31. L. Fellows, D. Nowell, D. Hills, *On the Initiation of Fretting Fatigue Cracks*, Wear, 1997, Vol. 205, 120-129.

32. W. N. Findley, *Fatigue of Metals Under Combinations of Stresses*, Transactions, ASME, Vol. 79, pp. 1337-1348, 1957.

33. D. Hills and D. Nowell, *Mechanics of Fretting Fatigue*, Kluwer Academic Publishers, Netherlands, 1994.

34. L. Fellows, D. Nowell, D. Hills, *Contact Stresses in a Moderately Thin Strip (with Particular Reference to Fretting Experiments)*, 1995, Wear, Vol 185, 235-238.

35. K. Chan and Y. Lee, *Ruiz Program*, South West Research Institute, Personal Communication, 1998.

36. E. R. De Los Rios, M. W. Brown, et al, *Effect of Shot-Peening on the Fretting Fatigue Behavior of BS L65 Aluminum Alloy*, International Committee on Aeronautical Fatigue, 25th Conference, Seattle WA, 1999.

37. E. R. De Los Rios, M. Trooll, and A. Levers, *Improving the Fatigue Crack Resistance of 2024-T351 Aluminum Alloy by Shot-Peening*, Life Extension– Aerospace Technology Opportunities, The Royal Aeronautical Society Publication, pp 26.1-26.8, 1999.

38. Y. Mutoh, T. Satoh, and E. Tsunoda, *Improving Fretting Fatigue Strength at Elevated Temperatures by Shot-Peening in Steam Turbine Steel*, Standardization of Fretting Fatigue Test Methods and Equipment, ASTM STP 1159, M. Helmi Attia and R. B. Waterhouse, Eds., American Society for Testing and Materials Philadelphia, pp 199-209, 1992.

39. Kaleidagraph, Curve Fitting Software, Kaleidagraph for Windows 2.

40. K. Iyer and S. Mall, *Effects of Cycling Frequency and Contact Pressure on Fretting Fatigue under Two-Level Block Loading*, Fatigue and Fracture of Engineering Materials and Structures, Vol. 23, pp 335-346, 2000.

Vita

1 LT, Halil I Yuksel, Turkish Air Force, was born in Eskisehir, Turkey. He graduated from Maltepe Military High School in Izmir, Turkey in 1992. He then entered Turkish Air Force Academy, Istanbul for undergraduate studies. He graduated from Turkish Air Force Academy with a Bachelor of Science degree in Aeronautical Engineering in August 1996.

After graduation, he was trained as a transportation officer in Bursa, Turkey. He worked as a transportation officer until July of 2000 in Istanbul, Turkey. In August 2000, he entered the Graduate School of Engineering and Management, Air Force Institute of Technology. Upon graduation, he will be assigned in Turkey working for Turkish Air Forces.

REPORT DOCUMENTATION PAGE

Form Approved
OMB No. 074-0188

1. REPORT DATE *(DD-MM-YYYY)*	2. REPORT TYPE	3. DATES COVERED *(From – To)*
26-03-2002	**Master's Thesis**	Sep 2000 – Mar 2002

4. TITLE AND SUBTITLE

EFFECTS OF SHOT-PEENING ON HIGH CYCLE FRETTING FATIGUE BEHAVIOR OF Ti-6Al-4V

5a. CONTRACT NUMBER

5b. GRANT NUMBER

5c. PROGRAM ELEMENT NUMBER

6. AUTHOR(S)

Yuksel, Halil, I, 1LT, TUAF

5d. PROJECT NUMBER

5e. TASK NUMBER

5f. WORK UNIT NUMBER

7. PERFORMING ORGANIZATION NAMES(S) AND ADDRESS(S)

Air Force Institute of Technology
Graduate School of Engineering and Management (AFIT/EN)
2950 P Street, Building 640
WPAFB OH 45433-7765

8. PERFORMING ORGANIZATION REPORT NUMBER

AFIT/GAE/ENY/02-12

9. SPONSORING/MONITORING AGENCY NAME(S) AND ADDRESS(ES)

AFRL/MLLMN
Attn: Dr. Jeffrey Calcaterra
2230 Tenth Street, Suite 1 DSN: 785-1360
WPAFB OH 45433-7817 e-mail: Jeffrey.Calcaterra@wpafb.af.mil

10. SPONSOR/MONITOR'S ACRONYM(S)

11. SPONSOR/MONITOR'S REPORT NUMBER(S)

12. DISTRIBUTION/AVAILABILITY STATEMENT

APPROVED FOR PUBLIC RELEASE; DISTRIBUTION UNLIMITED.

13. SUPPLEMENTARY NOTES

14. ABSTRACT

Effects of shot-peening on High Cycle Fretting Fatigue behavior of Ti-6Al-4Vwere investigated. Experiments were performed with 6.35 mm thick specimens which provided S / N curves. After the tests, it was observed that the specimens failed near the trailing edge of contact. Scanning Electron Microscopy showed that cracks initiated on the contact surface for 6.35 mm, and at the depth of specimen ranging from 200 to 300 microns for 3.81 mm thick specimens. Initial crack orientation was around 37 and 42 degrees respectively for 6.35 and 3.81 mm thicknesses. Finite Element Analysis (FEA) was conducted, and using FEA results, Smith-Watson-Topper, Findley, Shear Stress Range and Modified Shear Stress Range parameters were evaluated. Stress relaxation was observed after the failure of the specimens, and evaluations were repeated for different percentages of stress relaxation. Based on specific assumptions about stress relaxation, Modified Shear Stress Range parameter was determined to be the only appropriate fatigue parameter that could meet all the required conditions for shot-peened fretting fatigue specimens. Also thickness effects on shot-peened specimens were investigated and discussed in this study.

15. SUBJECT TERMS

Fretting Fatigue, High Cycle Fatigue, Shot-Peening, Shot-Peening Effects in Fretting Fatigue

16. SECURITY CLASSIFICATION OF:			17. LIMITATION OF ABSTRACT	18. NUMBER OF PAGES	19a. NAME OF RESPONSIBLE PERSON
a. REPORT	b. ABSTRACT	c. THIS PAGE			Prof. Dr. Shankar Mall, AFIT (ENY)
U	U	U	UU	142	19b. TELEPHONE NUMBER *(Include area code)* (937) 255-3636, ext 4587; e-mail: Shankar.Mall@wpafb.af.mil

Standard Form 298 (Rev. 8-98)
Prescribed by ANSI Std. Z39-18